Aus dem Institut für Molekular- und Zellbiologie
der Hochschule Mannheim
(Direktor: Prof. Dr. rer. nat. Mathias Hafner)

Development and characterization of a novel, simple, spheroid-based tri-culture model composed of fibroblasts, keratinocytes, and melanoma cells

Inauguraldissertation
zur Erlangung des Doctor scientiarum humanarum (Dr. sc. hum.)
der
Medizinischen Fakultät Mannheim
der Ruprecht-Karls-Universität
zu
Heidelberg

vorgelegt von
Julia Klicks

aus
Mannheim
2019

Dekan: Prof. Dr. med. Sergij Goerdt
Referent: Prof. Dr. rer. nat. Mathias Hafner

TABLE OF CONTENTS

Page

ABBREVIATIONS

ABCB5	ATP-binding cassette sub-family B member 5
ADME	absorption, distribution, metabolism and excretion
AF	AlexaFluor
ALCAM	activated leukocyte cell adhesion molecule
ANOVA	analysis of variance
BME	basement membrane extract
BRAF	B-rapidly accelerated fibrosarcoma
CAM	cell adhesion molecule
CLS	Cell Line Service
CTLA-4	cytotoxic T-lymphocyte antigen-4
DMEM	Dulbecco's Modified Eagle Medium
DMSO	Dimethylsulfoxid
ECM	Extracellular matrix
ERK	extracellular signal-regulated kinase
IFN	interferon
IKVAV	Ile-Lys-Val-Ala-Val
IL	interleukin
IMDM	Iscove's Modified Dulbecco's Medium
KRT	keratin
MAPK	mitogen-activated protein kinase
MEK	mitogen-activated extracellular signal-regulated kinase
Mel-CAM	melanoma cell adhesion molecule

PCNA   Proliferating Cell Nuclear Antigen

PCR   Polymerase Chain Reaction

PDMS   polydimethylsiloxane

PD-1   programmed cell death protein 1

PEG   polyethylene glycol

PI3K   phosphatidylinositol 3-kinase

PLA   polylactic acid

PLG   polylactide-co-glycolide

PVA   polyvinyl alcohol

RGD   Arg-Gly-Asp

RGP   radial growth phase

RTK   receptor tyrosine kinase

SMART   substrate modification and replication by thermoforming

TGF   transforming growth factor

TNF   tumor necrosis factor

UV   ultraviolet

VCAM   vascular cell adhesion molecule

VGP   vertical growth phase

2D   two-dimensional

3D   three-dimensional

1 INTRODUCTION

1.1 3D cell culture

Cell-based assays play a central role in the process of drug discovery. They provide simple, fast, and cost-effective tools to avoid large-scale and cost-intensive animal testing. Until now, the majority of cell-based assays are based on traditional two-dimensional (2D) monolayer cells cultured on flat and rigid substrates. While the widely used 2D cell culture has proven to be a valuable method for cell-based studies, it has also serious restrictions. In the *in vivo* environment, where cells grow in a three-dimensional (3D) manner, almost all cells are surrounded by other cells and the extracellular matrix (ECM). In contrast, 2D cell culture does not sufficiently take into account the natural 3D environment of cells. As a consequence, results achieved by 2D cell culture experiments are often misleading and their predictive value for *in vivo* responses is rather limited [1,2]. Nonetheless, in drug discovery, the standard procedure of screening compounds still starts with 2D cell culture-based studies, followed by animal tests and clinical trials. Only about 10 % of the compounds are successful in clinical development. The majority of drugs fail during clinical trials, especially during phase III, which is the most expensive phase in this process [3,4]. This is mostly due to a lack of clinical efficacy and/or acceptable toxicity [5,6]. A reason for this failure is caused by data collected from the 2D monolayer culture studies where, owing to the artificial microenvironment, the cellular response to drugs is altered. Thus, the development of more realistic and predictive *in vitro* cell-based systems is essential to identify non-specific, ineffective, or toxic compounds early in the drug development process, ideally before animal tests. 3D and organoid cell cultures promise to be a big step forward in that direction.

1.2 Types of 3D cell cultures

While most studies on 3D cultures use established cell lines, organoid cell cultures using patient-derived primary cells or stem cells in 3D cultures are on the rise.

Organoids are capable of self-renewal, self-organization and exhibit organ functionality [7]. They provide similar composition and architecture to primary tissue, relevant models of *in vivo* conditions, and a stable system for extended cultivation [8]. Conversely, established cell lines are cost effective, easy to handle, provide an

unlimited source of material, and avoid ethical concerns associated with the use of animal and human tissue. Furthermore, cell lines represent a pure cell population allowing reliable samples and reproducible results [9].

3D cell culture techniques are classified as scaffold-based and non-scaffold-based techniques.

1.2.1 Scaffold-based and non-scaffold-based techniques

In 3D cell cultures, cells grow into 3D aggregates/spheroids using a scaffold/matrix or they develop in a scaffold-free way. The generation of scaffold/matrix-based 3D cell cultures is performed by either seeding cells on an acellular 3D matrix or by dispersing cells in a liquid matrix and a further solidification or polymerization. Scaffold/matrix materials that are commonly used include biologically derived scaffold systems and synthetic-based materials. Biologically derived matrices that are commercially available products are for example BD Matrigel™ basement membrane matrix (BD Science), Cultrex® basement membrane extract (BME; Trevigen), and hyaluronic acid. To form synthetic scaffolds, polyethylene glycol (PEG), polyvinyl alcohol (PVA), polylactide-co-glycolide (PLG), and polylactic acid (PLA) are commonly used materials [10–13].

Scaffold-free techniques allow cells to self-assemble and to form non-adherent cell aggregates mimicking solid tissues that secrete their own extracellular matrix and exhibit an inherent gradient of nutrients, oxygen, and metabolites within themselves [14]. The generation of scaffold-free 3D cell spheroids is made in suspensions by the forced floating method, the hanging drop method, or agitation-based approaches [4] (figure 1). The forced floating method uses low adhesion polymer-coated well-plates to produce spheroids. An advantage of this method is that it can be used for high-throughput screening due to its possible automation [15]. The hanging drop method consists of a cell suspension inside a tray. By inverting the plate/tray, cell suspensions become droplets presenting cell aggregates on their tip and thereby creating compact spheroids [16,17]. Spheroids produced by this method have a relatively higher gas exchange [18] and possible effects of contact materials on cells are avoided. Nevertheless, to use these spheroids in cell-based assays, they need to be transferred to other standard plates after spheroid formation [18]. Finally, the agitation-based method uses bioreactors to obtain 3D spheroids. Herein, cell suspensions are placed into a

rotating bioreactor that gradually turns isolated cells into aggregates that cannot adhere to the container wall due to continuous stirring. Consequently, a wide range of non-uniform spheroids is generated. Each of the above mentioned methods allow cells to grow naturally in a 3D environment with cells interacting with other cells, the ECM, and their microenvironment. These interactions in such 3D spatial arrangement affect a variety of cellular functions, such as cell proliferation, differentiation, morphology, gene and protein expression, and cellular responses to external stimuli [19].
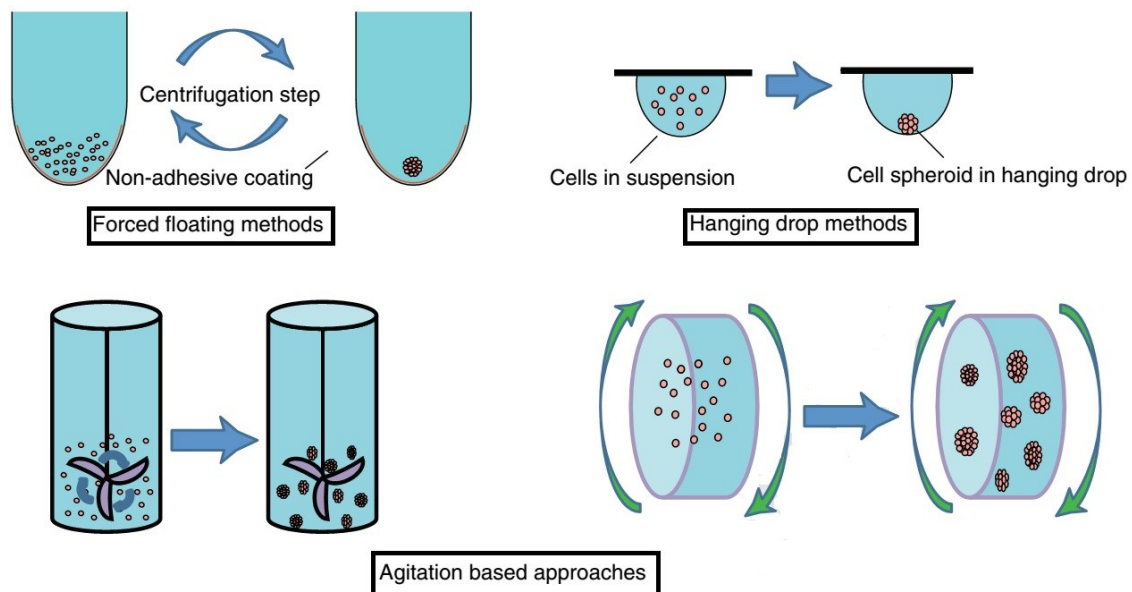
Figure 1: Scaffold-free 3D cell culture techniques. Scaffold-free techniques allow cells to self-assemble. The forced floating method uses low adhesion plates to produce spheroids. The hanging drop method creates spheroids by inverting a tray with cell suspensions that become droplets presenting cell aggregates on its tip. And the agitation-based approaches uses bioreactors to obtain 3D spheroids. *Adapted from Breslin et al 2013.*

1.2.2 Microfluidic 3D cell culture: Organs-on-chips

The transition from 2D to 3D cell culture techniques is an important step to gain more physiological relevant models. However, most 3D cell culture systems do not take into account the multicellular complexity of tissues and do not present tissue vasculature. Furthermore, they do not offer gradients and continuous perfusion [20]. Microfluidic 3D cell cultures allow co-culturing of cells in a spatially controlled manner, generation and control of gradients, and a continuous perfusion/flow. Combining multiple cell types represents the organization of tissues and organs more closely. By culturing them in a spatially controlled manner, the *in vivo* situation can be mirrored. For example, the interaction between stromal cells with cancer cells can be mimicked [21]. Microfluidics

are also a useful tool for co-cultivation of whole tissues, so called organs-on-chips, and interconnecting them with microfluidic channels for media circulation [22,23]. To further include vasculature, seeding of endothelial cells inside the interconnecting channels can be performed [24]. In the *in vivo* environment, many soluble molecular gradients are found in different biological processes such as angiogenesis, invasion, and migration [20]. To study these processes, microfluidic devices have been developed. The flow of fluids can be spatially controlled by microfluidics, and therefore gradients can be achieved. For example, it is possible to build a hydrogel between fluids that forms a stable linear gradient, or to alter the geometry of channels and apply flow rates to gain more complex gradients [25]. Perfusion inside microfluidic 3D cell culture devices enables stable nutrient and oxygen supply and constant removal of waste products. Furthermore, it is essential in terms of vasculature, since the flow of fluids provides shear stress that affects cell morphology and gene expression [26,27]. Figure 2 displays such a microfluidic 3D cell culture device. It allows efficient human-like tissue nutrition, flexible combination of different tissues, and long-term performance.
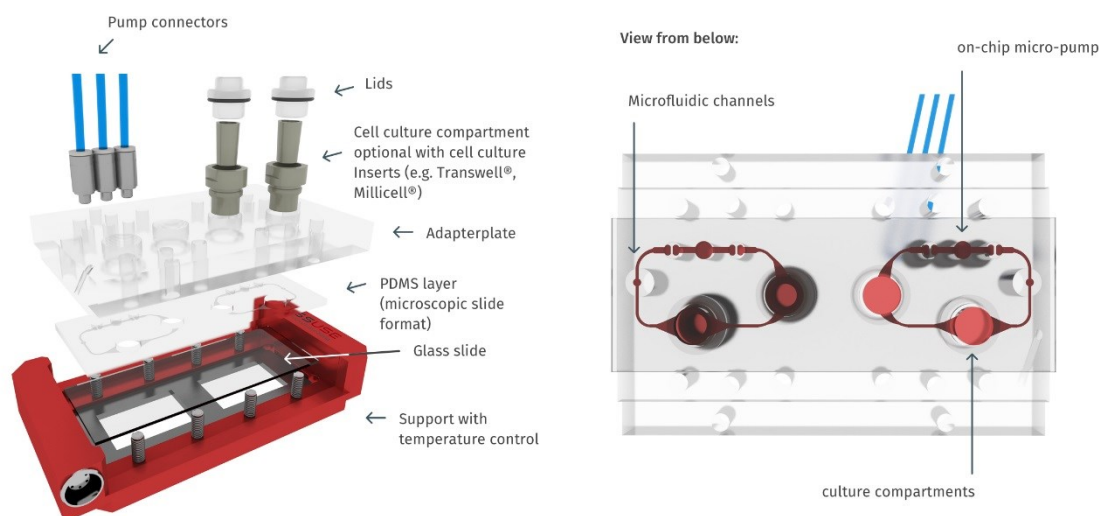
Figure 2: Microfluidic organ-on-chip. A microfluidic device allows cultivation of different organ models in a common media perfusion circuit in a miniaturized format. Adapted from Tissuse, 2-Organ-Chip (2-OC), URL: https://www.tissuse.com/en/products/2-organ-chip/ [15.02.2019].

1.3   Modeling cancer in 3D for drug discovery

One of the numerous advantages of 3D cell culture is the reflection of the tumor *in vivo* situation by the possibility to incorporate elements of the tumor microenvironment such as fibroblasts, immune and inflammatory cells, the blood and lymphatic vascular network, adipose cells, and neuroendocrine cells [28,29]. The tumor microenvironment displays following properties: (I) oxygen and nutrient gradients, (II) non-uniform

exposure to drug/compounds, (III) increased cell-cell interactions, (IV) cell-matrix interactions, (V) influence of stromal/tumor site specific cells via paracrine signaling, and (VI) dissimilar proliferation rates throughout the 3D structure (figure 3) [30]. These characteristics are closely mimicked by 3D cell culture models. Hence, drug research is much more efficient when performed in such 3D cell cultures. Several 3D cell culture systems with different cancer cell types have been developed to test various anti-cancer drugs. Direct comparison of the same cancer cells revealed a lower/reduced sensitivity to the anti-cancer agent when performed in 3D systems as compared to 2D growth [31–33]. On the other hand, there are studies showing that cancer cells cultured in 3D models are equal or even more susceptible to a drug compared to 2D monolayer cultures [34–36].
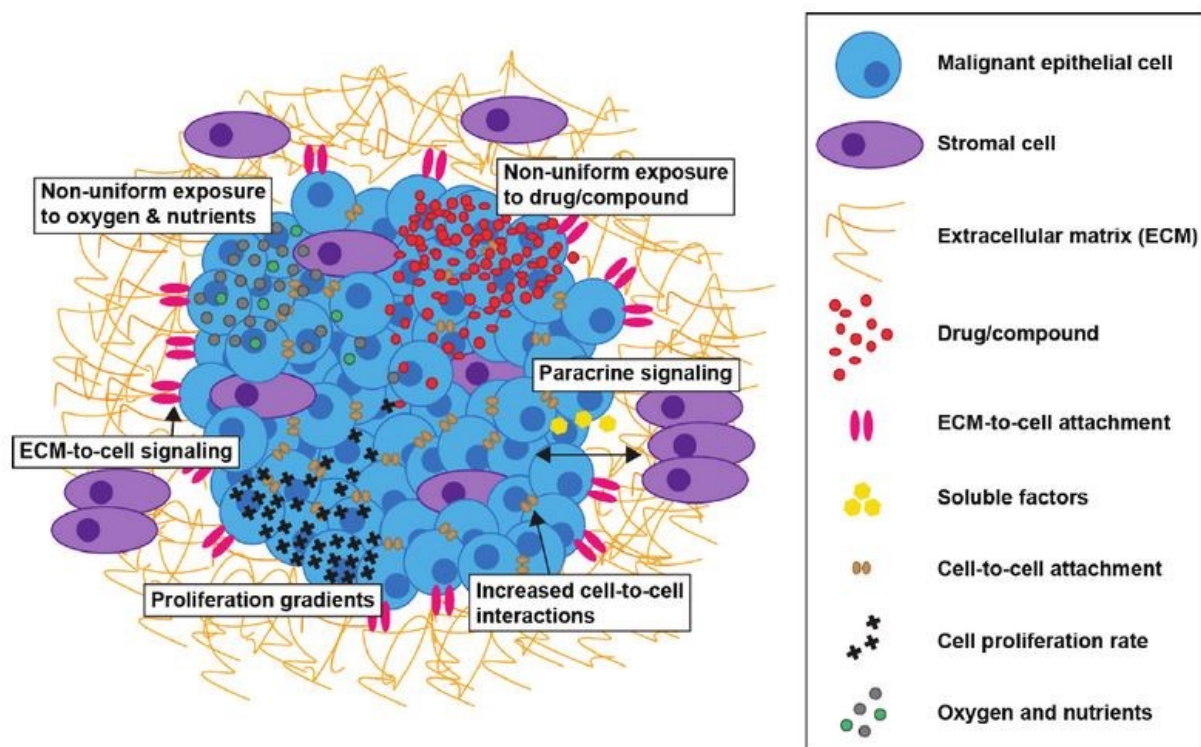
Figure 3: Properties of the tumor microenvironment. 3D architecture of tumors presents (I) oxygen and nutrient gradients, (II) uneven exposure to drug/compounds, (III) enhanced cell-cell interactions, (IV) cell-matrix communications, (V) effect of stromal/tumor site specific cells through paracrine signaling, and (VI) different proliferation rates throughout the 3D structure. *Adapted from Lovitt et al 2014.*

1.4 Skin

1.4.1 Composition and function

Human skin covers an area of almost 2 m^2 in the adult and thus represents our second largest organ only exceeded by the vascular system [37]. It consists of the three major layers, subcutis, dermis, and epidermis. The subcutis comprises primarily adipose tissue and epithelial cells. Adipose tissue consists of clusters or sheets of lipid-filled cells, called adipocytes. Furthermore, the subcutis is composed of blood vessels, neurites of peripheral neurons, Vater-Pacini mechanosensors, and, partially, also sweat glands and hair follicles [38]. Moreover, it connects the skin to periosteum and fascia, absorbs forces, and adds thermal insulation [39].

The dermis of the skin is stratified into an inner, reticular, and an outer, papillary, area. It supplies the epidermis with mechanical support and nutrients. Most sebaceous glands, sweat glands, hair follicles, smooth muscle cells, and capillary beds are located in the dermis. Thus, the dermis regulates skin moisture and body temperature, and performs the secretory function of the skin [38]. The papillary layer houses loose connective tissue. Herein, Meissner corpuscles are located that are responsible for sensitivity to gentle touch [40]. On the contrary, the reticular layer is characterized by dense connective tissue. Additionally, immune cells, especially mast cells and dendritic cells, are placed in the papillary layer and mediate local inflammatory reactions and immune surveillance [38]. Finally, tensile strength and elasticity of skin are mediated by dermal fibroblasts. These also secrete extracellular matrix and basement membrane components which are primarily collagens I and III, and a proteoglycan-rich ground substance [37]. The two skin compartments, dermis and epidermis, are separated from each other by a special basement membrane (figure 4). This comprises a laminin/collagen IV rich scaffold and components that are typical for the basement membrane such as perlecans and nidogens [37].

The epidermis of the skin is a 50-150 μm thick squamous epithelium. It contains keratinocytes, Merkel cell mechanosensors, Langerhans immune cells, and melanocytes [38]. Keratinocytes give mechanical strength to the skin through a dense network of intracellular intermediate filament systems built up of keratins (KRT). They interconnect neighboring cells via desmosomes containing desmoplakin [41] and link to the basement membrane via hemidesmosomes containing plectin [42,43] (figure 4).
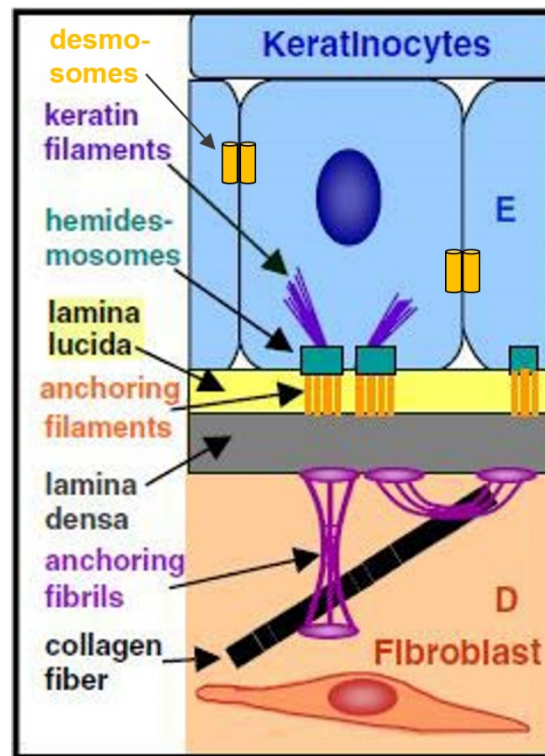
Figure 4: Elements of the basement membrane. Schematic draft shows the anchorage between epidermis (E) and dermis (D) centered around a special basement membrane. Dermal fibroblasts secrete collagens and keratinocytes in the epidermis, interconnected via desmosomes, give strength to the skin through keratin filaments that connect the cells to the basement membrane via hemidesmosomes. *Adapted and modified from Breitkreutz et al 2009.*

Epidermal keratinocytes are organized in four well-defined strata with increasing differentiation status from the inner to the outer side (figure 5). In detail, it first shows two germinal layers, the stratum basale and stratum spinosum. In the stratum basale, the inner layer, where the cells are linked to the lamina basale via hemidesmosomes, the keratinocytes divide and give rise to cells that constitute in the spinous layer. In the spinous layer, the cells exit from the cell cycle and reinforce their cytoskeletal keratin and desmosome network [44]. In the stratum granulosum, keratinocytes display a more flattened shape and express late differentiation markers such as filaggrin and loricrin. Finally, keratinocytes undergo terminal differentiation to become dead, flattened corneocytes in the outer layer of the epidermis, the stratum corneum [45]. During this process, a cornified envelope is created at the inner side of the cytoplasmic membrane, that is composed of keratins, involucrin, filaggrin, and loricrin [45,46]. Additionally, lipids are stored in secreted lamellar bodies that consist of ceramides, cholesterol, and fatty acids [47] to form a water-repelling envelope around the cornified envelope as a permeability barrier function [44,45,48]. Terminal differentiation of keratinocytes depends

on temperature and Ca^{2+} [46,49]. In fact, in the presence of millimolar amounts of Ca^{2+} and lowered temperature, the formation of such envelopes is preferred [46,49]. Furthermore, the secretion of lamellar bodies is triggered by Ca^{2+}-influx into keratinocytes [46] and occurs at the same time as keratinocytes convert to corneocytes by apoptotic cell death, indicated by the marker cleaved caspase 3 (table 1) [50]. In contrast, cells in the basal layer require low, micromolar amounts of Ca^{2+} for their proliferation [38]. A common marker of proliferation is ki67 (table 1). To ensure this variable function of Ca^{2+}, a sharp gradient is essential between the inner and outer layers of the epidermis. Between the stratum granulosum and stratum corneum, thick skin on palms of hands and feet features an additional layer, the stratum lucidum [51].
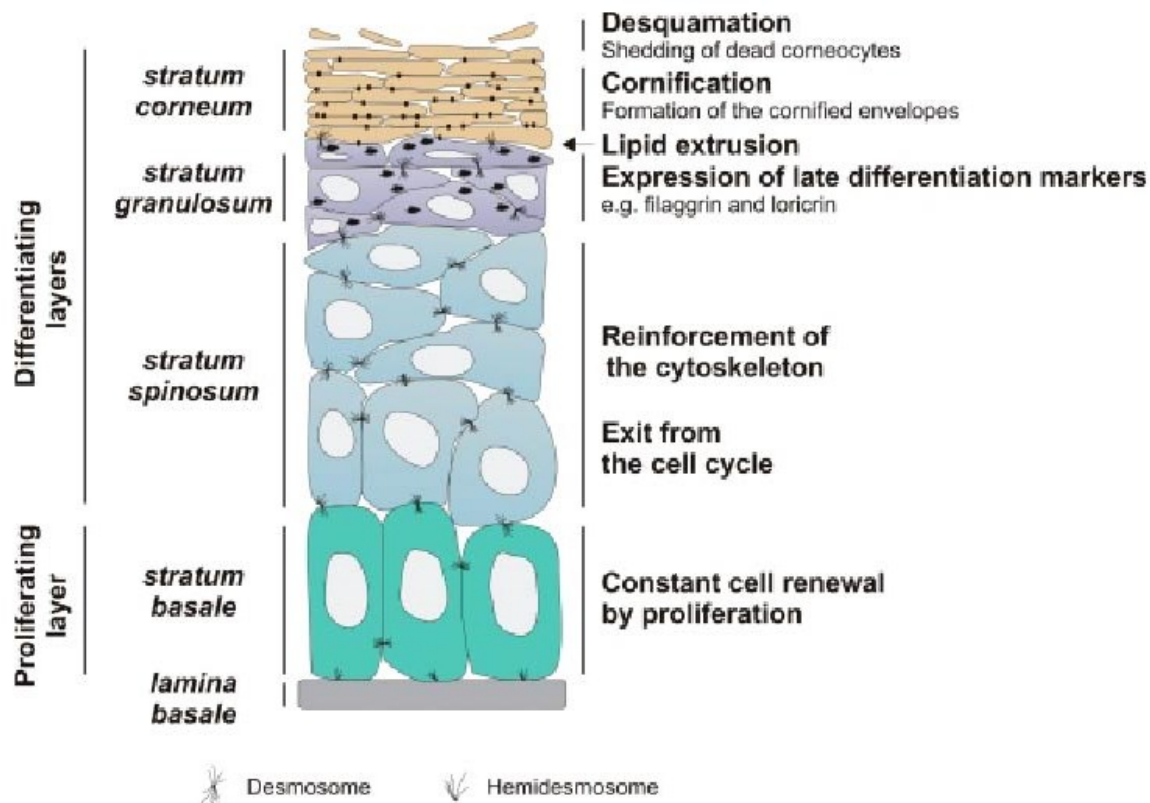
Figure 5: Layered structure of the epidermis. Keratinocytes located at the lamina basale proliferate to form the stratum basale. Then, they differentiate and build up the stratum spinosum, where they exit from the cell cycle and reinforce their cytoskeleton. In the stratum granulosum, they express late differentiation markers and, finally, become corneocytes in the outer most layers of the epidermis, the stratum corneum. *Adapted and modified from Denecker et al 2008.*

1.4.2 Role of cytokeratins in skin development and disorders

In a normal healthy adult, epidermis undergoes a complete renewal every 60 days [46]. Consequently, keratinocytes undergo a robust longitudinal change in gene expression.

This is particularly well understood and characterized for keratins [43,52–54]. As mentioned in table 1, KRT5 and KRT14 are typical markers for basal keratinocytes, while KRT1 and KRT10 are mainly expressed during differentiation in the stratum spinosum. The transition from KRT5/14 to KRT1/10 is a gradual process, typically resulting in a mixed expression of different keratins at several differentiation stages [43].

Table 1: Major markers of epidermal stratification

Protein	Epidermal layer	Physiological function	Ref.
KRT5/KRT14	Stratum basale	Resilience	[43,55]
KRT1/KRT10	Stratum spinosum	Resilience, part of cornification	[43,55]
KRT6/KRT16	Activated keratinocytes	Resilience	[53]
KRT17	Contractile keratinocytes	Resilience, regulation of protein synthesis and cell size	[53,54,56]
Involucrin	Stratum spinosum, Stratum granulosum, Stratum corneum	Cornification of plasma membrane, scaffold for other envelope proteins	[45,57]
Loricrin	Stratum granulosum, Stratum corneum	Major cornified envelope component	[45,58]
Profilaggrin	Stratum granulosum	Filaggrin precursor	[45,59,60]
Filaggrin	Stratum corneum	Keratin crosslinking	[45,59,60]
Ki67	Stratum basale, Stratum spinosum	Undefined role in cell division, rRNA synthesis, maintenance of mitotic spindle	[61–63]
Cleaved caspase 3	Stratum granulosum	Execution of apoptosis	[63–65]

Disturbance of keratinocyte differentiation can lead to chronic skin disorders such as atopic dermatitis and psoriasis [38]. In psoriatic epidermis, immune cells secrete inflammatory cytokines like TNF-alpha and IL-17, which results in a strongly altered gene expression [66]. This leads to an enhanced proliferation and an incomplete terminal differentiation of keratinocytes [66]. While the hyperproliferation-associated markers KRT6, KRT16, and KRT17 are highly expressed in psoriatic keratinocytes [67,68], the differentiation markers KRT1 and KRT10 are downregulated [68]. Consequently, psoriatic skin is associated with massive epidermal hyperplasia but poorly adherent stratum corneum leading to the characteristic flakes of psoriasis lesions [66]. In case of wound healing, keratinocytes undergo a different pathway called keratinocyte activation cycle [53] (figure 6). This process is initiated by the release of IL-1 from keratinocytes, which leads to the formation of blood vessels and immune response [38]. IL-1 functions as chemoattractant to trigger lymphocyte migration to the injury [69]. In

addition, IL-1 turns keratinocytes into hyperproliferative, migratory cells and changes their gene expression [53]. The cytokine TNF-α and growth factor TGF-α are induced and transmit the signal of injury to surrounding cells [53]. Furthermore, they are responsible for the maintenance of activation [53]. Activated keratinocytes express KRT6, KRT16, and KRT17 (table 1) and produce paracrine factors to alert fibroblasts, endothelial cells, melanocytes, and lymphocytes [53]. This activates fibroblasts to form a new ECM. Moreover, activated keratinocytes release autocrine signals targeting neighboring keratinocytes [53]. The next step of wound healing is the contraction of newly synthesized ECM. Therefore, keratinocytes become contractile caused by the signaling molecule IFN-γ. This, in turn, leads to the expression of KRT17. KRT17 is usually not found in healthy epidermis, but only at the end of the wound-healing process or in certain pathologies like psoriasis and allergic reactions [70]. To finish the process of wound healing, keratinocytes have to revert to their basal cell phenotype. Therefore, they need the signal that the injury is healed and the tissue repaired. This signal is caused by TGF-β released by fibroblasts [53]. TGF-β suppresses cell proliferation, reactivates the standard keratinocyte differentiation program, and induces expression of ECM and basement membrane components like fibronectin [71], laminin [72], and collagen IV [72] and VII [73,74]. Particularly, TGF-β induces the synthesis of the basal keratinocyte markers KRT5 and KRT14 [75].
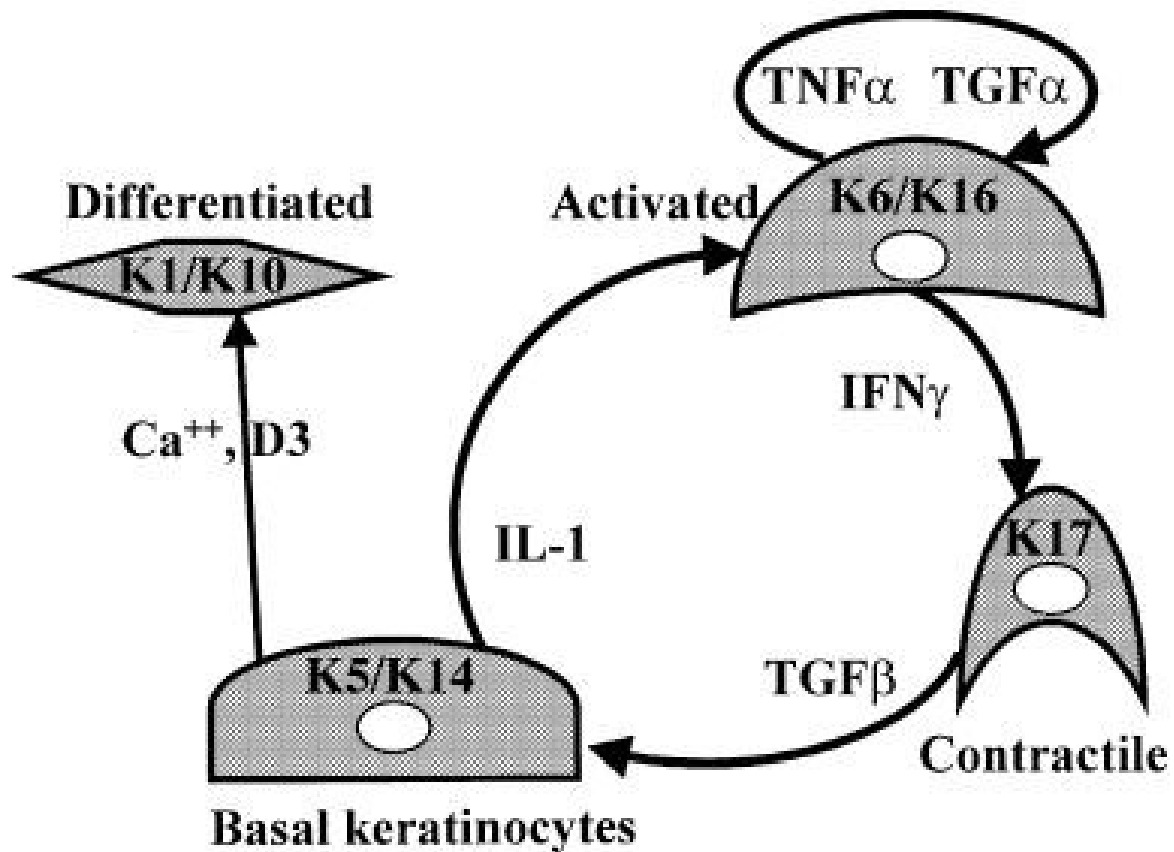
Figure 6: The keratinocyte activation cycle. Basal keratinocytes express KRT5 and KRT14. They can either differentiate, which depends on Ca^{2+} and vitamin D3, and produce KRT1 and KRT10, or become activated and produce KRT6 and KRT16. For this activation process, IL-1 has to be released. TNF-α and TGF-α are responsible for the maintenance of activation until another factor like IFN-γ is received. IFN-γ triggers KRT17 expression and induces contractility in keratinocytes. TGF-β reverts this pathway by induction of KRT5 and KRT14 expression. *Adapted from Freedberg et al 2001*.

1.5 From melanocytes to malignant melanoma

Melanoma is a malignant tumor that arises from the uncontrolled proliferation of melanocytes. Melanocytes are derived from the neural crest and produce the pigment melanin, which is responsible for human skin pigmentation [76]. Melanin can be classified into two major types of pigments: eumelanin (dark brown and black) and pheomelanin (yellow, red, and light brown) [77–79]. Both are produced and deposited in melanosomes. In human skin, melanocytes are located at the most basal epidermal layer, attached to the basement membrane, which separates epidermal and dermal compartments of the skin. In addition, they also mediate pigmentation of hair and iris [80]. Moreover, melanocytes are present in the inner ear for normal development of the cochlea [81], nervous system, sharing common embryologic origin [82], heart, influencing atrial reactive oxygen species [83,84], and probably many more locations [80]. Besides

melanocytes, also other cells have the ability to produce melanin. These include cells of pigmented epithelia of retina and iris, the ciliary body of the eye [85], some neurons [86], and adipocytes [87]. Melanocytes, placed at the basal layer of the epidermis, together with approximately 36 associated keratinocytes, form the epidermal melanin units [80,88,89]. In order to maintain this balance, melanocyte division is carefully regulated. Indeed, for proliferation, melanocytes need to detach from the basement membrane and neighboring keratinocytes, pull in their dendrites, divide, and finally migrate along the basement membrane, where they re-attach to the matrix and to keratinocytes to form a new epidermal melanin unit [90]. This growth of melanocytes is under the control of surrounding keratinocytes through (I) extracellular communication via paracrine growth factors, (II) intracellular communication via second messengers as well as signal transduction, and (III) intercellular communication via cell-cell adhesion molecules, cell-matrix adhesion, and gap junctions [90–92]. In normal skin, homeostasis decides whether a cell is quiescent, proliferative, differentiates, or undergoes apoptosis [90]. If this homeostasis is disturbed, the resulting imbalance of the epidermal melanin unit might cause a continuous proliferation of melanocytes, leading to the development of melanoma [90,92].

1.5.1 Cell-cell adhesion of melanocytes and melanoma cells

Normal melanocytes interact with the ECM through collagen IV and laminin. But in melanoma cells, this attachment is altered and they rather interact with collagen I and vitronectin [90]. This change is often associated with the aggressive potential of melanoma cells to invade from the epidermis to the dermis [93]. Cell-cell adhesion is also changed during tumor progression. While normal melanocytes connect to keratinocytes via E-cadherins (figure 7A), melanoma cells exhibit N-cadherins in order to attach to fibroblasts and endothelial cells in the tumor environment (figure 7B) [94]. Normal melanocytes were found to express only few cell-cell adhesion receptors of the family of cell adhesion molecules (CAMs) [90]. In contrast, melanoma cells display an increased expression of melanoma cell adhesion molecule (Mel-CAM), vascular cell adhesion molecule 1 (VCAM-1), L1 cell adhesion molecule (L1-CAM), and activated leukocyte cell adhesion molecule (ALCAM) [90].
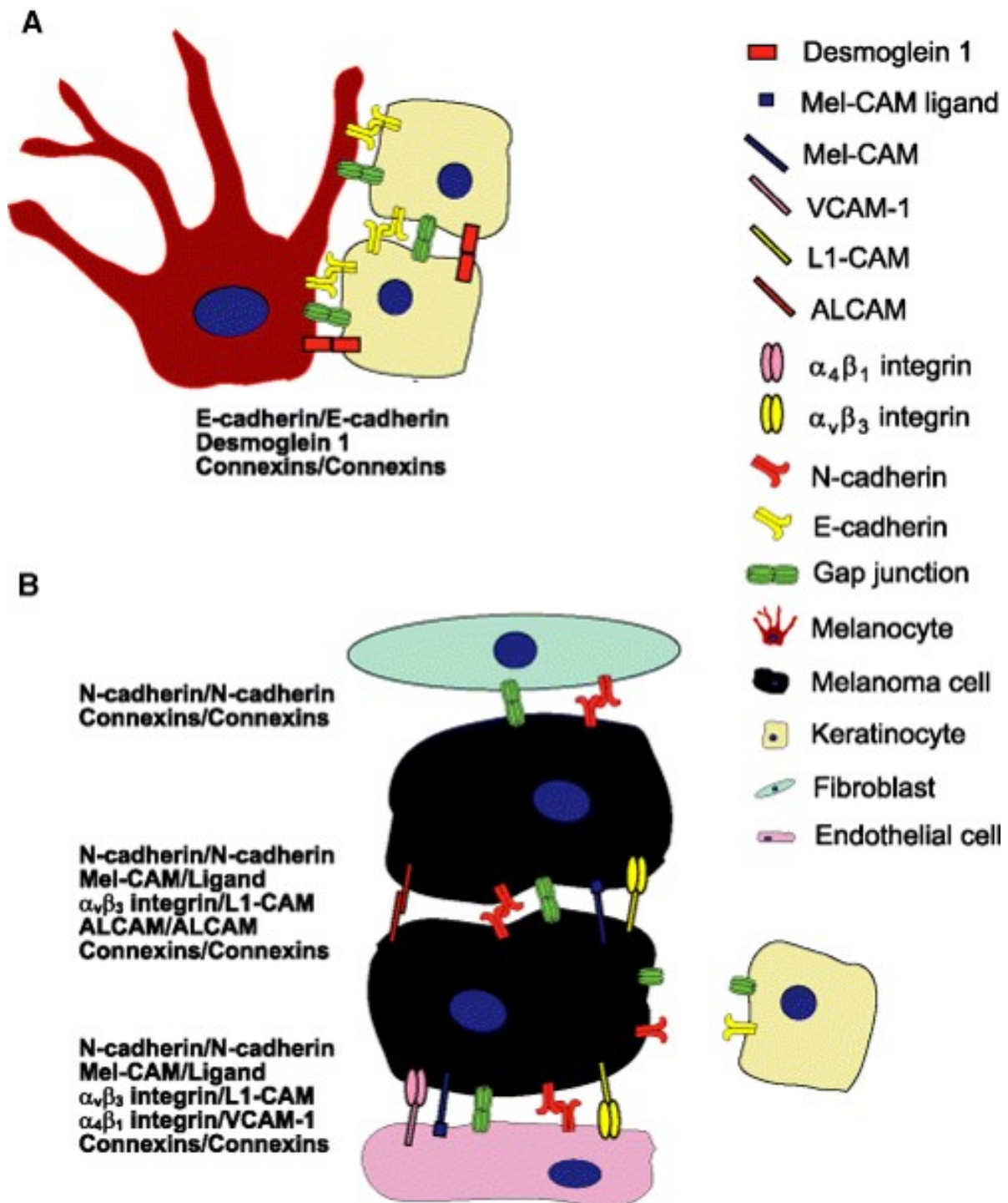
Figure 7: Difference in cell-cell adhesion in melanocytes versus melanoma cells. Normal melanocytes are interconnected to keratinocytes via E-cadherin and desmoglein allowing for communication through gap junctions **(A)**. Melanoma cells interact with each other via N-cadherin, Mel-CAM/Mel-CAM ligand, ALCAM, $\alpha_v\beta_3$ integrin/L1-CAM, and connexins, with fibroblasts via N-cadherin, and with endothelial cells via N-cadherin, Mel-CAM/Mel-CAM ligand, $\alpha_v\beta_3$ integrin/L1-CAM, $\alpha_4\beta_1$ integrin/VCAM-1, and connexins **(B)**. *Adapted from Haass et al 2005.*

Mel-CAM mediates cell-cell adhesion between melanoma cells and endothelial cells through a heterophilic adhesion to a still unknown ligand [95]. Mel-CAM expression is first found in melanocytic cells in nevi, where they start to separate from epidermal

keratinocytes and migrate into the dermis [96]. With ongoing malignancy, the expression of Mel-CAM increases and is found to be highest in metastatic melanoma cells [97]. Moreover, a correlation between Mel-CAM expression and tumor thickness exists [97,98]. Inhibition of Mel-CAM expression in metastatic melanoma cells through genetic suppressor elements of Mel-CAM cDNA results in the inhibition of adhesion between melanoma cells and thus downregulates the tumorigenic phenotype [99]. L1-CAM mediates adhesion of melanoma cells to other melanoma cells as well as to endothelial cells through binding to $\alpha_v\beta_3$ integrin in a heterophilic way [100]. This binding appears to play a central role in transendothelial migration of melanoma cells [101]. Next, the adhesion molecule ALCAM is only expressed in metastatic melanoma cells and facilitates cell-cell adhesion in a homophilic manner [102]. Its expression correlates with melanoma progression [103]. Finally, VCAM-1, a cytokine inducible cell adhesion molecule, is predominantly present on endothelial cells [90]. It serves as a receptor for $\alpha_4\beta_1$ integrin, which is expressed by malignant melanoma, and therefore guides adhesion of melanoma cells to the vascular endothelium [104].

1.5.2   Melanoma genetics

Melanoma gene mutations are highly induced by carcinogenic ultraviolet (UV) light irradiation [105]. Most of these mutations are cytidine to thymidine (C>T) transitions [105]. About 50-60 % of melanoma cases are caused by B-rapidly accelerated fibrosarcoma (BRAF) V600E mutations [106] and 20–30 % by NRAS mutations [107]. Since the MAP (mitogen-activated protein) kinase/ERK (extracellular signal-regulated kinases)-signaling pathway is activated in the majority of melanoma cases, BRAF V600E and NRAS Q61R are seen as driver mutations for malignant melanoma [108]. The MAPK pathway is an important intracellular signaling pathway that involves a series of protein kinase cascades to regulate cell proliferation (figure 8). It is activated through binding of extracellular growth factors to receptor tyrosine kinases (RTKs) [109]. This binding activates a small G protein such as RAS. RAS proteins are usually in an inactive state but become active when binding to GTP. Activated RAS, in turn, activates BRAF, which subsequently phosphorylates and thereby activates MEK (mitogen-activated extracellular signal-regulated kinase). Finally, MEK phosphorylates and activates ERK causing a normal cell proliferation and survival [110].
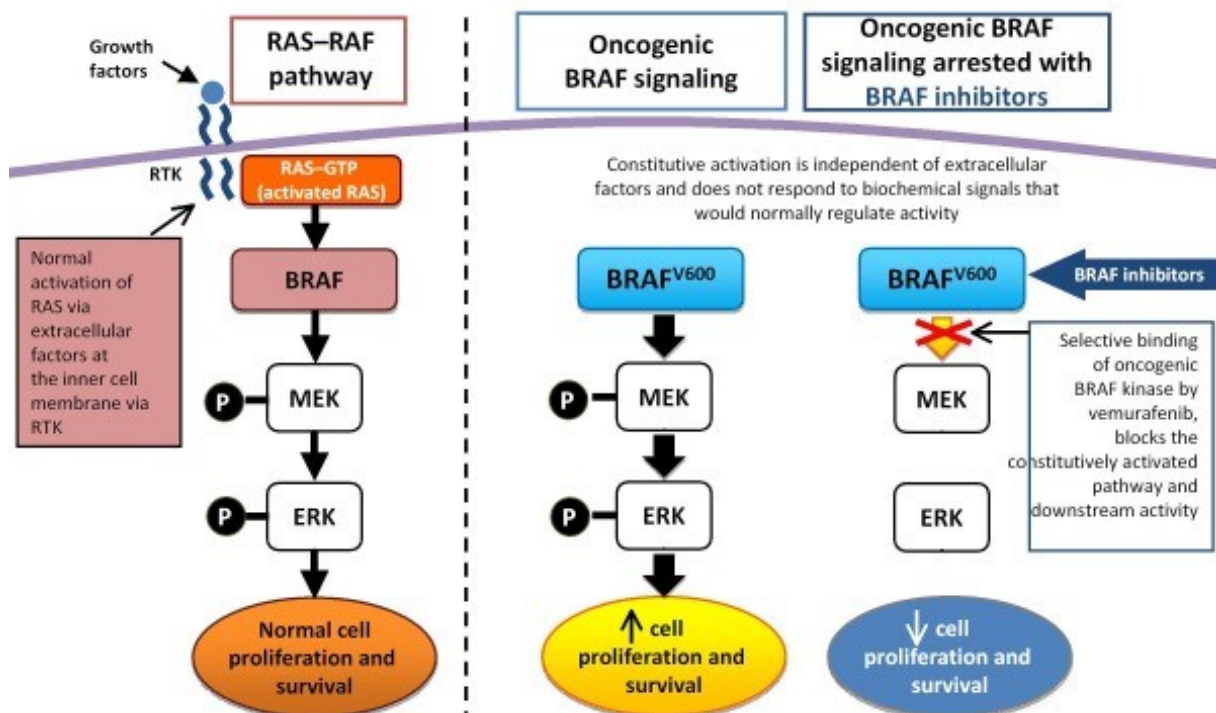
Figure 8: Normal and oncogenic BRAF signaling pathway. Normal cell proliferation and survival is triggered by activation of RAS via binding of extracellular factors to RTK. The following signaling involves the sequential activation of RAF, MEK and ERK. Point mutations like in BRAF V600E lead to an excessive activation of this pathway causing immense cell proliferation. Inhibition of BRAF V600E blocks the constitutively activated signaling and thereby hinders downstream activity. *Adapted from Ascierto et al 2012*.

However, in melanoma, where BRAF V600E is mutated, the MAPK pathway proceeds in a different way. Here, activation of BRAF V600E does not require RAS activation through extracellular factors. BRAF V600E is constitutively activated and continuously activates MEK followed by ERK. This leads to excessive cell growth and proliferation. BRAF inhibitors such as vemurafenib [111] aim to selectively bind to oncogenic BRAF kinase and thus block the signaling pathway [106,109,110]. However, the MAPK pathway is not the only signaling pathway that is critical for many essential cellular processes. The PI3K (phosphatidylinositol 3-kinase)-AKT pathway plays also an important role in normal cellular physiology and is frequently activated in melanomas [112].

1.5.3 Stages and types of melanoma

Melanoma is the most common form of cancer and its incidence is rising faster than any other cancer [107]. It is currently responsible for over 80 % of deaths from skin cancer [113]. Melanoma can be subdivided into two growth phases, radial and vertical. While in the radial growth phase, malignant cells stay in the epidermis and grow only radially, the vertical growth phase is characterized by the invasion of malignant cells into the dermis and the ability to metastasize beyond its primary site [114]. In more detail, melanoma can be grouped into different stages from 0-IV. Stage 0 melanoma (in situ) is characterized by restriction to the outer layer of the skin, the epidermis. It has not yet invaded the dermis but stays in place. Furthermore, it has not spread to the lymph nodes or distant sites. Stage I melanoma is divided into stage IA and stage IB. In stage IA, the tumor has no ulceration and is not more than 1 mm thick. In stage IB, the tumor is either not more than 1 mm thick but with ulceration, or between 1 and 2 mm thick and without ulceration. Moreover, the cancer cells have not spread to lymph nodes or distant sites. Stage II melanoma has invaded the dermis and is also divided into subclasses. Stage IIA melanoma is defined by either a thickness between 1 and 2 mm with ulceration, or between 2 and 4 mm thickness without ulceration. Stage IIB melanoma is either between 2 and 4 mm thick with ulceration, or more than 4 mm thick without ulceration. Stage IIC melanoma is more than 4 mm thick with ulceration. Stage III melanoma does not depend on thickness or ulceration. Here, the cancer cells have spread to one or more lymph nodes. And finally, in stage IV melanoma, the cancer has spread far away from its primary site to other places in the body including lung, liver, brain, bone or soft tissue [115]. Additionally, there are four types of melanoma, according to their growth pattern: (I) superficial spreading melanoma, the most common form, is flat but can become asymmetrical and elevated in advanced stages with various colors, (II) nodular melanoma, the second most common type, are normally blue-black but can also lack pigment, (III) lentigo maligna melanoma, which affects 4-10 % of melanomas, are often larger than 3 cm, flat, tan, and with marked notching of the borders, (IV) acral lentiginous melanoma, the rarest kind, appears on the palms and soles, or under the nails. They look flat, tan, or brown with irregular borders [114].

1.5.4 Treatment options of melanoma

When diagnosed in its early non-tumorigenic stages, resection of the lesion leads to promising survival rates [116]. However, melanoma is an aggressive malignancy that

tends to metastasize beyond its primary site. Once melanoma is advanced, surgery is no longer sufficient and the disease becomes more challenging to treat. Treatment options for late-stage melanomas include kinase inhibitors and immunotherapies. Vemurafenib is an approved BRAF inhibitor [117,118] and trametinib, an selective inhibitor for MEK1/2 [119]. Furthermore, pimasertib and binimetinib (MEK162) have been reported to be promising in patients with NRAS mutations [120]. Immunotherapies use checkpoint inhibitor antibodies against cytotoxic T-lymphocyte antigen-4 (CTLA-4) like ipilimumab [121] and/or programmed cell death protein (PD-1) [122,123]. However, monotherapy is unlikely to bring a long-term benefit due to drug resistance. Therefore, drug combinations with different targeted and immunotherapies as well as standard chemotherapeutics are the best option to overcome resistance and obtain long-term response [124–127]. For example, co-targeting the MAPK and PI3K/AKT signaling pathways, or the MAPK and p53 pathways, might be options [107].

1.5.5 Role of ABCB5 in drug resistance

Although there are some promising targeted therapies against metastatic melanoma such as the BRAF kinase inhibitor vemurafenib [117], melanomas constantly become resistant to these agents [128]. In addition to general mechanisms of resistance that are found in various cancers, including downregulation of drug uptake mechanisms, altered drug metabolism, and increased repair or cellular tolerance [129], melanomas exhibit specific features [130]. For example, it was shown that the melanogenesis-associated vesicles, the melanosomes, are involved in trapping and export of drugs [131]. Furthermore, melanoma cells express ATP-binding cassette (ABC) transporters, in particular of type ABCB5, which are related to multidrug resistance by decreasing the accumulation of cytotoxic drugs inside the cells [132]. ABCB5 was found to mediate resistance to the chemotherapeutics doxorubicin and temozolomide [130,133]. Although it is also present in several human tissues [134,135], ABCB5 is highly abundant in melanocyte progenitors, melanoma cell lines, and melanoma biopsies [133,136–139]. ABCB5-expressing cells in melanoma have the ability to self-renew, differentiate and become tumorigenic [130,140]. Furthermore, expression of ABCB5 correlates with tumor progression and metastasis competence [140]. Schatton and colleagues showed that the growth of melanoma xenografts in mice was delayed when treated with a monoclonal anti-ABCB5 antibody [140].

1.6 Current 3D *in vitro* test systems for skin and melanoma

The skin plays a central role in human health and physiology. Therefore, it is a principal organ of the human body. In order to find novel drugs and treatments in pharmacological and biomedical research, it is necessary to develop appropriate test systems. In both cases, animal models are not the first choice. The most common species used in animal models are rodents. However, their skin composition is too different to human skin to be comparable. Other animals with more human-like skin, such as pigs, are difficult to handle and too expensive for regular application. Furthermore, ethical reasons exclude them as well. Taken together, animal models turn out to be less and less attractive for skin and melanoma research [38]. Nonetheless, also 2D skin and melanoma cell cultures that have been used since decades are physiologically irrelevant. Most principal functions of skin, like barrier function, resilience, cell sheeting, cell layering, developmental profiles, immune function, blood perfusion, and innervation, cannot be addressed in simple 2D cultures [38]. In addition, melanoma cells do not grow in isolation rather interacting with their stroma and other cell types such as endothelial cells, fibroblasts, and immune cells [141]. Therefore, 3D cell cultures present a reasonable compromise between ease of use and predictability. Several 3D cell culture models have been developed to study skin and melanoma *in vitro*: spheroids, hydrogel systems, 3D bioprinting, and organ-on-a-chip.

1.6.1 Spheroids

The spheroid technology and its use in oncology came into existence, when Halpern and colleagues observed that malignant cells are more likely to form aggregates than normal cells when cultured in an Erlenmeyer on a shaker [142]. The team around Sutherland titled their Chinese hamster V79 lung cell aggregates "multicellular spheroids" and added a description of the three typical zones found in the majority of these 3D spherical cultures, i.e. an inner necrotic core, an intermediate zone of quiescent cells as well as an outer stratum of proliferating cells [143]. Spheroids are primarily formed by the Hanging Drop method [17] or by the use of non-adherent U-bottom shaped plates [144]. Sometimes, the addition of coatings is essential for the formation of spheroids. For example, melanocytes need the addition of chitosan [145]. Recently, new technologies have been developed and are now commercially available that force aggregation via magnetized cells [146]. However, spheroids are not the classical model for 3D cultivation of skin cells. They are more suitable when addressing

cancer, such as melanoma. 3D melanoma spheroids embedded in a collagen matrix closely resemble the *in vivo* tumor structure and microenvironment [147,148]. It mirrors the heterogeneity of a tumor with oxygen/nutrient gradients, a hypoxic area, and a necrotic core, and lets melanoma cells interact with their stroma. For example, it was found that ERK is homogeneous in 2D cell cultures and can be totally inhibited by treatment with small-molecule inhibitors of the MAPK pathway [149], whereas in 3D spheroids, ERK-activity is restricted to the periphery, which is similar to the *in vivo* situation [150]. This indicates the heterogeneous expression of signaling molecules inside a tumor and, thus, its implications for cancer therapies [141]. Okochi and colleagues used the spheroid technique to investigate the interaction of fibroblasts on the invasion of melanoma. In order to generate a co-culture spheroid, they magnetically labelled fibroblasts and melanoma cells [146]. Another melanoma model used a bioreactor system to produce HaCaT spheroids as a scaffold for melanoma cells [151]. Peura et al. highlight the importance of paracrine factors released by fibroblast spheroids to produce an active matrix [152]. Nevertheless, none of these publications describes a skin spheroid model with the typical stratification pattern observed in the epidermal layer of the skin. First promising attempts have been reported, describing a spherical microtissue that contains different keratinocyte sheets and a dermal fibroblast core producing extracellular matrix proteins so that no exogenous collagen is required [153]. Due to their simplicity, low cost, and high reproducibility, spheroids are very interesting 3D models, even for skin research (table 2). They could be used for high-throughput cell function and cytotoxicity analysis [38,154]. Most spheroids can be disassembled by lysis buffer or enzymes, allowing them for biochemical analysis [155]. Imaging of whole mount spheroids can be performed by confocal microscopy [156] or light-sheet microscopy [157], whereas conventional microscopy requires sectioning of spheroids prior imaging [158].

1.6.2 Hydrogel systems

Besides spheroids as the easiest 3D cell culture method, the most dominant system to create an *in vitro* skin model is the use of hydrogels. Hydrogels function as a scaffold for dermal fibroblasts, which are then co-cultured with keratinocytes on top. Typically, hydrogels are made of collagen I, the leading class of ECM protein, and usually dermal fibroblast cells are embedded in the collagen gel mimicking the dermal layer of the skin [159,160]. Bell and colleagues were the first to describe a hydrogel system containing

epidermal cells on top of a primary rat fibroblast-seeded collagen matrix [161]. However, there are also other ECM-related proteins that can be used for the generation of hydrogels. For instance, Alameda et al. created a 3D model comprising HaCaT keratinocytes and fibroblasts in fibrin gels to achieve a human skin equivalent that includes both, a dermal and epidermal compartment. This resembled the structure and stratification found in normal human skin [162]. Apart from that, there are numerous commercially available skin models based on hydrogels, such as EpiDerm (MatTek, Ashland, MA, USA), Episkin (L´Oreal; SkinEthic, Nice, France), Apligraf (Organogenesis Inc., Canton, MA, USA), and Labskin (Innovenn, Dublin, Ireland). Taken together, hydrogels are a good technique to assemble the dermal stratum and the stratified layers of the epidermis. Moreover, complete stratification of keratinocytes, including cornification, can be achieved by special protocols of air exposure [163,164] or combination of high Ca^{2+} and low temperature [49]. The principal advantage of hydrogel systems is their high level of differentiation. This makes it a good approach to study effects on specific epidermal layers [38]. The most common used cell types are primary human dermal fibroblasts and primary keratinocytes [159,165]. However, also keratinocyte cell lines, like HaCaT cells, are used [163]. For example, Zanoni and co-workers investigated the cytotoxicity of different chemicals, such as hair dyes on a hydrogel-based skin system using HaCaT keratinocytes [160]. In order to study diseases of the skin, such as psoriasis, simple models are on the market (MatTek Corp., Ashland, MA, USA), comprising healthy keratinocytes and diseased fibroblasts isolated from psoriatic lesions of patients. Still, the use of psoriatic epidermal keratinocytes is more appropriate to mirror the psoriatic situation [166]. Furthermore, it is possible to assemble a human skin equivalent including all three major skin layers, even the subcutis, with human adipose derived stem cells and adipocytes [167]. To address melanoma, melanocytes and/or melanoma cells can be added [168]. Melanoma cells from different stages of progression share similar properties in human skin reconstructs as in the skin of a patient. For example, cells derived from melanoma *in situ* (RGP) do not invade the dermis, whereas advanced primary VGP and metastatic melanoma cells are able to invade the dermal compartment in such a model [90,169,170]. Meier and colleagues used the reconstruction of melanoma in an organotypic human skin culture technique to show that combinations of MAPK and AKT inhibitors totally suppressed invasive tumor growth of melanoma cells [171]. Since melanoma, psoriasis, and other skin diseases involve cross-talk between different cell types and cytokines,

the addition of immune cells to the 3D skin model is very helpful [38]. The first 3D skin equivalent including different T-cell populations was described by van den Bogaard et al. It was used to study the migration of immune cells and the secretion of proinflammatory cytokines in psoriasis [172]. However, this system lacked hyperproliferation and the cytokine levels were much lower compared to the *in vivo* condition, suggesting that there are still components and cell types missing to create an accurate model of psoriasis [38].

While 3D *in vitro* hydrogel systems are mainly used to study epidermal behavior, biology of melanoma, and drug response of melanoma cells at early stages [141], spheroid models can be used for high-throughput assays to evaluate proliferation, invasion, and drug response of distant metastatic melanoma [141]. As summarized in table 2, the major advantage of 3D *in vitro* hydrogel systems is their defined biomimetic properties. Their site of cell adhesion can be adjusted by the use of peptides like RGD or IKVAV [173,174]. Additionally, the cell-degradability, the stiffness of the gels as well as the material of the gels itself can be varied (e.g. collagen, fibrin, gelatin) [38,162,175,176]. Since the hydrogel systems allow the cells to recover from the gels by proteases, they are also applicable for molecular analysis like Western Blot and Polymerase Chain Reaction (PCR) [165,168]. Due to their transparency, they can be imaged by microscopy [163]. Regarding costs, hydrogels are in a moderate range. They are much cheaper than microfluidic devices but more expensive than simple spheroid systems [38]. Even though their handling is easy, they need a constant monitoring throughout the whole culture time of up to 21 days or even longer [155,177,178]. Since the hydrogels involve biological components, the gels might have a high batch-to-batch variability which makes it difficult to reproduce the same results [38] (table 2).

1.6.3 3D bioprinting

Using the 3D bioprinting technique, complex tissue structures can be generated automatically [179]. Therefore, different layers of a desired material, which is in most cases a hydrogel or biodegradable matrix, are printed creating such arrangements. Afterwards, cells or biomolecules are added in a defined way to form the desired biological structure [180]. In 1986, Charles W. Hull presented the stereolithography method, where he combined thin layers of certain materials with UV light [181]. Then, the method was further improved leading to methods like the laser printing [182] and ink printing [183]. Later, soft lithographic methods have been developed. This technique uses

stamps to form cell-containing sheets and stacks these layers to create a 3D shape [184,185]. However, these approaches are often associated with complex manufacturing processes to ensure precise positioning of the cell-containing layers [38]. Since 3D bioprinting is able to produce 3D structures in an on-demand fashion, it was used to manufacture diverse biomimetic architectures, such as fluidic channels [186], vascular-like structures [187], growth-factor releasing matrices [188], neural tissues [189], and cancer cell-holding tissues as a model for angiogenesis [190]. Regarding bioprinted skin, complex skin tissues were generated comprising dermal and epidermal layers made of keratinocytes, melanocytes, and fibroblasts [179,191–193]. However, so far, there is no attempt to emulate a more complete 3D bioprinted skin including subcutis or disease models such as melanoma. Using 3D bioprinting, Lee et al. generated a human skin that is biologically and morphologically representative of human skin tissue *in vivo*. It comprises keratinocytes and fibroblasts resembling epidermis and dermis, and collagen resembling the dermal matrix [179]. Koch and colleagues used the laser-assisted bioprinting to embed keratinocytes and fibroblasts in collagen. Then, they evaluated the influence of the printing procedure on the cellular proliferation, survival rate, and apoptotic activity. All cells maintained their proliferation ability, were able to differentiate, and formed functional gap and adherent junctions [192].

Current 3D bioprinting techniques are mostly automated, hence they provide a good reproducibility and allow for high-throughput (table 2). 3D bioprinting is a highly flexible method, since the scaffold as well as the cell types and active molecules can be varied on demand. Therefore, this system is potentially applicable in tissue engineering, cytotoxicity assays, and pathophysiology of skin diseases [38,179]. Moreover, bioprinted tissue can be further analysed by biochemical methods and imaged by fluorescence microscopy [179,194]. However, 3D bioprinting is a cost-intensive, complex method (table 2). Consequently, it is only available in a few laboratories.

1.6.4 Organ-on-a-chip

The term organ-on-a-chip stands for cell culture devices for the cultivation of living cells under continuous perfusion to simulate tissue and organ physiology with high spatiotemporal control [195,196]. These aim to create minimal functional units of tissue and organs rather than forming a completely living organ. The easiest system consists of only one cell type presenting functions of one tissue and is perfused in a single microfluidic chamber [38]. More complex approaches exhibit two or more microfluidic

chambers containing different cell types. They are connected by porous membranes mimicking the borders between different tissues [196]. Microfluidic devices usually rely on soft lithography, a complementary extension of photolithography. Replicating patterns are etched into silicon chips in more biocompatible and flexible materials. A liquid polymer like polydimethylsiloxane (PDMS) is poured on an etched silicon substrate. After its polymerization, it is an optically clear, rubber-like material serving as a stamp [197]. Most microfluidic chips are perfused with a pumping system [198], but some are pumpless using a rocking platform [199]. Compared to the other 3D *in vitro* systems, microfluidic devices are the best option to emulate skin physiology and functionality. Perfusion produces shear stress increasing cell viability and proliferation which is not achieved in static cultures [200]. Furthermore, almost all systems are able to cultivate with an air-liquid interface [200]. Depending on the application, either cell lines, primary cells, or skin biopsies are used [198,200,201]. An additional source of cells are presented by human induced pluripotent stem cells. As they have the ability to differentiate into keratinocytes [202], fibroblasts [203], melanocytes [204], and endothelial cells [199], human induced pluripotent stem cells can be used in healthy and diseased skin models. Simple skin models include epidermis and dermis, but there are also more complex models with hair follicles and adipocytes [22], immune cells [205], and structures similar to sweat gland pores [206]. Additionally, skin-on-a-chip can be combined with other tissues to study drug metabolism. For that reason, Maschmeyer et al. and Wagner et al. created two and four organ chips with intestine, liver, skin, and kidney [207–209]. Besides, skin disease models such as inflammation and edema are present [210]. The integration of microfluidics in 3D tumor environment may provide a powerful platform for the precise and fast monitoring of the response of cancer cells to drugs [211]. Furthermore, the small amounts that are needed in such systems make it a cost-effective tool for drug screening applications [211]. Mori and co-workers used a perfusable skin equivalent model with vascular channels composed of endothelial cells to evaluate the amount of drug absorbed by the vascular channels [212]. Pandya and colleagues used mouse melanoma cells in a microfluidic platform for drug screening [213]. In addition, Mattei and co-workers co-cultivated mouse melanoma cells and immune cells to explore their cross-talk [214].

One of the major advantages of microfluidic chips is the physiological flow of medium allowing a constant oxygen and nutrient supply. This has an effect on cell-cell interactions and local concentrations of secreted ligands of tissues [215]. Combining skin

with the organ equivalents of intestine, liver, and kidney, an *in vitro* ADME (absorption, distribution, metabolism and excretion) profiling is possible [209]. Molecular analysis, like PCR, can be performed [210], and, since the chips are typically made of PDMS, microscopy is feasible [208]. However, the great disadvantage of PDMS is that it absorbs small molecules such as drugs [216]. The central constraints of microfluidic devices are the high costs and the expertise needed for the complex assembly of such systems [38] (table 2). Another fact is that arising air bubbles within the system can harm biological function and viability [217,218].

Table 2: Advantages and disadvantages of different 3D *in vitro* test systems

System	Advantages	Disadvantages
Spheroids	Ease of use Low costs High reproducibility Allow for high-throughput screening	Simplified architecture
Hydrogel systems	Ease of use Defined biomimetic properties Applicable to microplates High reproducibility Allow for high-throughput and high-content screening	Simplified architecture Constant monitoring required High batch-to-batch variability
3D bioprinting	High reproducibility Custom-made architecture Allow for high-throughput screening	High costs Complex method Difficult to be adapted to high-throughput and high-content screening
Organ-on-a-chip	*In vivo* like architecture	High costs Complex assembly

1.7 Aims of the project

Melanoma is the most common form of cancer [107]. Thus, test systems resembling the *in vivo* situation are required for the development of new drugs and therapies. Several 3D cell culture approaches have been developed to test drugs and perform mechanistic studies on melanoma. They all exhibit varying degrees of complexity [211]. Although 3D cultures are superior to traditional 2D approaches, these cultures are either composed of only one cell type, the melanoma cells, or they are so complex that it is difficult to study the behavior of a single cell type. Moreover, they are hard to establish and expensive.

Therefore, the aim of this project was to establish a novel, simple, spheroid-based melanoma model composed of human fibroblasts, keratinocytes, and melanoma cells. Furthermore, this study aimed to characterize the melanoma tri-culture model in a cell-type specific way and to study the effect of the cytostatic drug, docetaxel, on this system. In order to avoid batch-to-batch variability and achieve a cost effective system, the established cell lines CCD-1137Sk fibroblasts, HaCaT keratinocytes, and SK-MEL-28 melanoma cells were used. To identify general features for 3D cultivation of normal and neoplastic cells, the prostate cancer cell lines LNCaP and PC-3 were used in addition. In order to study differences in culture conditions and behavior of these cell lines, they were cultivated in 2D and compared to 3D cultures. Furthermore, their proliferation and apoptosis potential was examined.

The established 3D melanoma model might now be complemented by the addition of further cell types like immune cells or, to address personalized medicine, primary cells. Moreover, this model might be applied to screen new drugs and analyze their mode of action in a cell-type specific manner.

2 MATERIAL AND METHODS

2.1 Cell Culture

The human fibroblast cell line CCD-1137Sk (ATCC® CRL-2703™) was cultured in Iscove's Modified Dulbecco's Medium (IMDM), with L-Glutamine, supplemented with 10 % fetal bovine serum (Sigma), and 1 % Penicillin Streptomycin (Capricorn). HaCaT cells (immortal human keratinocytes, order no. 300493) and SK-MEL-28 cells (human malignant melanoma cell line, order no. 300337), both from Cell Line Service (CLS) GmbH (Heidelberg/Germany), were cultured in Dulbecco's Modified Eagle Medium (DMEM) High Glucose (4.5 g/l), with L-Glutamine, with Sodium Pyruvate (Capricorn) supplemented with 10 % fetal bovine serum, and 1 % Penicillin Streptomycin. LNCaP (ECACC Catalogue no. 89110211) and PC-3 (DSMZ order no. ACC 465), human prostate carcinoma cell lines, were cultured in RPMI 1640 Medium, with L-Glutamine (Capricorn), supplemented with 10 % fetal bovine serum, and 1 % Penicillin Streptomycin. All cells were maintained under standard conditions at 37 °C in 5 % CO_2. 0.05 % Trypsin EDTA in DPBS (1x) (Capricorn) was used to detach the cells. Mycoplasma tests using the MycoAlert™ Mycoplasma Detection Kit (Lonza) were routinely performed to ensure mycoplasma-free cell cultures. Thawing of cells was performed rapidly in a 37 °C water bath. Then, thawed cells were diluted in pre-warmed growth medium and centrifuged for 6 min at 800 rpm. Afterwards, the cell pellet was resuspended in fresh growth medium and plated in a T75-flask. In order to freeze cells, they were detached from the tissue culture plates by trypsinization and counted using a VI-CELL XR cell counter (Beckman Coulter) (1 x 10^6 cells/cryovial). Required volume of cell suspension was centrifuged at 800 rpm for 6 min and cell pellet was resuspended in appropriate amount of cold freezing medium containing 20 % fetal bovine serum and 10 % dimethylsulfoxide (DMSO). Aliquots of the cell suspension were dispensed into cryovials, placed in an isopropanol chamber and stored at -80 °C overnight. Next day, frozen cells were transferred to liquid nitrogen.

2.2 3D spheroid cultures and docetaxel treatment

Spheroids were plated using 96- and 384-well cell-repellent plates from Greiner. For mono-culture spheroids, fibroblasts (10,000 cells/well), HaCaT cells (20,000 cells/well), SK-MEL-28 cells (5,000 cells/well), LNCaP cells (1,000 cells/well) and PC-3

cells (5,000 cells/well) were seeded. For skin bi-cultures, 10,000 cells of each, fibroblasts and keratinocytes, were used per well, whereas HaCaT cells were added three days after formation of the fibroblast core. Mono- and bi-cultures were cultured for 7 or 14 days as indicated. For tri-culture spheroids, fibroblasts (10,000 cells/well) were seeded. After three days, HaCaT (10,000 cells/well) and SK-MEL-28 cells (2,500 cells/well) were added simultaneously. Spheroid formation was facilitated by centrifugation of the plates for 4 min at 500 rpm after each seeding step. To distinguish between the different cell lines, CellTracker Fluorescent Probes (Life Technologies) were applied. Before adding cells to the 3D co-culture, HaCaT cells were labeled with CellTracker Red CMPTX dye (Life Technologies, C34552) and SK-MEL-28 cells were labeled with CellTracker Green CMFDA (Life Technologies, C2925), each for a time period of 45 min according to the CellTracker manuals. Another two days later, tri-culture spheroids were treated with 100 nM docetaxel or 0.01 ‰ of DMSO as control for 15, 24, 48, and 72 h, respectively. Stock solutions (10 mM) of docetaxel (Sigma) were prepared in DMSO. After treatments, spheroids were normally fixed and immunostained as described below. For some experiments, tri-culture spheroids were transferred to 3D agarose molds (Sigma, Z764051) on day five after seeding in cell-repellent plates. Treatment with DMSO or 100 nM docetaxel for 72 h, as well as fixation and cryosectioning were then carried out in the molds.

2.3   3D cultures using a microchip-based bioreactor system

2.3.1   Chip design and manufacturing

For microfluidic 3D cultivation of cells, Dynarrays were used (Dynarrays© MCA-C300-300-PC, 300MICRONS). They are made of polycarbonate and contain microcavities with 300 µm diameter and 300 µm in depth. For perfusion of the chips, they possess pore sizes from a few nanometers to several micrometers. The chip is made by a microthermoforming technique, the so-called SMART (substrate modification and replication by thermoforming) process, developed by 300MICRONS [219–221]. Briefly, thin polymer films with a thickness of only 50 µm are heated and pressed into a mold by applying appropriate pressure. Prior to microthermoforming, surface modifications onto the planar polymer film can be introduced leading to a translation of the surface modification from the planar state into the third dimension after thermoforming. In a post-process step, pores can be introduced into the polymer film leading to highly porous microcavities.

2.3.2 Bioreactor setup

The bioreactor for the housing of the Dynarrays can support perfusion as well as superfusion flow schemes (figure 9 A, C and D). When the superfusion mode is applied, the fluid flows in parallel to the surface of the tissue, leading to the supply of nutrients and gases in the depth of microcavities by diffusion over both, the top and bottom surfaces of the chip (figure 9 D). In contrast, in the perfusion mode, the medium is flowing vertically to the surface of the tissue, i.e. through the porous bottom of the chip and the tissue of each microcavity (figure 9 C) [222]. All experimental data presented in this work were generated by applying the superfusion flow regime at 130 µL/min.
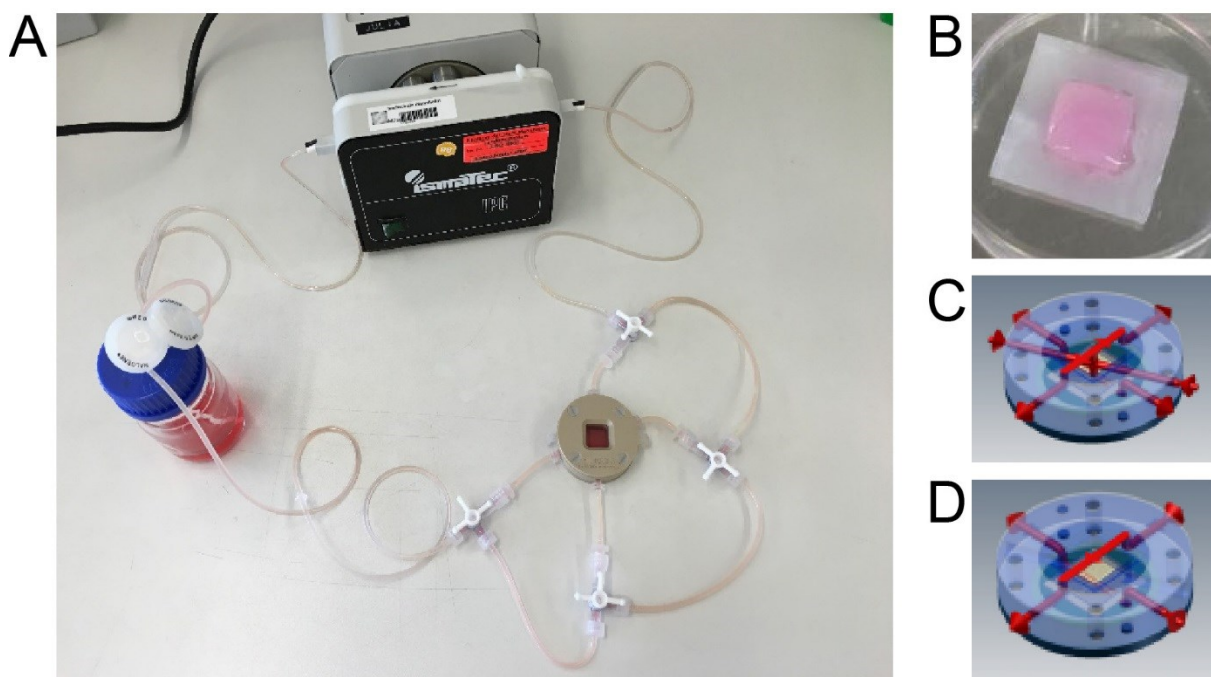

Figure 9: 300MICRONS Dynarray and bioreactor setup. Closed circulation loop of the bioreactor setup with bioreactor housing, medium reservoir, and pump (**A**). After cell seeding (**B**), the Dynarray is transferred into the bioreactor and cultivated with either the perfusion mode (**C**), or the superfusion flow scheme (**D**). *Adapted and modified from Wuchter et al 2016.*

2.3.3 3D chip culture

Prior to cell seeding, the air in the cavities of the chip was removed to ensure complete wetting of the microstructured surface area by applying a descending series of isopropanol/water. Since the micro-chips are made of polycarbonate, the microstructured area of the chips was coated with 30 µg collagen from rat tail tendon (Roche, #11179179001, stock solution 1 mg/mL) overnight at 4 °C to improve initial cell adhesion inside the cavities. Inoculation of the chips was achieved by pipetting

6 x 10^6 HaCaT cells or 3 x 10^6 SK-MEL-28 cells/150 µL culture medium onto the microstructured area of the chip, followed by 5 h incubation at 37 °C in an incubator to allow cell adhesion (figure 9 B). Afterwards, inoculated chips were transferred into the bioreactor and cultivated with superfusion for 7 or 9 days, respectively.

2.4 Sectioning and immunofluorescence staining

Immunostaining of spheroids used the following steps. After cultivation time, spheroids were collected in an Eppendorf tube, washed once with PBS (137 mM NaCl, 2.7 mM KCl, 10 mM Na$_2$HPO$_4$ x 2 H$_2$O, 2 mM KH$_2$PO$_4$, pH 7.4), and fixed with 4 % wt/vol paraformaldehyde in PBS at room temperature for 30 min. Next, spheroids were incubated overnight at 4 °C in 15 % sucrose (Roth, 4621.1) in PBS, followed by an incubation overnight at 4 °C in 25 % sucrose in PBS, before they were embedded in OCT (Leica). For preparing 10 µm thick sections, a CM-1950 cryostat (Leica Biosystems, Nussloch, Germany) was used. 3D molds were washed once with PBS and fixed with 4 % wt/vol paraformaldehyde in PBS at room temperature for 30 min. Then, molds were embedded in OCT and cut with the cryostat into 20 µm thick sections. All sections were permeabilized with 0.1 % Triton X-100 (Roth, 3051.4) in PBS, blocked with 3 % BSA (Roth, 8076.3) in PBS, and stained with rabbit anti-ki67 (Merck, AB9260), rabbit anti-cleaved caspase 3 (Cell Signaling, 9661), rabbit anti-cytokeratin 10 (Thermo Fisher Scientific, PA5-32459), rabbit anti-collagen IV (Rockland, 600-401-106S), mouse anti-cytokeratin 14 (Merck, MAB3232), or mouse anti-ABCB5 (3C2-1D12 and Thermo Fisher Scientific, MA5-17026) antibodies, followed by goat anti-rabbit Alexa Fluor 647 (Invitrogen, A21246), goat anti-mouse Alexa Fluor 555 (Invitrogen, A21424), or donkey anti-mouse Alexa Fluor 647 (Invitrogen, A31571) secondary antibody labeling. The corresponding dilutions of antibodies are outlined in table 3. Nuclei were stained with Dapi (Sigma, 10236276001; 1:1,000 dilution). As a final point, sections were washed with PBS and mounted with Mowiol (Roth, 0713.2) for confocal microscopy (SP8, Leica). Immunostaining of Dynarrays used the following steps. Dynarrays were washed once with PBS, and fixed with 4 % wt/vol paraformaldehyde in PBS at room temperature for 30 min. Then, they were washed 3 times for 10 min with PBS and embedded in 2 % agarose. For preparing 30 µm thick sections, a vibratome (Leica VT1000S) was used. At first, sections were washed at least 3 times (PBS, 0.5 % Triton X-100) and afterwards quenched with quenching buffer (PBS, 0.5 % Triton X-100, 20 % DMSO, 0.3 M

glycine) for 2 hours. Next, samples were permeabilized and blocked (PBS, PTwH (0.5 %Tween-20 with 10 µg/mL heparin in PBS), 0.5 % Triton X-100, 10 % DMSO, 6 % bovine serum albumin) overnight at 4 °C and then stained with rabbit anti-ki67, rabbit anti-cleaved caspase 3, rabbit anti-cytokeratin 10 or mouse anti-cytokeratin 14 followed by donkey anti-rabbit Alexa Fluor 488 (Invitrogen, A21206) or goat anti-mouse Alexa Fluor 555 secondary antibody labeling (table 3). Nuclei were stained with Draq5 (Thermo Fisher Scientific, 62251; 1:1,000 dilution). Slices were washed carefully, placed on a glass slide and embedded in Mowiol for confocal microscopy. Images were taken with an inverted Leica SP8 (Leica Microsystems CMS, Mannheim, Germany) confocal microscope equipped with a HC PL APO 20x /0.75 IMM CORR objective.

Table 3: Antibodies and their dilutions used for immunofluorescence (IF) and Western Blot (WB) analysis

Antibody	host, company, number	Dilution
anti-ki67	rabbit polyclonal, Merck, #AB9260	IF: 1:500
anti-cleaved caspase 3	rabbit polyclonal, Cell Signaling, #9661	IF/WB: 1:500
anti-cytokeratin 10	rabbit polyclonal, Thermo Fisher Scientific, #PA5-32459	IF/WB: 1:500
anti-collagen IV	rabbit polyclonal, Rockland, #600-401-106S	IF: 1:50
anti-cytokeratin 14	mouse monoclonal, Merck, #MAB3232	IF/WB: 1:500
anti-ABCB5	3C2-1D12	IF: 1:50
	mouse monoclonal, Thermo Fisher Scientific, #MA5-17026	IF: 1:200 WB: 1:500
anti-GAPDH	mouse monoclonal, Thermo Fisher Scientific, #MA5-15738	WB: 1:10,000
anti-PCNA	mouse monoclonal, Thermo Fisher Scientific, #13-3900	WB: 1:500
anti-rabbit-AF647	goat polyclonal, Invitrogen, #A21246	IF: 1:1,000
anti-rabbit-AF488	donkey polyclonal, Invitrogen, #A21206	IF: 1:1,000

anti-mouse-AF555	goat polyclonal, Invitrogen, #A21424	IF: 1:1,000
anti-mouse-AF647	donkey polyclonal, Invitrogen, #A31571	IF: 1:1,000
anti-rabbit-HRP	goat polyclonal, Dako, #P0448	WB: 1:3,000
anti-mouse-HRP	goat polyclonal, Thermo Fisher Scientific, #32430	WB: 1:3,000

2.5 *SDS PAGE* and Western Blotting

Cells grown in 2D cultures were harvested by trypsination. After centrifugation, the cell pellet was lysed with 100 µL lysis buffer (50 mM Tris-HCl (pH 7.5), 15 mM NaCl, 0.5 % NP-40, 50 mM NaF, 1 mM PMSF and Sigma Inhibitor Cocktail (1:100)) for 30 min on ice. Spheroids were washed once with PBS and then also lysed with 100 µL lysis buffer for 30 min on ice using a glass homogenizer. Afterwards, cells were centrifuged for 10 min at 10,000 g at 4 °C and the supernatant (=lysate) was stored at -20 °C. Protein concentration of respective lysates were colorimetric measured using BCA assay (Pierce™ BCA Protein Assay Kit, Thermo Fisher Scientific, #23225). For Western Blot, lysates containing an amount of 20 or 50 µg total protein in Laemmli buffer (200 mM Tris-HCl (pH 6.8), 40 vol % Glycerol, 8 vol % SDS, 0.01 vol % BPB, 100 mM β-mercaptoethanol) [223] were loaded on a 12 % polyacrylamide gel. Afterwards proteins were transferred to a PVDF membrane (Merck Millipore, #IPVH00010) using PerfectBlue® semi-dry electroblotter (Peqlab). Primary and secondary antibodies for detection of respective proteins and antibody dilutions are displayed in table 3. Bands were detected by using chemiluminescence analysis with G-Box Chemi XX6 (Syngene, Cambridge, UK).

2.6 Statistical analysis

Images were processed using ImageJ software (NIH, Bethesda, MD) and composed using Adobe Illustrator (Adobe Systems Software). All numeric data were handled using Microsoft Excel 2013 and were subsequently incorporated into the Adobe Illustrator composite. Quantitative analysis of ki67-, cleaved caspase 3-, and ck10-positive cells was performed using ImageJ. In brief, images were background subtracted and the channel containing Dapi or Draq5 was median filtered (kernel 1 x 1) and an appropriate threshold (pixel size of 10 to infinity) was set. Screening of Dapi or Draq5 signals yielded total amounts of nuclei structures, which were imported into a

ROI (region of interest) manager. Next, the segmented structures were screened in the ki67 and cleaved caspase 3 channel. Only those structures were considered, that showed a value higher than background plus two times standard deviation. For the case of ck10, only the peripheral nuclei were manually counted and colocalized ck10 stainings were counted as positive. For Western Blot analysis, densities of bands were quantified using the Gel Analysis plugin of ImageJ software. Relative values were then normalized to the housekeeping gene (GAPDH). Graphs are presented as mean ± S.E.M. or mean ± SD as indicated and statistically analyzed using one-way ANOVA with post-hoc Tukey HSD Calculator or Student`s t-test. P-values are indicated as *<0.05, **<0.01.

3 RESULTS

3.1 Spheroids of HaCaT keratinocytes and fibroblasts were shrinking in size over time

To study differences in culture conditions and behavior of normal and neoplastic cells, 3D cell cultures of different cell types were compared. For this purpose, stromal, skin, and cancer cells were used. In more detail, the fibroblast cell line CCD-1137Sk, HaCaT keratinocytes, SK-MEL-28 melanoma cells, as well as the prostate cancer cell lines LNCaP and PC-3, were grown as monoculture on cell-repellent plates to create 3D spheroids. In order to study their growth and stability, they were monitored over time. Cultivation of HaCaT keratinocytes on cell-repellent plates led to the formation of round spheroids (figure 10 A`). During seven days in 3D culture, their volume decreased from 1.4×10^8 µm^3 (day 1) to 2.7×10^7 µm^3 (day 7) (figure 10 A). The largest drop was visible in the first two days when the volume decreased by half. However, after seven days they were still forming round spheroids without dissociating. Similar to keratinocytes, also stromal fibroblast cells formed stable spheroids and those shrank in size over a period of 14 days (figure 10 B`). While on day 1, their volume was 2.7×10^7 µm^3, on day 14 it was only 8.2×10^6 µm^3 (figure 10 B). Within the first six days, their volume was reduced by half. Still, their shape was compact with a sharp boundary. Together, these results suggest that 3D cultivation of fibroblast and skin cells leads to compact round spheroids with decreasing sizes over time.
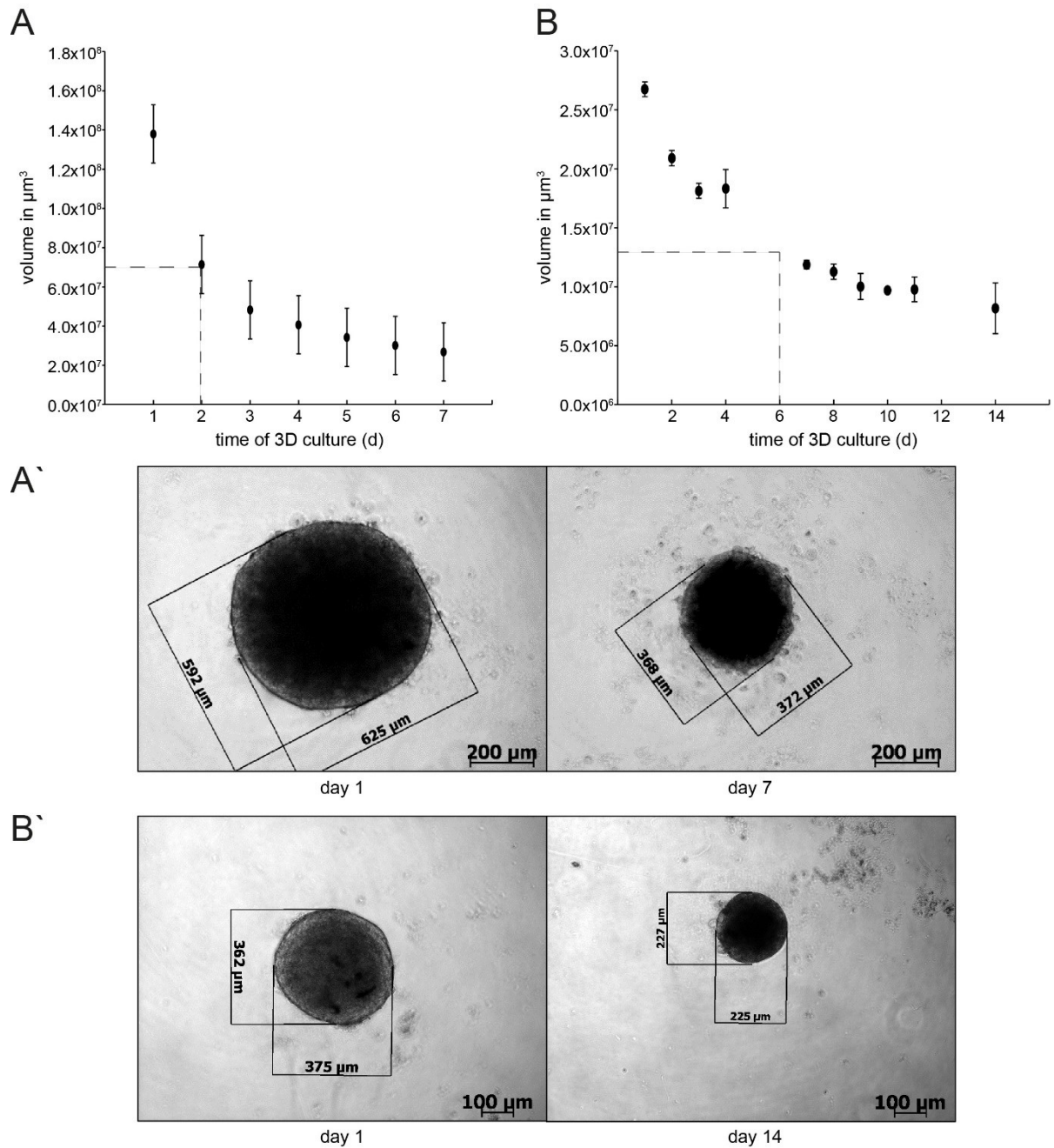
Figure 10: Spheroids of keratinocytes and fibroblasts were decreasing over time. HaCaT (**A and A`**) and fibroblast (**B and B`**) spheroids were cultivated on cell-repellent plates for 7 and 14 days, respectively. During this period, an exponential decrease in size was observed. Loss of volume by 50 % was observed after two and six days for keratinocytes and fibroblasts, respectively (dashed lines). The graphs show the volume of spheroids in μm^3 over time ± S.E.M. with n = 3 independent experiments. For each experiment and time point, 3 spheroids were measured.

## 3.2 Tumor spheroids were increasing in size over time

Previously, spheroids of cancer cells were found to increase in size over time [224]. To confirm this finding, 3D cultivation of SK-MEL-28 melanoma cells, and LNCaP and PC-3 prostate cancer cells was performed on cell-repellent plates to form spheroids.

Unlike SK-MEL-28 and LNCaP cells, PC-3 cells required the addition of 2.5 % Matrigel to create compact spheroids. Figure 11 displays an increase in spheroid volume for all three tumor cell lines over time. Since the melanoma spheroids were first becoming more compact, their volume was getting smaller at the beginning (figure 11 A). But then, these spheroids' volumes were continuously increasing from 1.2×10^8 µm^3 on day 4 to 1.8×10^8 µm^3 on day 7. The borders of the spheroid were not as sharp as those made from other cancer cells. Nevertheless, their structure was stable and they did not disaggregate during the time of cultivation (figure 11 A`). LNCaP spheroids were stable in size over seven days (figure 11 B). Even though this cell line formed compact spheroids with clear borders (figure 11 B`), they were not as round as SK-MEL-28 spheroids. The last cancer cell line, PC-3, was not able to make spheroids unless 2.5 % of Matrigel were added. Under these conditions, compact and round spheroids were obtained already after one day (figure 11 C) in culture. Here, the amount of their volume was 6.8×10^7 µm^3. The following days, the volume further increased to 4.6×10^8 µm^3 on day 7. Although they needed the addition of a basal membrane matrix, they aggregated to produce round compact spheroids (figure 11 C`). Altogether, these results suggest and thereby confirms previous studies that spheroids of cancer cells are increasing in size over time in 3D culture.
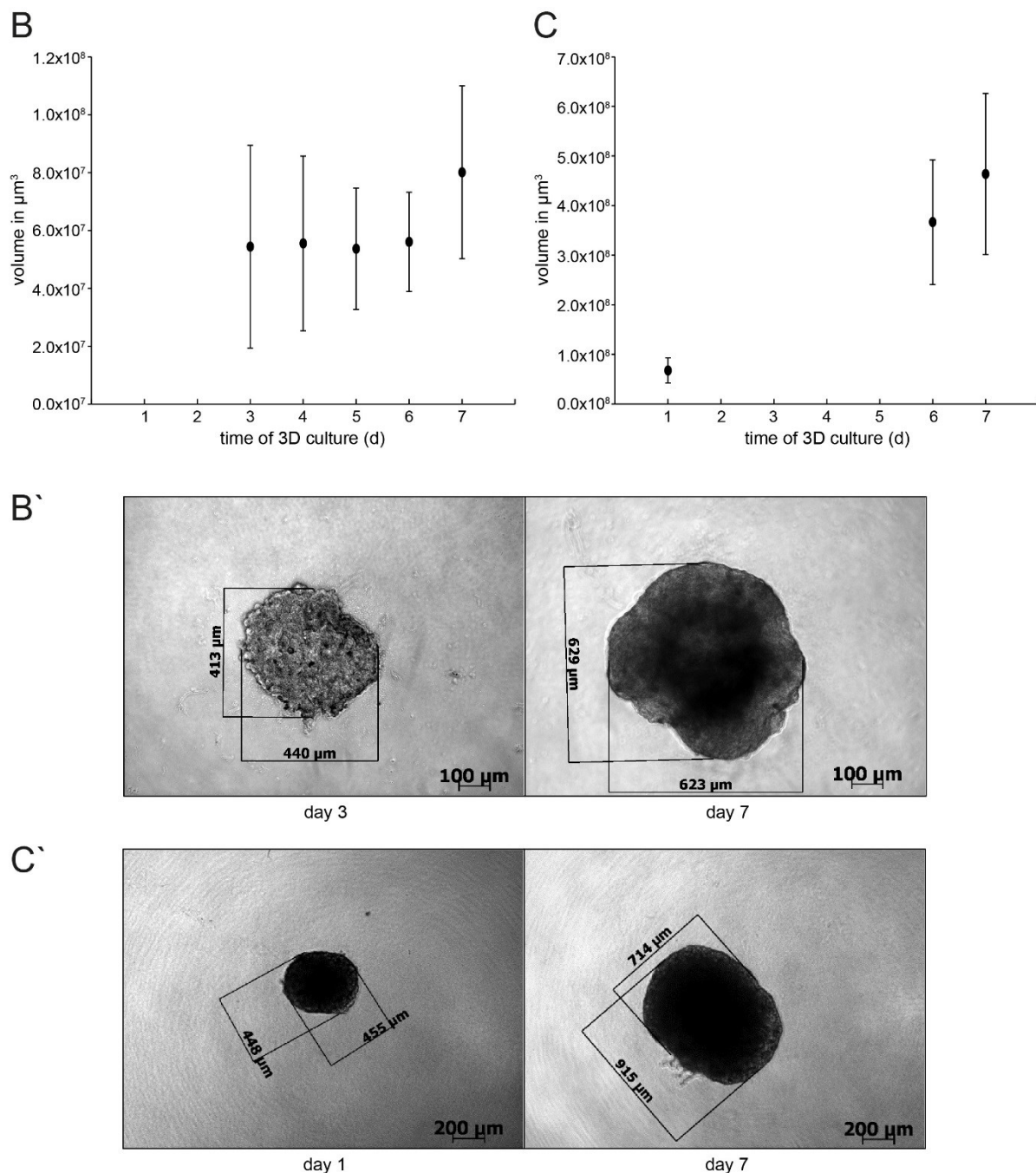
A

A`

day 1   day 7
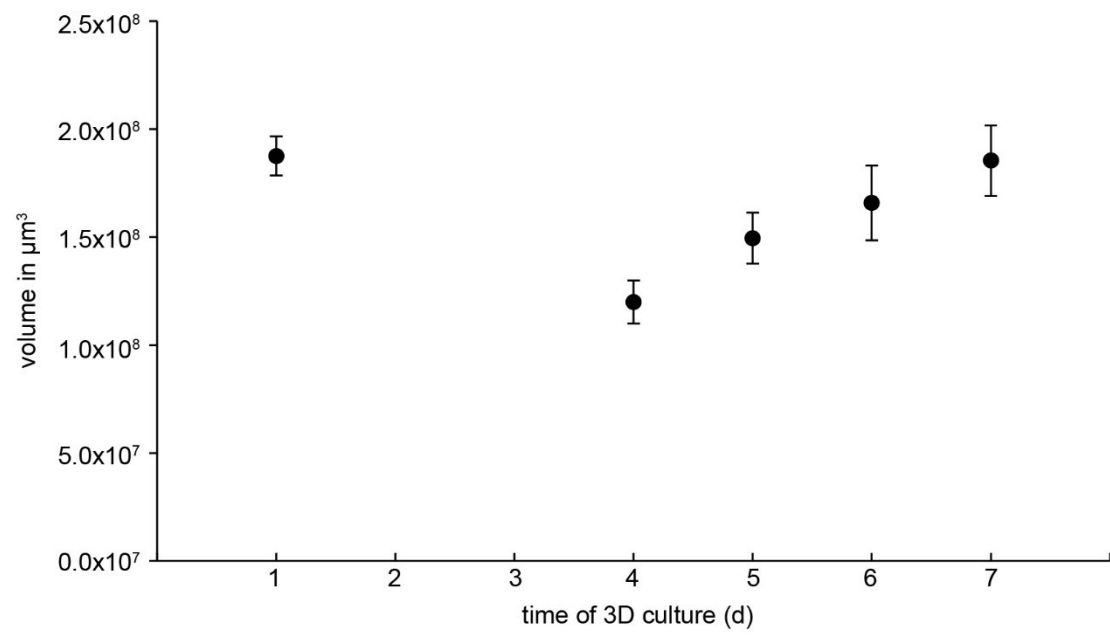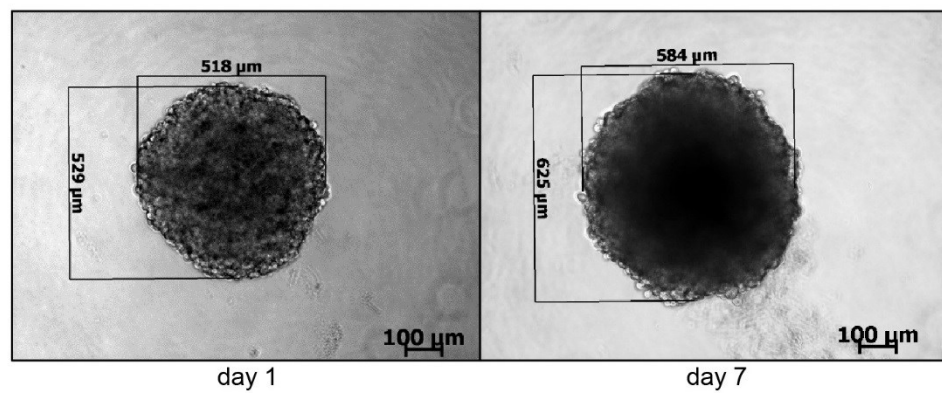
Figure 11: Spheroids of melanoma and prostate cancer cells were increasing over time. SK-MEL-28 (**A and A`**), LNCaP (**B and B`**), and PC-3 (**C and C`**) spheroids were cultivated on cell-repellent plates for 7 days. During this period, their size was rising. The graphs show the volume of spheroids in μm^3 over time ± S.E.M. with n = 3 independent experiments. For each experiment and time point, 3 spheroids were measured.

3.3 Proliferation of skin, melanoma, and prostate cancer cells was decreased when cultivated under 3D conditions

In order to analyze the effect of 3D cultivation on cell proliferation, HaCaT, SK-MEL-28, LNCaP, and PC-3 cells were grown in 2D and as spheroids. Additionally, HaCaT and

SK-MEL-28 cells were cultured on Dynarrays with superfusion. Cells were grown in 2D, as spheroids, and on Dynarrays. After seven days, spheroids and Dynarrays were fixed and sliced into 10 µm and 30 µm thick slices, respectively. Cell proliferation was analyzed by immunofluorescence for the proliferation marker ki67. When cultivated as 2D monolayers, HaCaT cells were highly proliferative with intense ki67 staining, while in spheroids as well as on Dynarrays, only few proliferating cells were observed at the periphery of the spheroids and at the bridges of the cavities on the Dynarrays (figure 12 A). The 3D cultivation of keratinocytes on Dynarrays generated only a few layers of cells, while in spheroids, HaCaT cells assembled numerous sheets of cells. Quantitative analysis revealed that 3D cultivation led to a significant decrease of the amount of proliferating ki67-positive cells with only 2.0 % ± 0.9 %, 6.1 % ± 1.7 %, and 74.7 % ± 17.5 % in spheroids, Dynarrays, and 2D culture, respectively (figure 12 B). Similarly, Western Blot analysis of HaCaT cells cultured in 2D as well as spheroids showed a significant decrease of the proliferation marker PCNA upon 3D cultivation (figure 12 C). Due to the insufficient quantity of proteins on Dynarrays, it was not possible to perform Western Blot analyses of HaCaT cells cultured on Dynarrays.
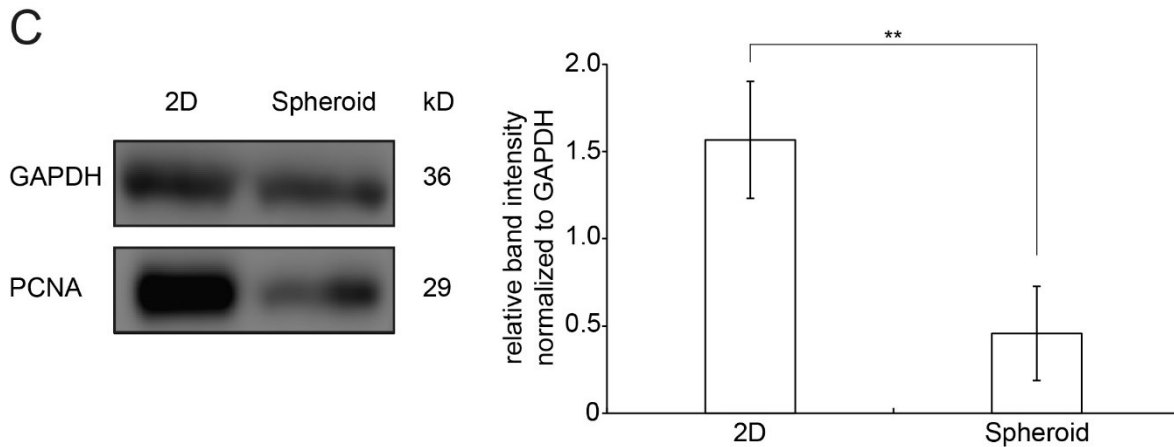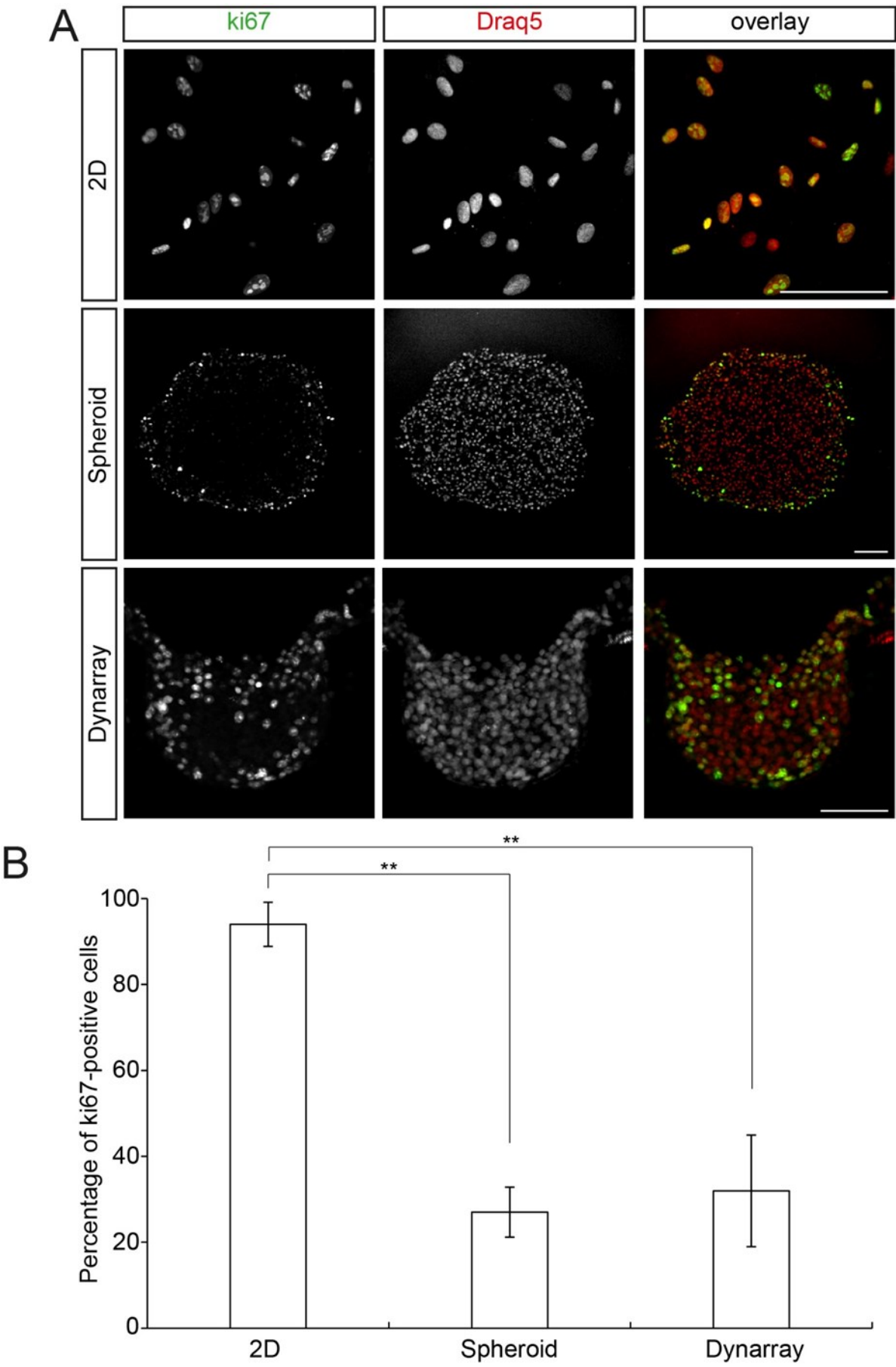
C
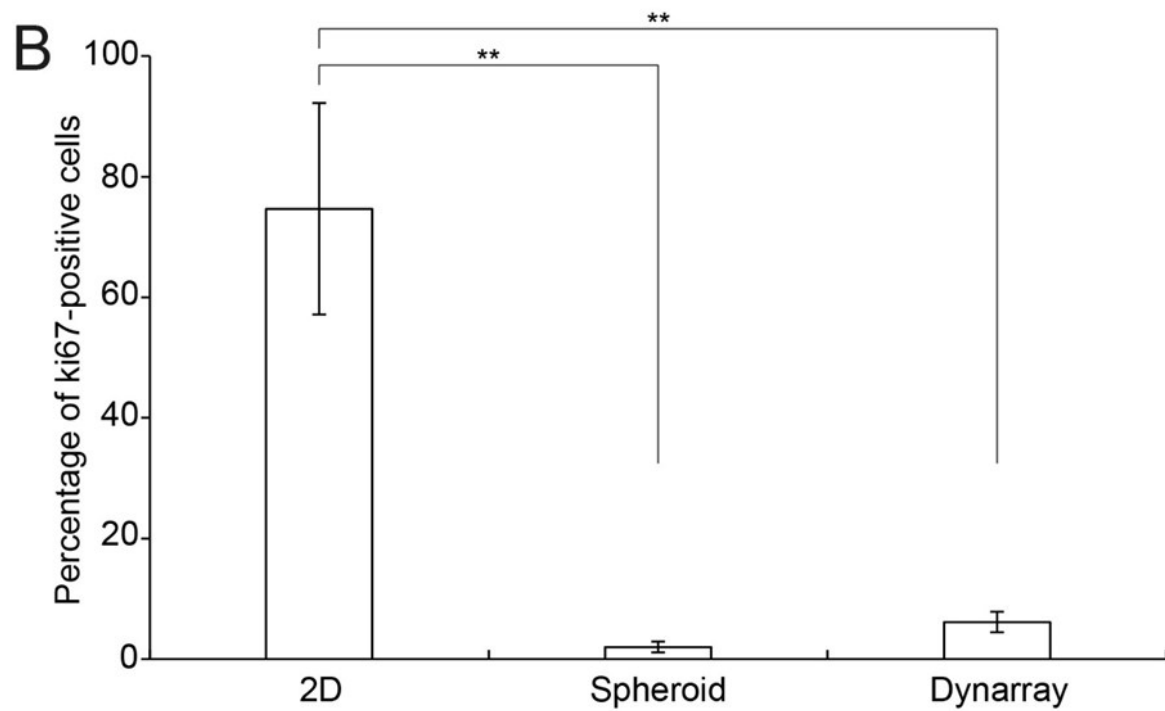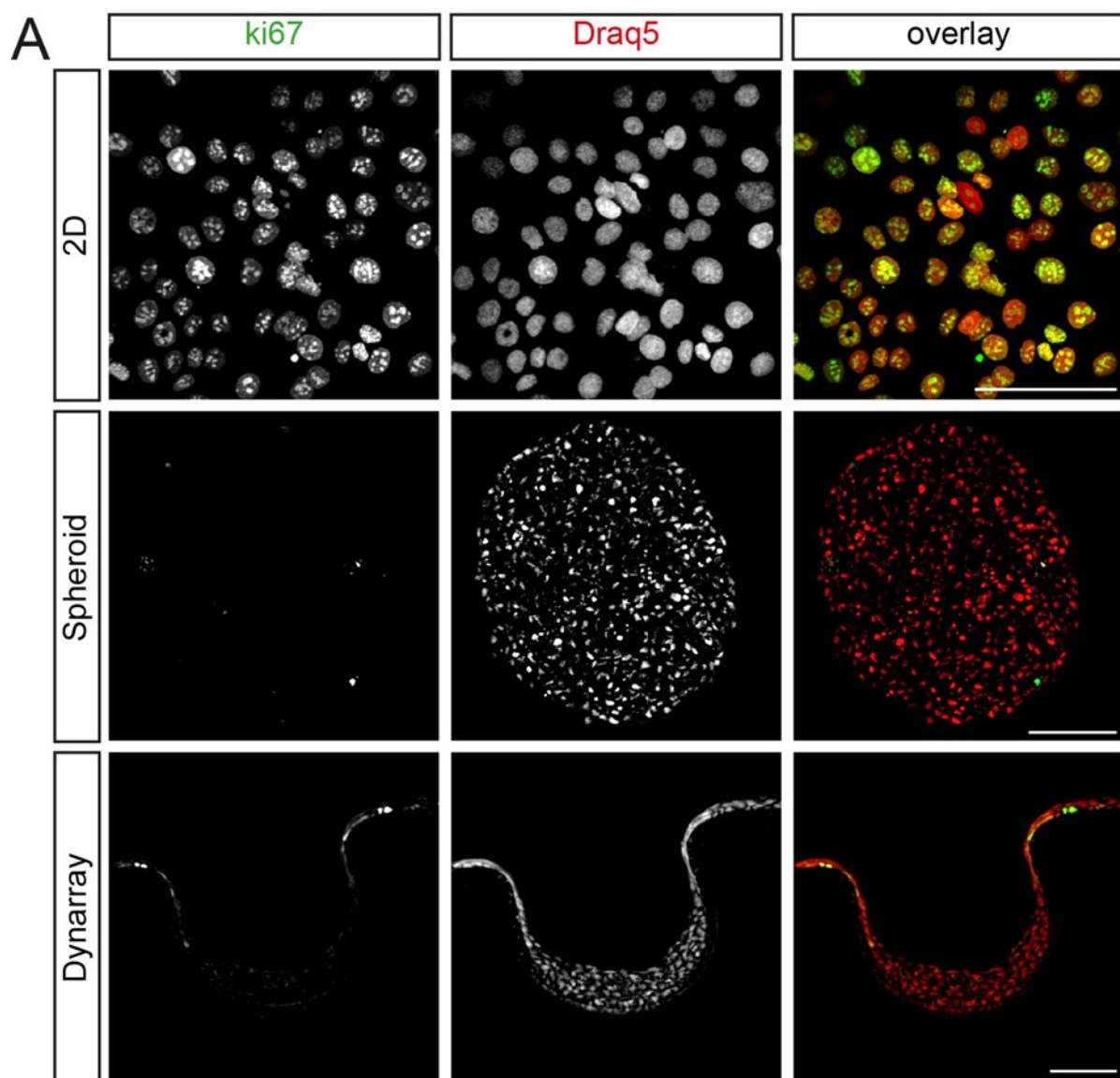
Figure 12: Decreased proliferation of HaCaT keratinocytes upon 3D cultivation. HaCaT cells were grown in 2D, as spheroids, and on Dynarrays. After 7 days, spheroids and Dynarrays were sectioned into 10 µm and 30 µm thick slices, respectively. All samples were immunostained for the proliferation marker ki67 and the nuclear dye Draq5. Images were taken at the confocal microscope. **A** Representative images of 2D and 3D samples are shown as indicated, exhibiting fluorescence signal from ki67 and Draq5 and overlay of both. In overlay, ki67 is coloured in green and Draq5 signals in red. Scale bar is 100 µm. **B** Quantitative analysis of ki67-positive cells in 2D cultures, spheroids, and Dynarrays. Numbers are depicted in mean ± S.E.M. with n = 3 for all conditions. Statistical significance was probed by ANOVA with **p<0.01. **C** Western Blot analysis of HaCaT cells cultured in 2D and as spheroids. Relative band intensities were normalized to internal GAPDH control. A number of three independent samples was analysed. Values are mean ± SD with n = 3. Significance was tested by t-test (**p<0.01). *Adapted and modified from Klicks et al 2017.*

Figure 13 shows the same trend for the cultivation of SK-MEL-28 cells. 2D cultures exhibited high amounts of ki67 staining, whereas spheroids and Dynarrays only displayed proliferating cells at the outer layers of 3D cultures (figure 13 A). Statistical analysis of ki67-positive cells confirmed this finding. 2D cultivation of melanoma cells yielded 94.0 % ± 5.1 % of ki67-positive cells, whereas the number of ki67-positive cells is significantly less in spheroids with 27.0 % ± 5.8 % and in Dynarrays with 32.0 % ± 13.0 % (figure 13 B). Western Blot analysis displayed the same trend. 3D cultivation of melanoma cells revealed a significant reduction of proliferating cells in spheroids as well as on Dynarrays (figure 13 C).
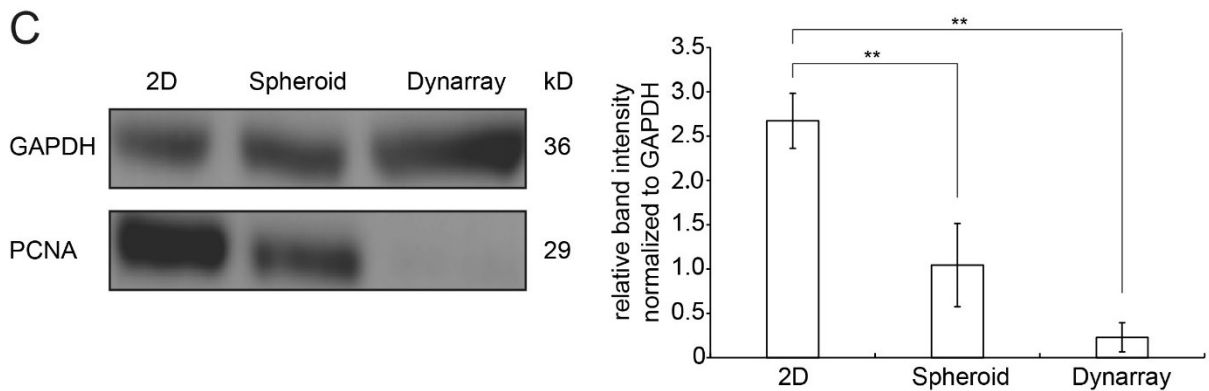
C

Figure 13: Proliferation of SK-MEL-28 melanoma cells was reduced when cultivated under 3D conditions. SK-MEL-28 cells were grown in 2D, as spheroids, and on Dynarrays. After 7 days in 3D culture, spheroids and Dynarrays were sectioned into 10 μm and 30 μm thick slices, respectively. All samples were stained with an antibody against ki67 and nuclei were stained with Draq5. **A** Representative confocal images of 2D and 3D samples are shown as indicated, presenting fluorescence staining of ki67 and Draq5 and overlays of both. Overlay shows ki67 signals in green and nuclei signals in red. Scale bar is 100 μm. **B** Quantitative analysis of ki67-positive cells in 2D cultures, spheroids, and Dynarrays. Numbers are depicted in mean ± S.E.M. with n = 3 for 2D and 3D. Statistical significance was probed by ANOVA (**p<0.01). **C** Relative intensity of respective bands were measured and normalized to internal GAPDH loading control. Given is mean ± SD from three independent experimental sets with statistical significance probed using ANOVA (**p<0.01).

Finally, LNCaP and PC-3 cells were also analyzed in 2D and 3D cultures similar to the melanoma cells. Both cell lines were actively proliferating when grown in 2D monolayers, but, in spheroids, only those cells that are at the periphery were proliferating (figure 14 A and B). Quantitative analysis of ki67-positive cells of both, LNCaP and PC-3 cells, displayed a significant reduction of proliferation in spheroids compared to 2D cultures (figure 14 C). 82.3 % ± 3.3 % of LNCaP cells were ki67-positive in 2D cultures and 13.2 % ± 1.4 % in spheroids. For PC-3 cells, it was similar. Here, 92.4 % ± 9.7 % were ki67-positive in 2D and only 22.9 % ± 3.6 % in 3D cultures.
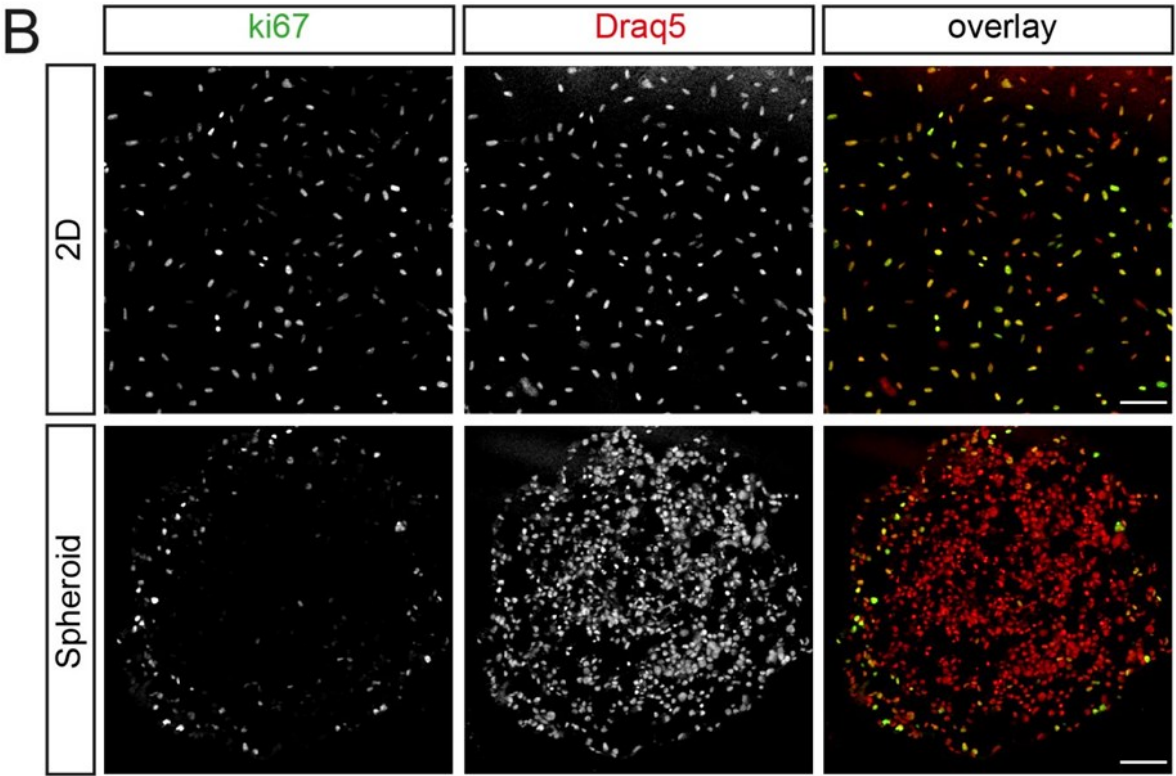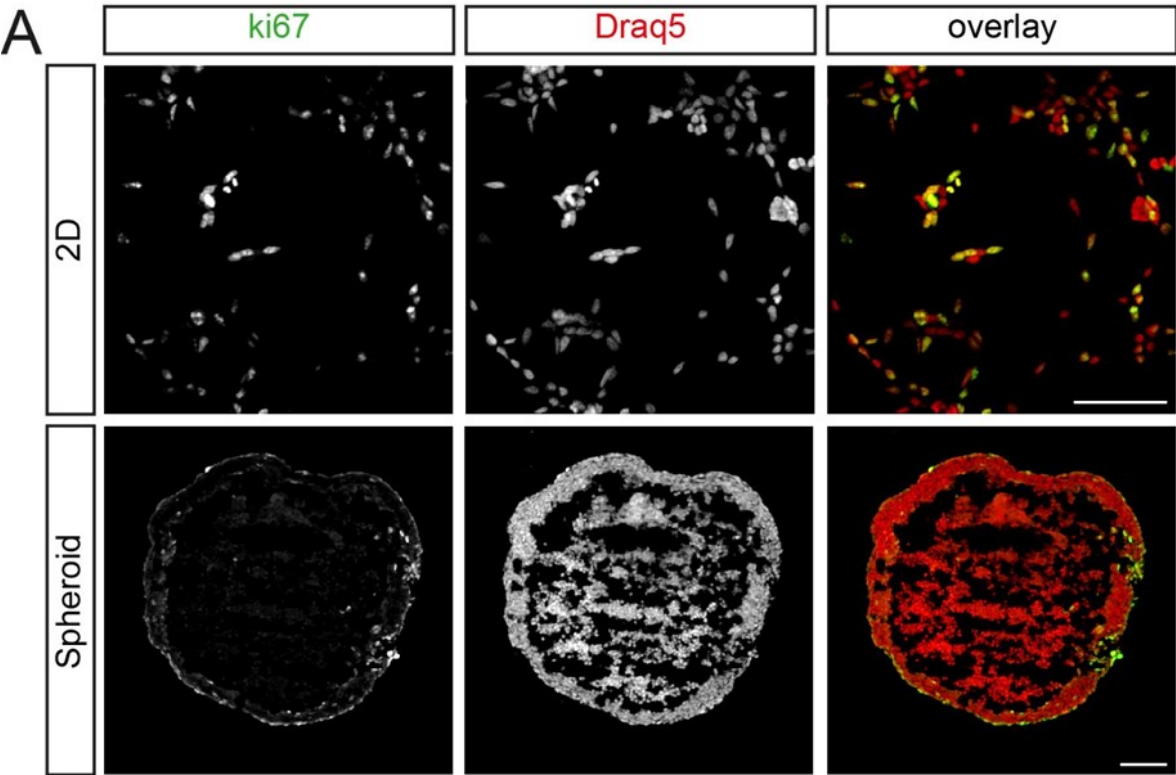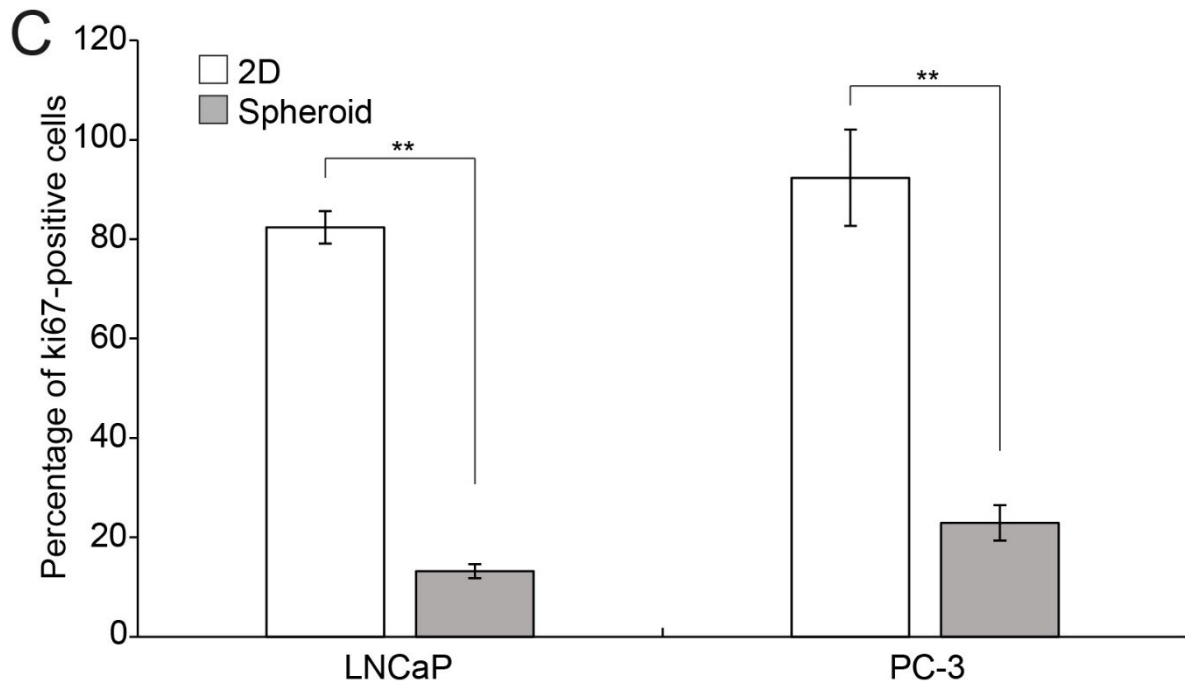
Figure 14: 3D cultivation effected cell proliferation in prostate cancer cell lines. LNCaP and PC-3 cells were grown in 2D and as spheroids. After 7 days in 3D culture, spheroids were sectioned into 10 µm thick slices. All samples were stained for ki67 and Draq5. **A and B** Representative confocal images of 2D monolayers and spheroid sections of LNCaP (**A**) and PC-3 (**B**) cells are shown as indicated, demonstrating fluorescence signals of ki67 and Draq5 and overlays of both. Overlay displays green ki67 signals and red nuclei signals. Scale bar: 100 µm. **C** Quantitative analysis of ki67-positive cells in 2D cultures and spheroids. Numbers are depicted in mean ± S.E.M. with n = 3 for 2D and 3D. Statistical significance was probed using t-test (**$p < 0.01$).

In summary, these findings show that 3D cultivation of skin, melanoma, and prostate cancer cells has a significant effect on the number of ki67-positive cells, i.e. a reduction of proliferation. Although cancer cells were proliferating on the periphery of the spheroids and Dynarrays, respectively, the overall amount of proliferation was diminished.

3.4 Apoptosis in 3D cultures differed among cell types

To further characterize the 3D structures of HaCaT, SK-MEL-28, LNCaP, and PC-3 cells and analyze the effect of 3D cultivation on apoptosis, cells were grown in 2D monolayers, as spheroids, and on Dynarrays. After seven days in 3D culture, spheroids and Dynarrays were fixed and sliced into 10 µm and 30 µm thick slices, respectively. All samples were then stained for the apoptosis marker cleaved caspase 3. Confocal microscopy revealed that there was almost no signal for cleaved caspase 3 in HaCaT cells when cultivated in 2D (figure 15 A). Conversely, cleaved caspase 3-positive cells

were equally distributed in the whole spheroid. 3D cultivation of keratinocytes on Dynarrays produced less apoptotic cells. Counting of cleaved caspase 3-positive cells in HaCaT 2D and 3D cultures revealed that spheroids exhibit significant more apoptotic cells than 2D and Dynarray cultures. While the amount of cleaved caspase 3-positive cells in spheroids was 32.1 % ± 2.7 %, it was only 11.0 % ± 5.9 % in 2D cultures and 8.3 % ± 1.4 % on Dynarrays (figure 15 B).
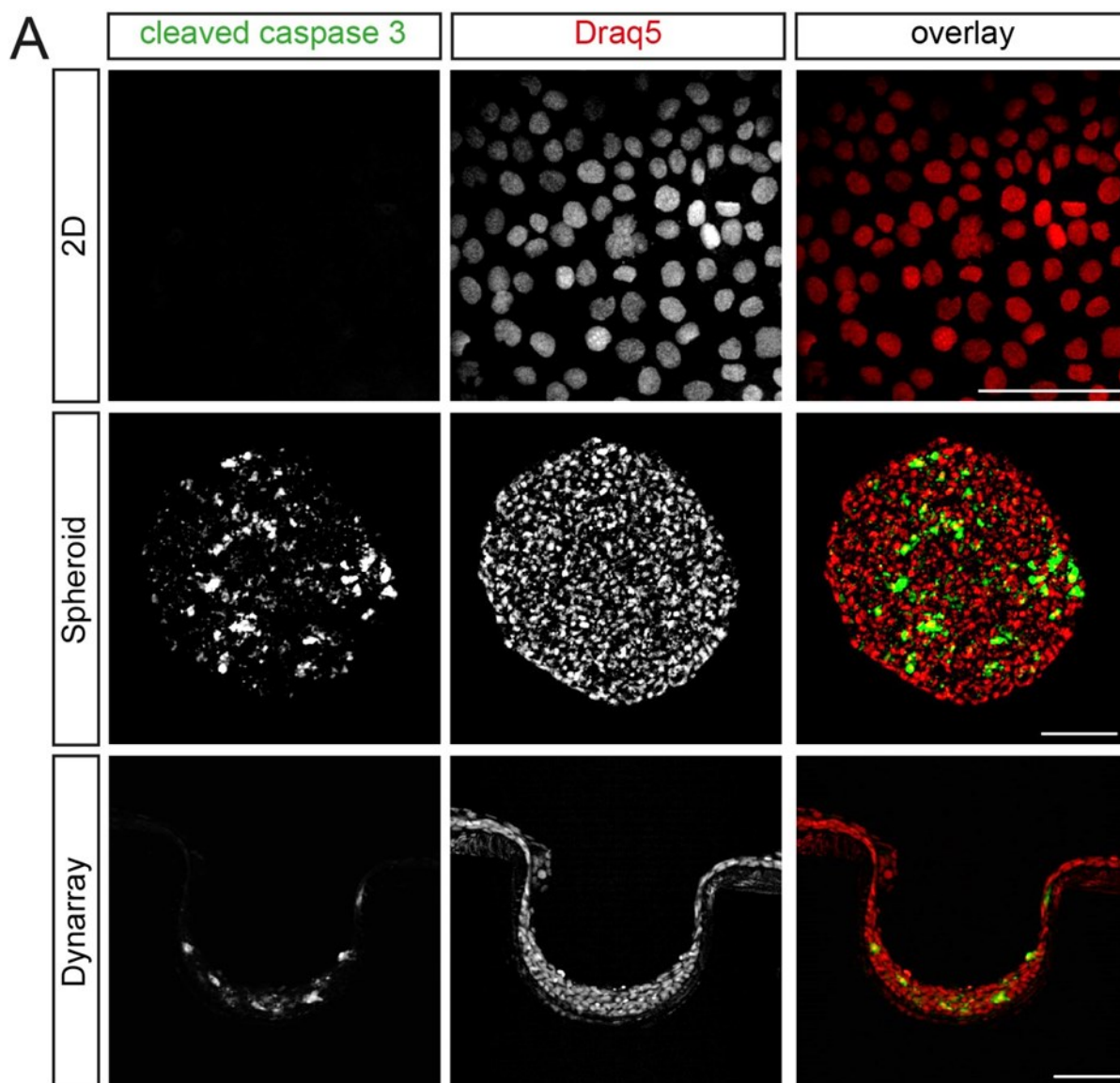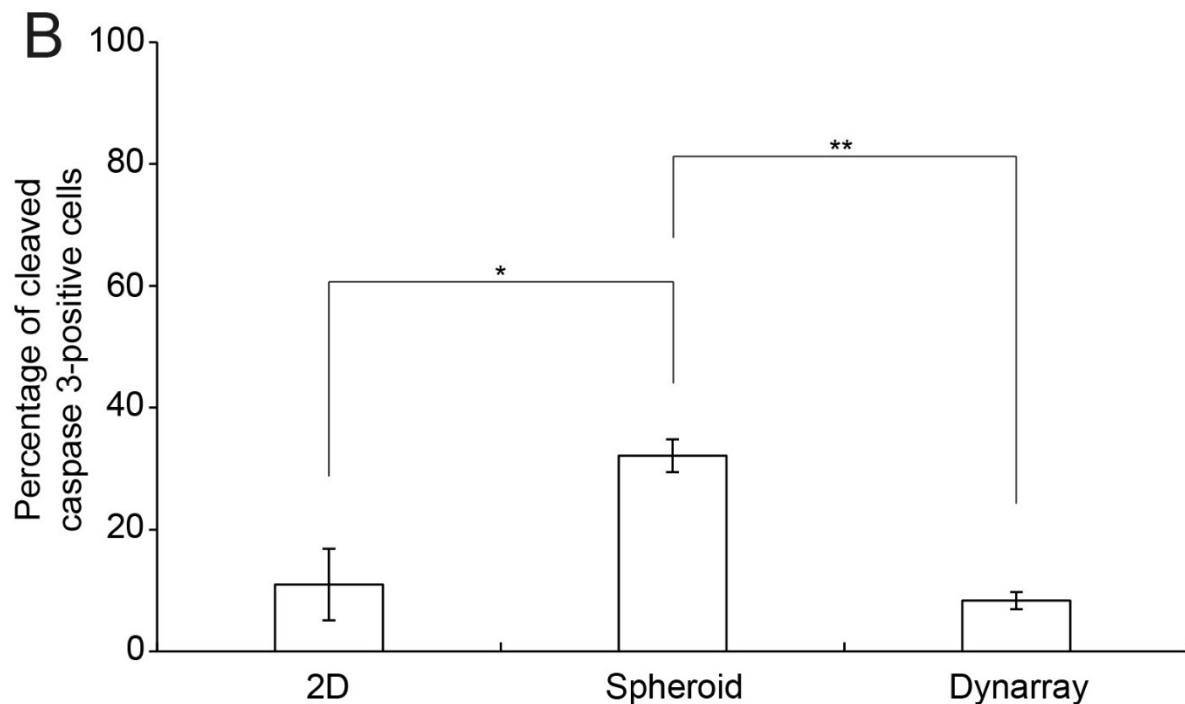
Figure 15: HaCaT keratinocytes displayed an increase in apoptosis when cultivated as spheroids compared to 2D and Dynarrays. HaCaT cells were grown in 2D, as spheroids, and on Dynarrays. After 7 days, spheroids and Dynarrays were sectioned into 10 µm and 30 µm thick slices, respectively. All samples were immunostained for the apoptosis marker cleaved caspase 3 and the nuclear dye Draq5. Images were taken at the confocal microscope. **A** Representative images of 2D and 3D samples are shown as indicated, exhibiting fluorescence signal from cleaved caspase 3 and Draq5 and overlay of both. In overlay, cleaved caspase 3 is coloured in green and Draq5 signals in red. Scale bar is 100 µm. **B** Quantitative analysis of cleaved caspase 3-positive cells in 2D cultures, spheroids, and Dynarrays. Numbers are depicted in mean ± S.E.M. with n = 3 for all conditions. Statistical significance was probed by ANOVA with *p<0.05 and **p<0.01. *Adapted and modified from Klicks et al 2017.*

Figure 16 shows the cultivation of SK-MEL-28 cells in 2D and 3D. Similar to HaCaT keratinocytes, melanoma cells were not apoptotic when cultivated as 2D monolayers. Spheroids of SK-MEL-28 cells were found to be only sparsely cleaved caspase 3-positive. On Dynarrays, apoptotic cells were unevenly distributed throughout the 3D structure (figure 16 A) and more cleaved caspase 3-positive cells were found. This observation was confirmed by quantitative analysis of cleaved caspase 3-positive cells in all samples. Melanoma cells in 2D cultures display no apoptotic cells at all, and spheroids exhibited only 2.9 % ± 3.7 % of cleaved caspase 3-positive cells. Although Dynarrys were cultivated in a bioreactor with superfusion, SK-MEL-28 cells were significantly more apoptotic in this condition (14.3 % ± 5.4 % of apoptotic cells) than in 2D or spheroids (figure 16 B).
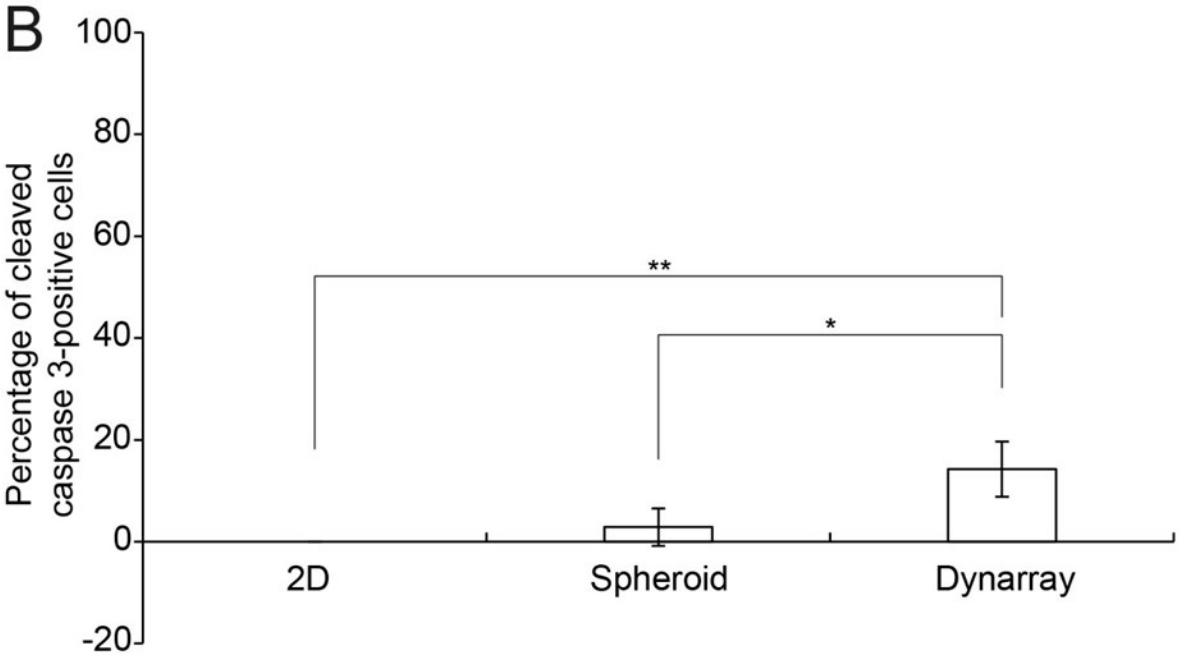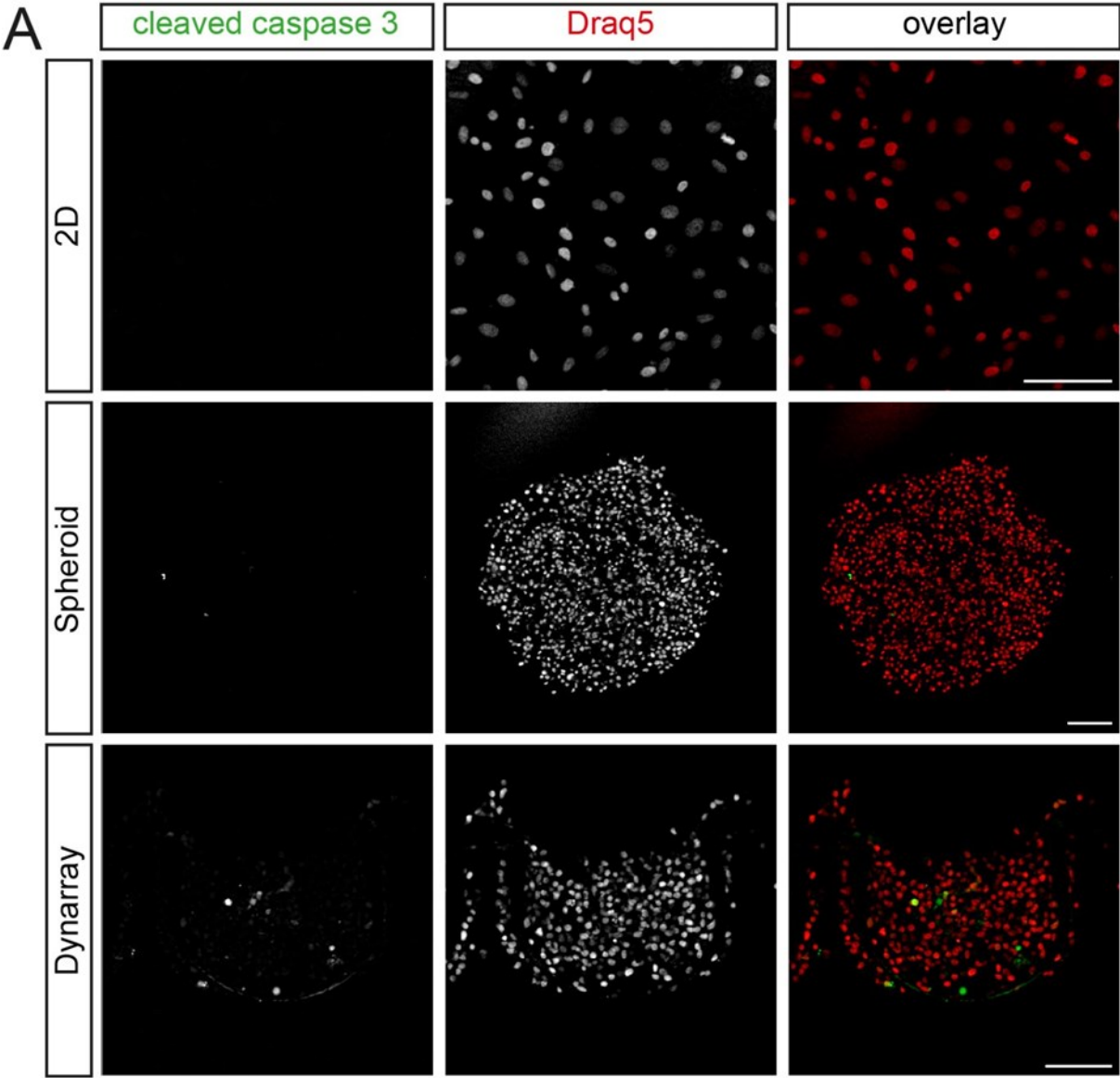
Figure 16: Apoptosis of SK-MEL-28 melanoma cells was enhanced when cultivated under perfused 3D conditions. SK-MEL-28 cells were grown in 2D, as spheroids, and on Dynarrays. After 7 days in 3D culture, spheroids and Dynarrays were sectioned into 10 µm and 30 µm thick slices, respectively. All samples were stained with an antibody against cleaved caspase 3 and nuclei were stained with Draq5. **A** Representative confocal images of 2D and 3D samples are shown as indicated, presenting fluorescence staining of cleaved caspase 3 and Draq5 and overlays of both. Overlay shows cleaved caspase 3 signals in green and nuclei signals in red. Scale bar is 100 µm. **B** Quantitative analysis of cleaved caspase 3-positive cells in 2D cultures, spheroids, and Dynarrays. Numbers are depicted in mean ± S.E.M. with n = 3 for 2D and 3D cultures. Statistical significance was probed by ANOVA (**p<0.01 and *p<0.05).

Finally, the prostate cancer cells LNCaP and PC-3 were analyzed in terms of apoptosis. Both cancer cell lines showed a similar behavior upon 3D cultivation. Compared to 2D cultures, where almost no apoptotic cells were visible, spheroids had an apoptotic core after 7 days in 3D culture (figure 17 A and B). Statistical analysis of fluorescent signals revealed that spheroid cultivation leads to a significant higher amount of cleaved caspase 3-positive cells (19.7 % ± 3.4 % in LNCaP and 8.7 % ± 1.5 % in PC-3) compared to 2D cultures (0.6 % ± 1.3 % in LNCaP and 0.0 % ± 0.0 % in PC-3) (figure 17 C).
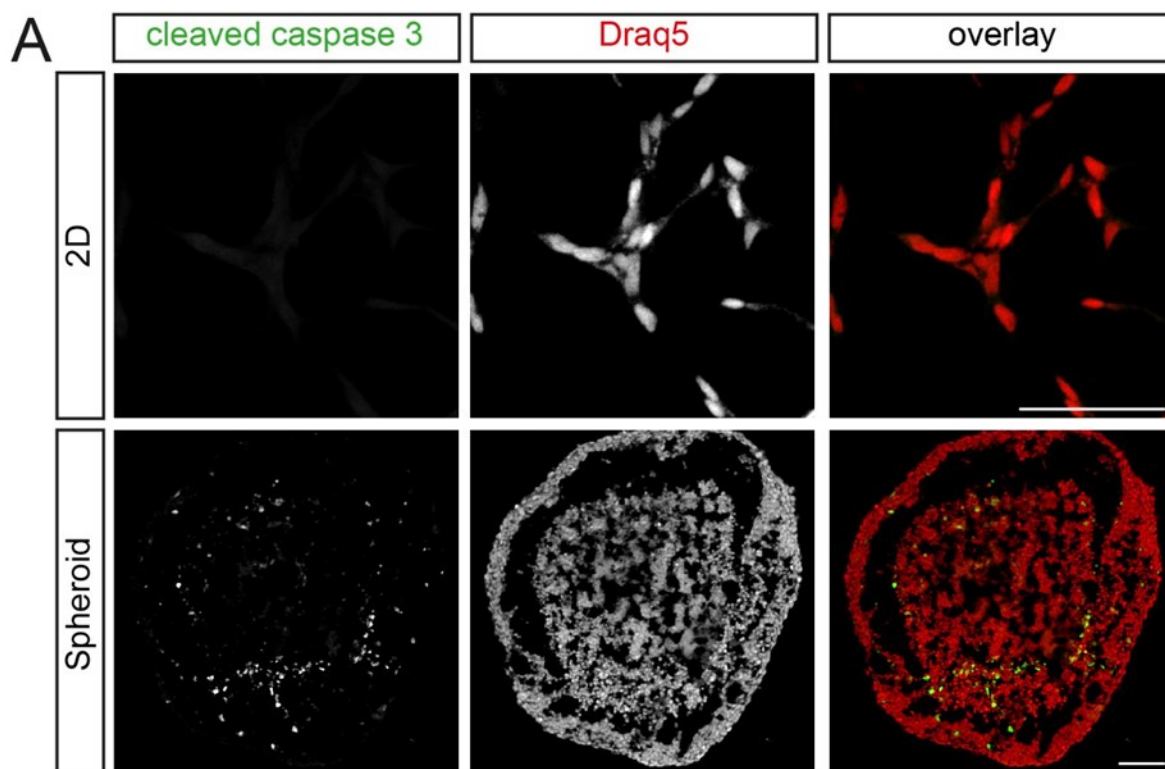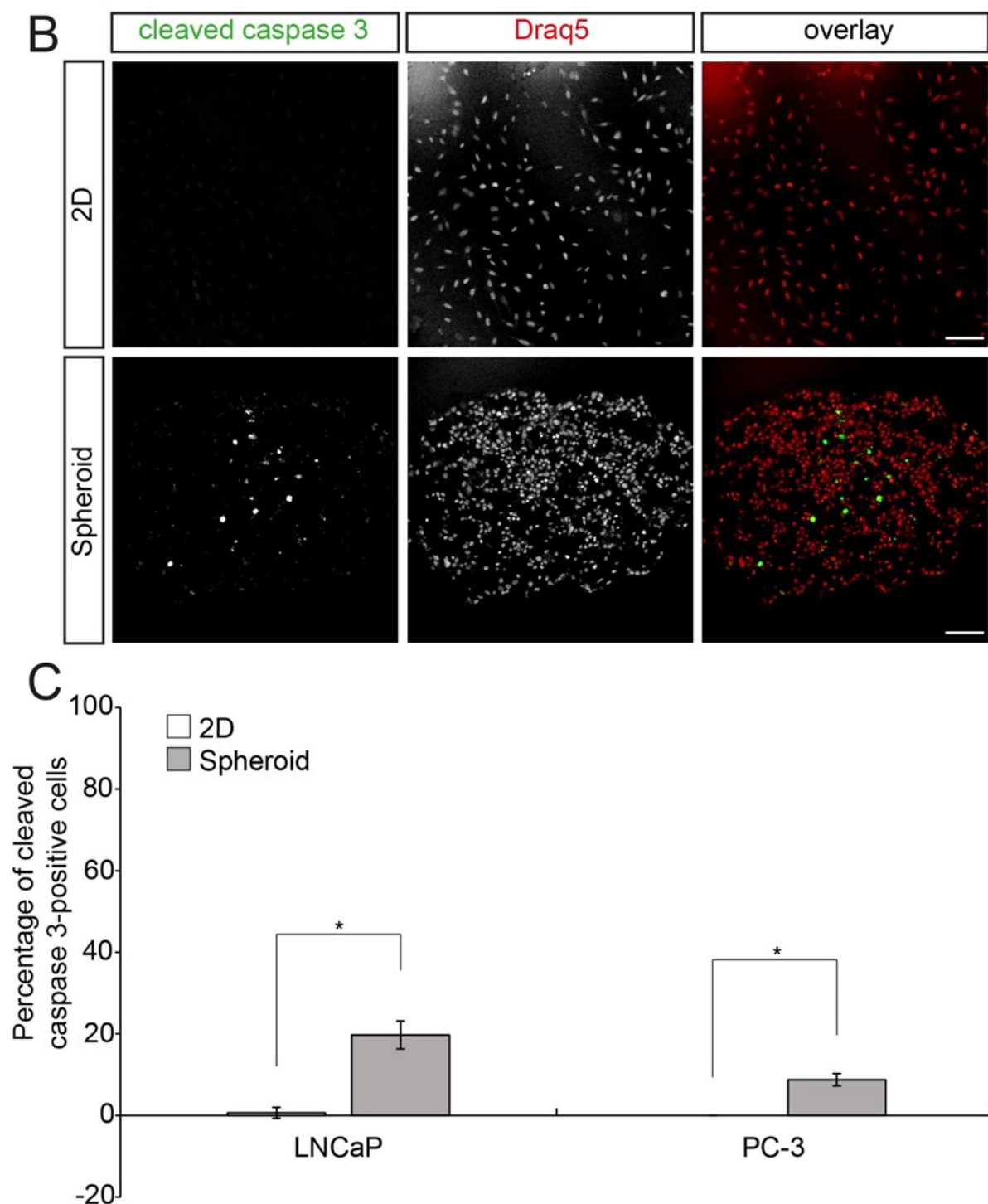
Figure 17: 3D cultivation effected cell apoptosis in prostate cancer cell lines. LNCaP and PC-3 cells were grown in 2D and as spheroids. After 7 days in 3D culture, spheroids were sectioned into 10 µm thick slices. All samples were stained for cleaved caspase 3 and Draq5. **A and B** Representative confocal images of 2D monolayers and spheroid sections of LNCaP (**A**) and PC-3 (**B**) cells are shown as indicated, demonstrating fluorescence signals of cleaved caspase 3 and Draq5 and overlays of both. Overlay displays green cleaved caspase 3 signals and red nuclei signals. Scale bar: 100 µm. **C** Quantitative analysis of cleaved caspase 3-positive cells in 2D cultures and spheroids. Numbers are depicted in mean ± S.E.M. with n = 3 for 2D and 3D cultures. Statistical significance was probed using t-test (*p<0.05).

3.5 Qualitative assessment of HaCaT differentiation

After the study of proliferation and apoptosis, the effect of 3D cultivation on keratinocyte differentiation was assessed. Therefore, HaCaT cells were cultured in 2D, as spheroids, and on Dynarrays. After seven days in 3D culture, spheroids and Dynarrays were fixed and sliced into 10 µm and 30 µm thick sections, respectively. Then, all samples were stained for the basal keratinocytes marker ck14 and the differentiation marker ck10. As displayed in figure 18, confocal microscopy revealed differences in the location and amount of ck10- and ck14-positive cells. HaCaT cells in 2D were sometimes ck10-positive when grown to confluency but with random distribution. Conversely, spheroids regularly assembled to form a ck14-positive core and a ck10-positive external layer of cells. Similarly, also Dynarrays showed a clearly layered expression of keratinocyte differentiation markers, ck14 and ck10. To sum up, 3D cultivation allowed keratinocytes to build up layers of cells that show a stratification of keratin differentiation markers ck14 and ck10, which was not observed in 2D cultures.
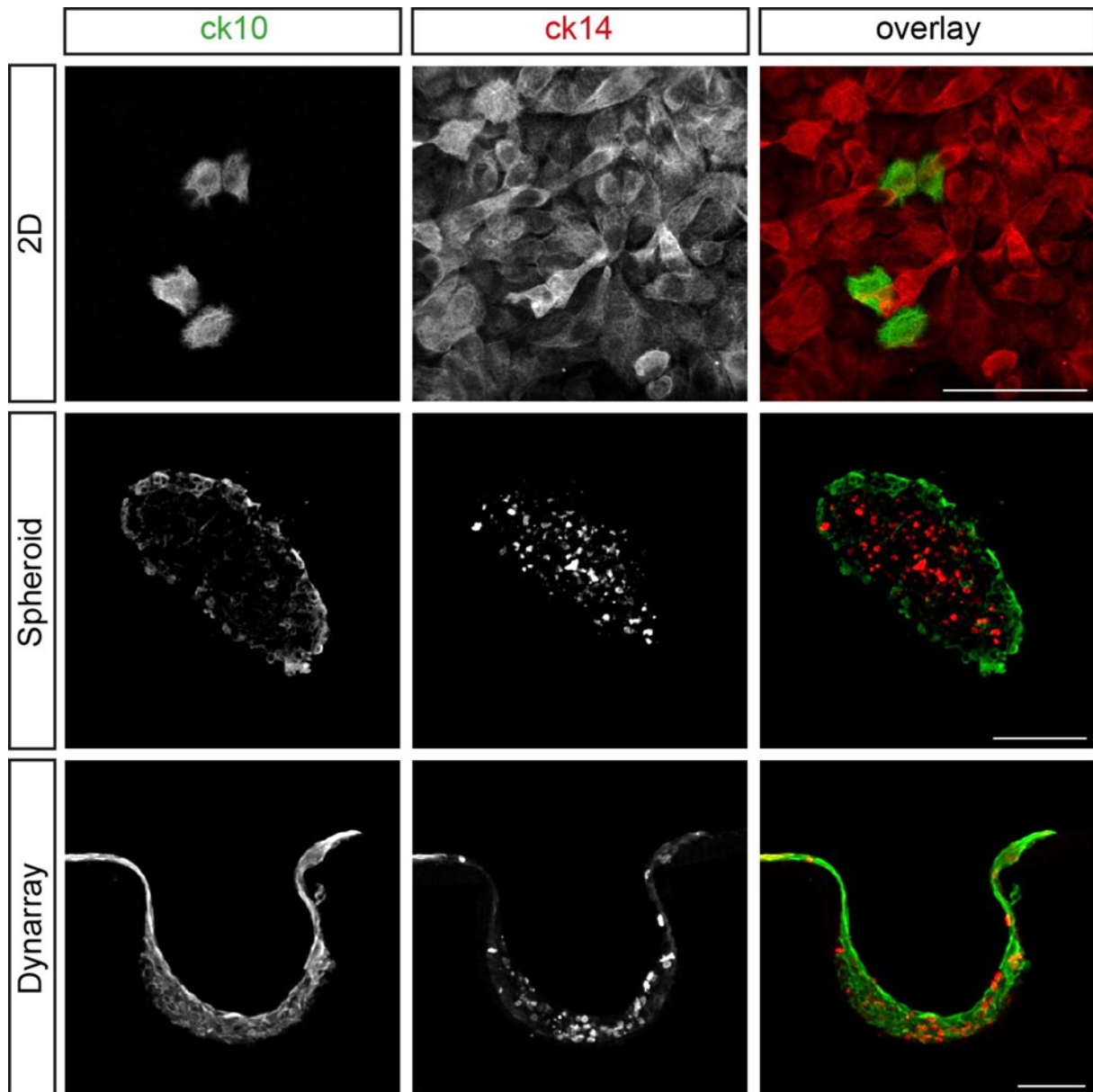
Figure 18: Differentiation of HaCaT keratinocytes was promoted by 3D cultivation. HaCaT cells were grown in 2D, as spheroids, and on Dynarrays. After 7 days, spheroids and Dynarrays were sectioned into 10 µm and 30 µm thick slices, respectively. All samples were immunostained for ck14 and ck10 to mark basal cells and more differentiated keratinocytes, respectively. Images were taken at the confocal microscope. The panels show representative images of 2D and 3D samples as indicated, exhibiting fluorescence signal from ck10 and ck14 and overlay of both. In overlay, ck10 is coloured in green and ck14 signals in red. Scale bar is 100 µm. *Adapted and modified from Klicks et al 2017.*

3.6 Characterization of spheroid keratinocyte and fibroblast mono- and bi-cultures

After the successful establishment of 3D cultures of various cell types, further investigation was restricted to stromal, skin, and melanoma cells. Here, the goal was to set up a simple, robust and multiplexable 3D melanoma test system. Due to their ease of preparation and clear stratification of keratinocytes, investigations were limited

to spheroids. In addition, potential effects of co-culturing were analyzed. Thus, HaCaT cells and CCD-1137Sk fibroblast cells were either cultured as mono- or co-cultures on cell-repellent plates with a culture time of seven days. Then, spheroids of all types were cryosectioned into 10 µm thick slices and immunostained for ki67 or cleaved caspase 3. Cytokeratins ck10 and ck14 were immunostained to assess keratinocyte stratification. Nuclei were labeled with Dapi. Figures 19 A-C show representative confocal images of these samples as indicated. While proliferation was restricted to few cells in the periphery of spheroids (figure 19 A), apoptotic cells were found throughout the whole spheroid diameter (figure 19 B). In mono-cultures as well as in bi-cultures, HaCaT keratinocytes showed a clear stratification with basal-like ck14-positive cells in the center of the spheroid and more differentiated ck10-positive cells on the periphery of the spheroids (figure 19 C). In bi-cultures, fibroblasts formed a central core, and keratinocytes were located in a ring-like fashion around this fibroblast core. Quantitative analysis revealed that co-culturing significantly reduced the number of proliferating and increased the amount of ck10-positive peripheral keratinocytes (figure 19 D). These results suggest that the 3D spheroid skin model mirrors some stratification and differentiation characteristics of skin even without the use of a pH or Ca^{2+} gradient or an air-liquid interface to induce differentiation.
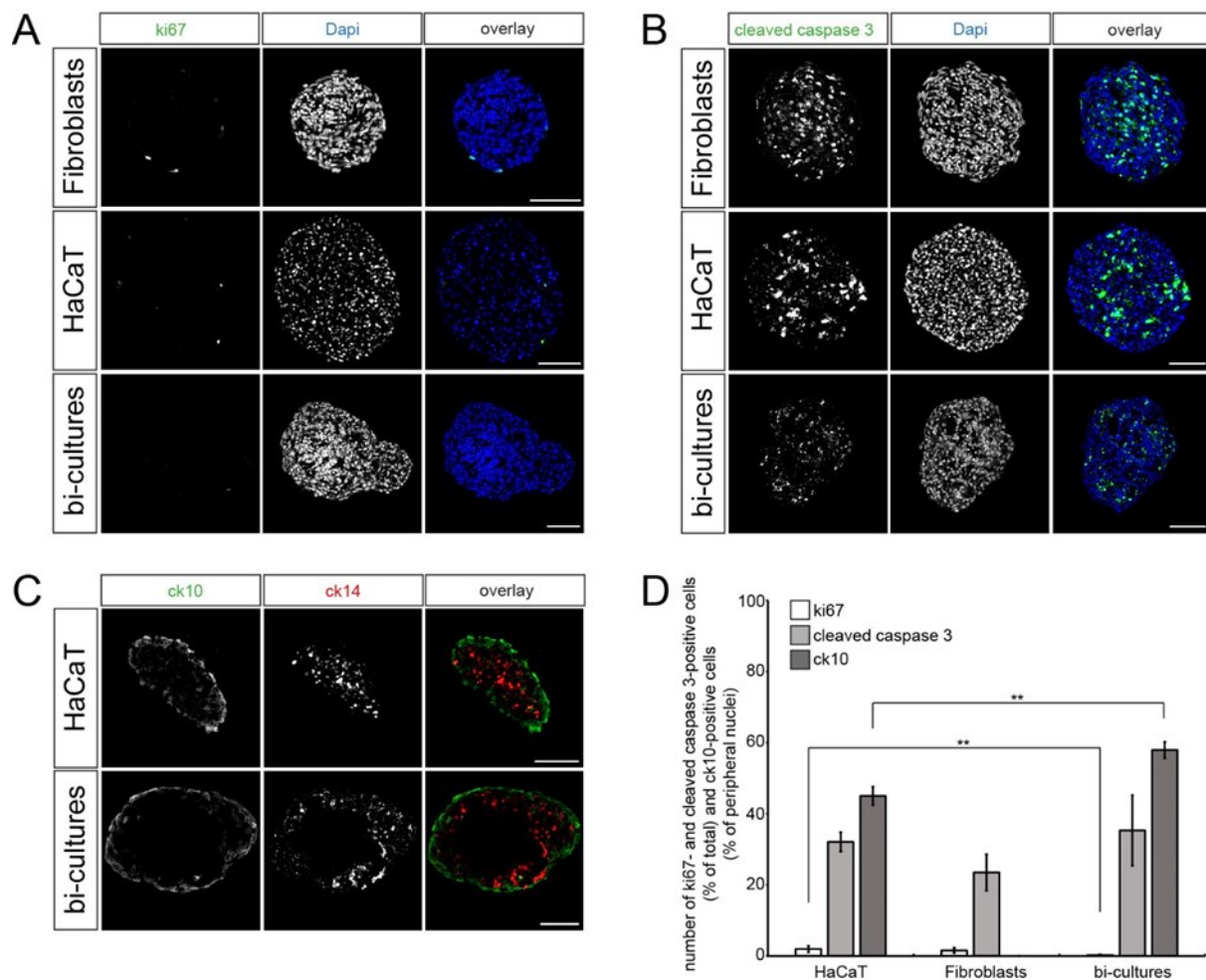
Figure 19: Proliferation, apoptosis, and differentiation of fibroblasts and HaCaT cells in mono- and bi-culture spheroids. Spheroids were cultured as mono- and bi-cultures for seven days, cryosectioned into 10 μm thick slices, and then stained for markers for cell proliferation (A, ki67, green), apoptosis (B, cleaved caspase 3, green), differentiated (C, ck10, green) and basal keratinocytes (C, ck14, red). In A and B, nuclei were stained with Dapi (blue). **A-C** Representative confocal images. Scale bars: 100 μm. **D** Quantification of ki67- and cleaved caspase 3-positive cells in percentage of total and ck10-positive cells in percentage of peripheral nuclei. Given is mean ± S.E.M. with n ≥ 3 independent experiments and **p<0.01 according to ANOVA. *Adapted and modified from Klicks et al 2019 (revised revision)*.

3.7 Melanoma cells invaded the fibroblast core and decreased keratinocyte differentiation in tri-cultures

After these first characterizations, the spheroid skin model was supplemented by the addition of SK-MEL-28 melanoma cells. For that reason, fibroblasts were seeded and cultivated in 3D. Three days later, HaCaT keratinocytes and SK-MEL-28 melanoma cells were added simultaneously. To distinguish between the different cell types, HaCaT cells were labeled with CellTracker Red CMPTX and SK-MEL-28 cells with CellTracker Green CMFDA. After another four days, tri-culture spheroids were

collected, cryosectioned into 10 µm thick slices and stained for ki67, cleaved caspase 3, ck10 and ck14, or the basement membrane marker collagen IV. As shown in figure 20 A, collagen IV rich fibroblasts stayed in the central core of these tri-cultures, followed by a few layers of basal ck14-positive and a sheet of more differentiated ck10-positive keratinocytes. Most melanoma cells were clustered on the shell of the cultures. However, a few melanoma cells were also very regularly found in the fibroblast core, but almost never in the keratinocyte layers. For simplicity, in the following, SK-MEL-28 cells in the outer border of the tri-cultures will be termed 'external' (figure 20 A zoom out, arrows), those in the fibroblast core as 'internal' (figure 20 A zoom out, arrowhead) melanoma cells. The qualitative examination further showed that plenty of external melanoma cells were proliferating, while internal melanoma cells, keratinocytes, and fibroblasts were rarely doing so. Remarkably, ck10 expression, which indicates keratinocyte differentiation, was strongly diminished at the contact sites with melanoma cells. Furthermore, most external melanoma cells got lost upon treatment with docetaxel (figure 20 B).
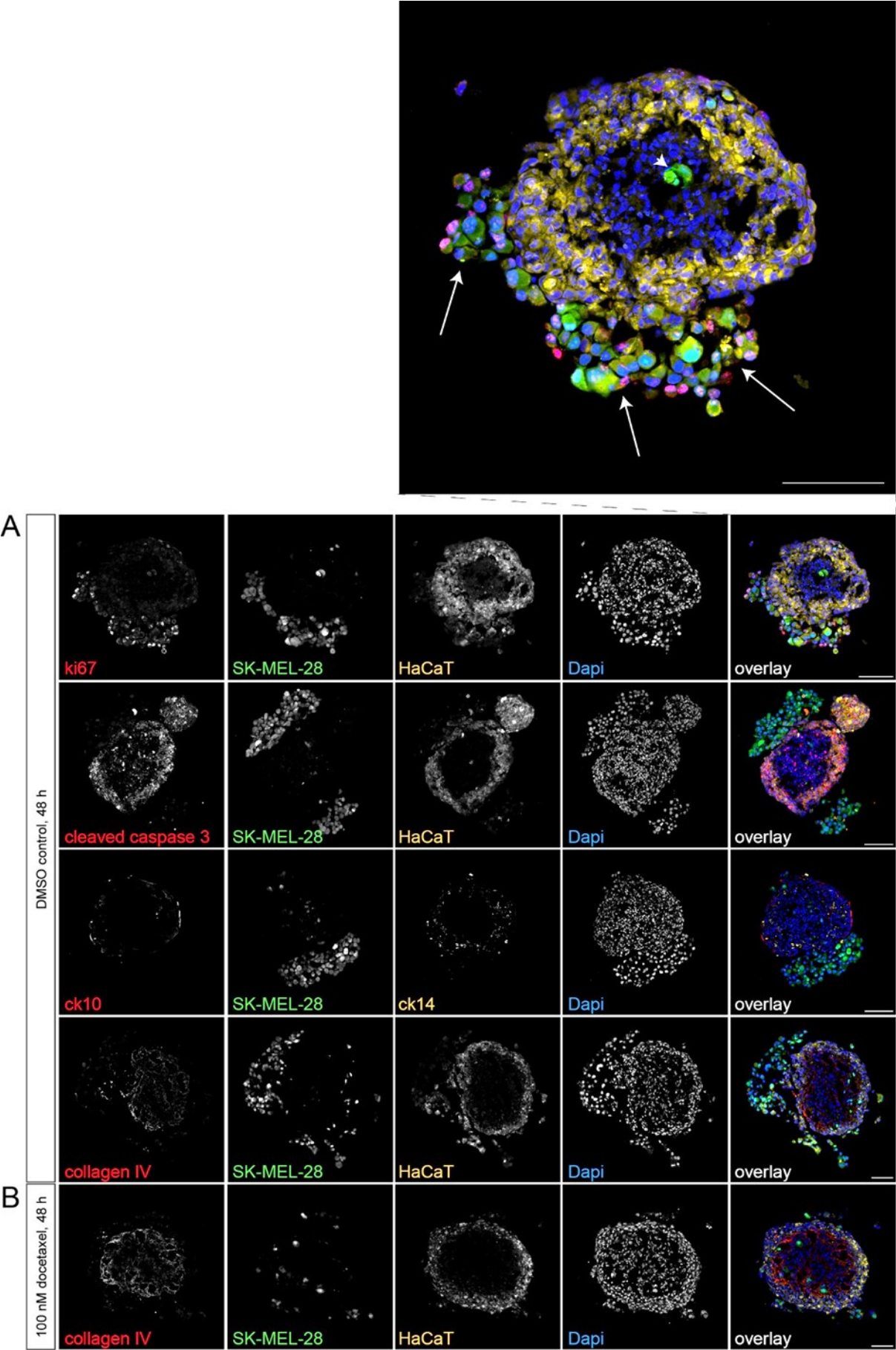
Figure 20: Features of a melanoma tri-culture spheroid model. Tri-culture spheroids were produced

by 3D cultivation of CCD-1137Sk fibroblasts for three days, followed by the simultaneous addition of HaCaT keratinocytes and SK-MEL-28 melanoma cells. Afterwards, they were cultured for another four days. HaCaT and SK-MEL-28 cells were labeled with CellTrackerRed CMPTX and CellTrackerGreen CMFDA dyes, respectively. As indicated, spheroids were incubated on day five after seeding either with 0.01 ‰ DMSO as control (**A**) or 100 nM docetaxel in DMSO (**B**) for 48 h, then cryosectioned into 10 µm thick slices and stained for ki67, cleaved caspase 3, ck10, ck14, or the basal membrane marker collagen IV. Nuclei were labeled with Dapi. Most melanoma cells were clustered on the shell of the cultures (**A** zoom out, arrows). However, a few melanoma cells were also very regularly found in the fibroblast core (**A** zoom out, arrowhead). Images show representative confocal sections of these samples. In overlay panels, all immunostainings except for ck14 are depicted in red, SK-MEL-28 cells in green, HaCaT cells or ck14 in yellow, and nuclei in blue. Scale bars are 100 µm. *Adapted and modified from Klicks et al 2019 (revised revision)*.

To address, whether melanoma cells distributed passively or actively into the fibroblast core or on the periphery of the tri-cultures, we harvested tri-culture spheroids after four and five days in culture. After fixation, they were sliced into 10 µm thick sections and stained for the nuclear dye Dapi (figure 21). On day four, which is one day after the simultaneous seeding of melanoma cells and keratinocytes, most melanoma cells were embedded in the keratinocyte ring, while on day five, they segregated from keratinocytes and either accumulated in the periphery of the culture ('external' melanoma cells) or within the fibroblast core ('internal' melanoma cells). This suggests that the separation of melanoma cells into the fibroblast core as well as the periphery of the tri-cultures is an active process.
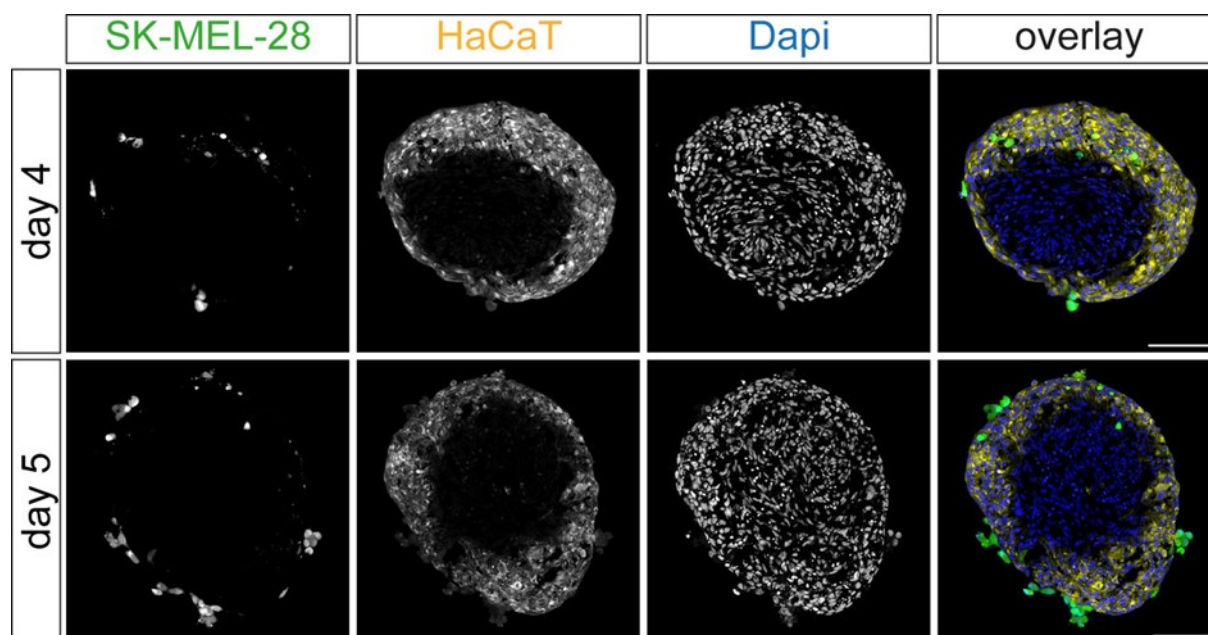

Figure 21: Melanoma cells in tri-cultures separated actively to form external melanoma cells. Tri-culture spheroids were generated by 3D cultivation of fibroblasts for three days, followed by the

combined addition of keratinocytes and melanoma cells. HaCaT and SK-MEL-28 cells were labeled with CellTrackerRed CMPTX and CellTrackerGreen CMFDA dyes, respectively, prior seeding. After one ('day 4', upper row) or two ('day 5', lower panels) more days, tri-culture spheroids were cryosectioned into 10 µm thick slices and stained with Dapi. Representative confocal sections are shown. While on day four, most melanoma cells were located in the keratinocyte ring, on day five, they separated from keratinocytes and either accumulated in the periphery of the culture ('external' melanoma cells) or within the fibroblast core ('internal' melanoma cells). The fibroblast core is found in the center of the tri-culture and marked as Dapi-positive plus CellTracker-negative. Scale bars: 100 µm. *Adapted and modified from Klicks et al 2019 (revised revision)*.

3.8   Docetaxel treatment affected external melanoma cells

Since the tri-culture system was established to serve as a model for testing drug candidates, docetaxel, which is being explored in particular for combination treatments of malignant melanoma [225–227], was tested. In order to find a suitable concentration for *in vitro* tests, a dose-response curve was set up. Therefore, fibroblasts were cultivated for three days in 3D culture, followed by the simultaneous addition of HaCaT and SK-MEL-28 cells. Two days later, tri-cultures were incubated for 48 h with various concentrations of docetaxel, i.e. 0 nM, 10 nM, 50 nM, 100 nM, 500 nM, and 1,000 nM. Remaining external melanoma cells after 48 h were used as an end point measurement for docetaxel assessment. As demonstrated by the dose-response curve shown in figure 22, the number of remaining external melanoma cells decreased with increasing concentration of docetaxel. Already the lowest docetaxel concentrations slightly reduced external melanoma cells, but the effects were statistically significant in this setting only at concentrations ≥ 100 nM of docetaxel. Therefore, in all following experiments, this drug concentration was used. In comparison, SK-MEL-28 cells were also cultured in 2D and incubated with various concentrations of docetaxel for 24 h. Here, melanoma cells appeared much more susceptible to docetaxel treatment. Already a docetaxel concentration of 10 nM significantly reduced the number of cells (figure 22). Higher concentrations of docetaxel did not change the number of remaining cells compared to 10 nM.
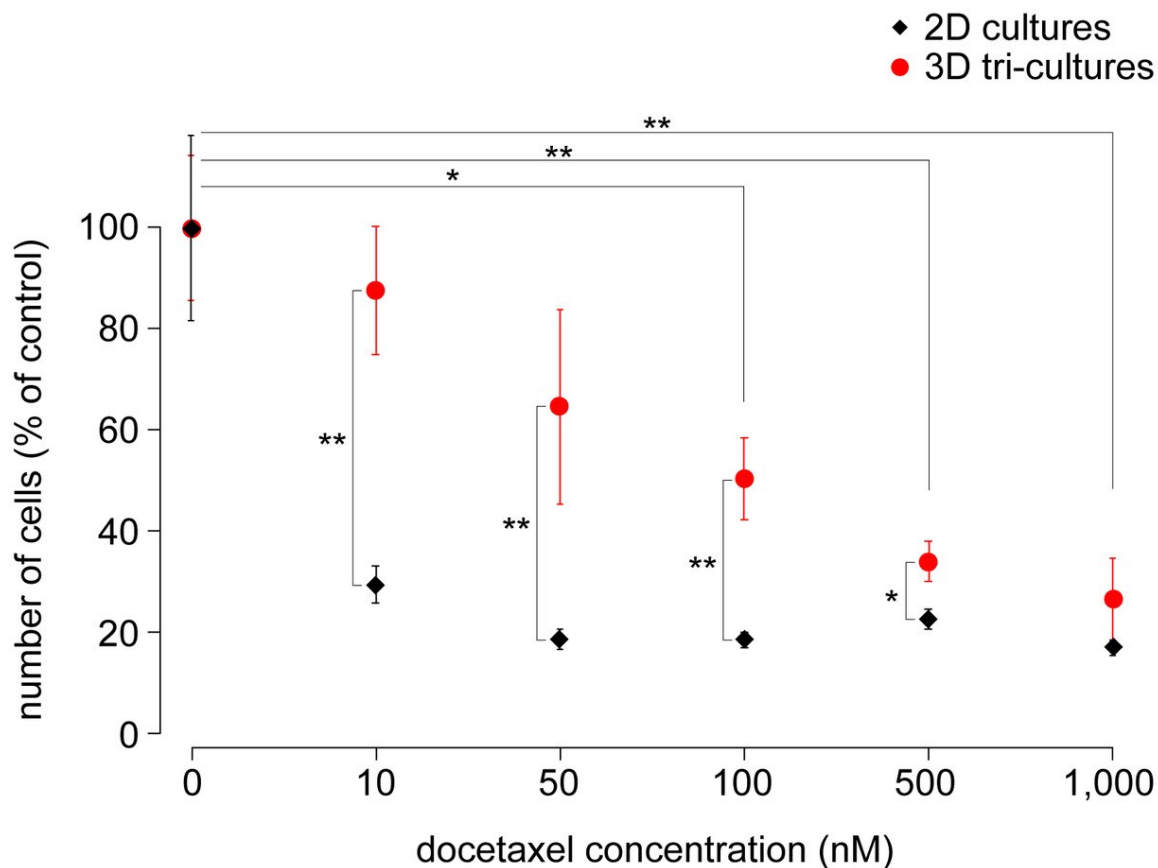
Figure 22: SK-MEL-28 cells were more susceptible to docetaxel in 2D compared to 3D. 2D cultures of SK-MEL-28 cells were grown until they reached 50 % of confluency. Tri-culture spheroids were made by 3D cultivation of fibroblasts for three days, followed by the combined addition of keratinocytes and melanoma cells, and another two days without treatment. Then, all cultures were treated with different concentrations of docetaxel for 24 h (2D) or 48 h (spheroids). Spheroids were cryosectioned into 10 μm thick slices, 2D cultures were directly fixed. Subsequently, all samples were labeled with Dapi and then imaged by confocal microscopy. The numbers of remaining SK-MEL-28 cells (2D cultures) or of external SK-MEL-28 cells (spheroids) were determined. The graph shows the amounts of SK-MEL-28 cells as a function of docetaxel concentration and normalized to the control condition without docetaxel. Given is mean ± S.E.M. with n ≥ 3, *$p<0.05$ and **$p<0.01$ according to ANOVA. *Adapted from Klicks et al 2019 (revised revision)*.

3.9 Docetaxel treatment of tri-culture spheroids reduced melanoma cell proliferation

In order to get an insight into the kinetics of docetaxel effects on the proliferation of the tri-culture spheroids, they were treated with 100 nM docetaxel for 15, 24, 48, and 72 h prior harvesting. Samples were then cryosectioned and slices were immunostained for the proliferation marker ki67. Figure 23 A and B depict representative fields of view.

C
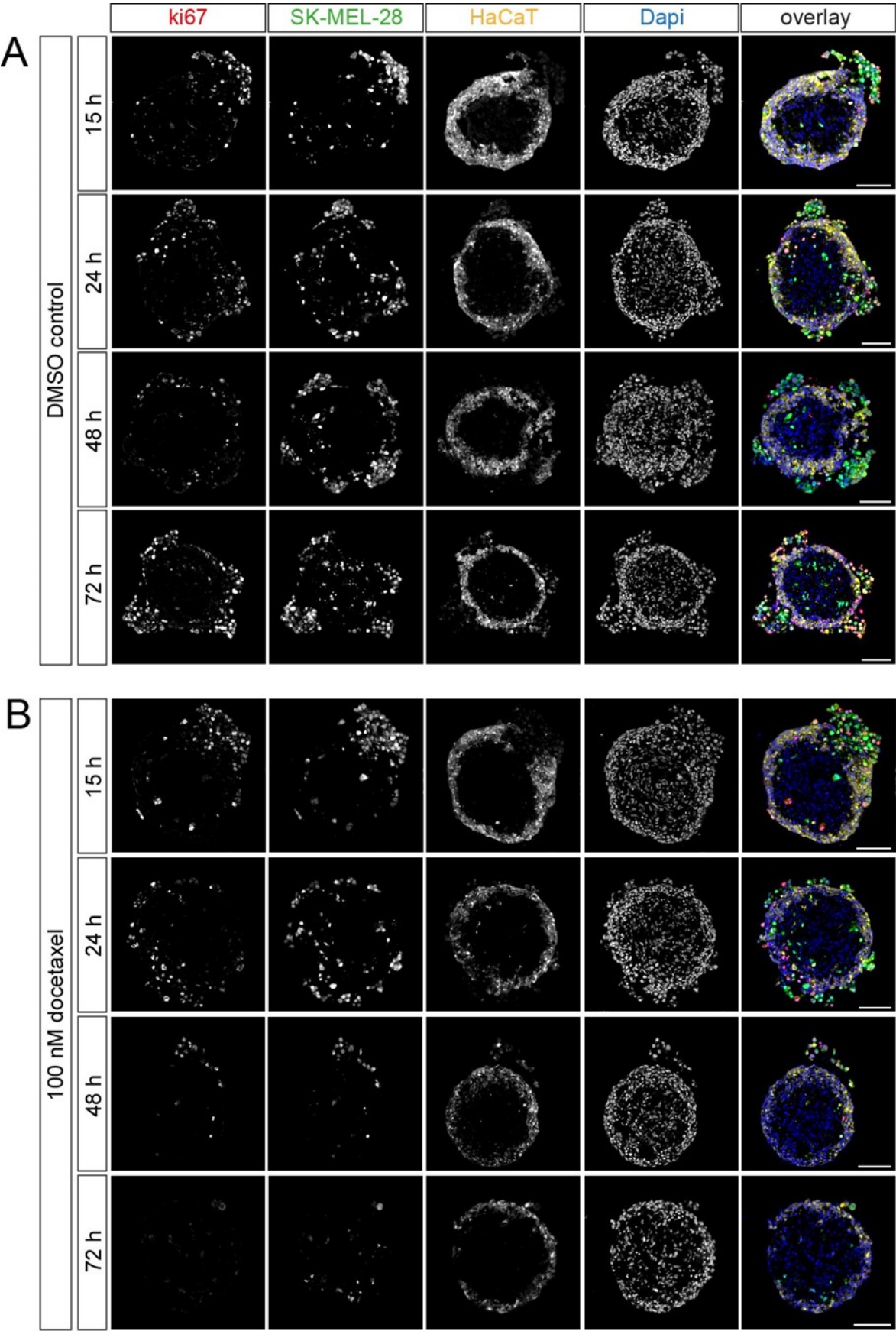
Figure 23: Docetaxel treatment led to a reduction of proliferating cells in melanoma 3D tri-cultures. Tri-culture spheroids were created by 3D cultivation of fibroblasts for three days, followed by simultaneous addition of keratinocytes and melanoma cells. HaCaT cells were marked with CellTrackerRed CMPTX dye and SK-MEL-28 cells with CellTrackerGreen CMFDA. After another cultivation period of two days, tri-culture spheroids were treated either with 0.01 ‰ DMSO as 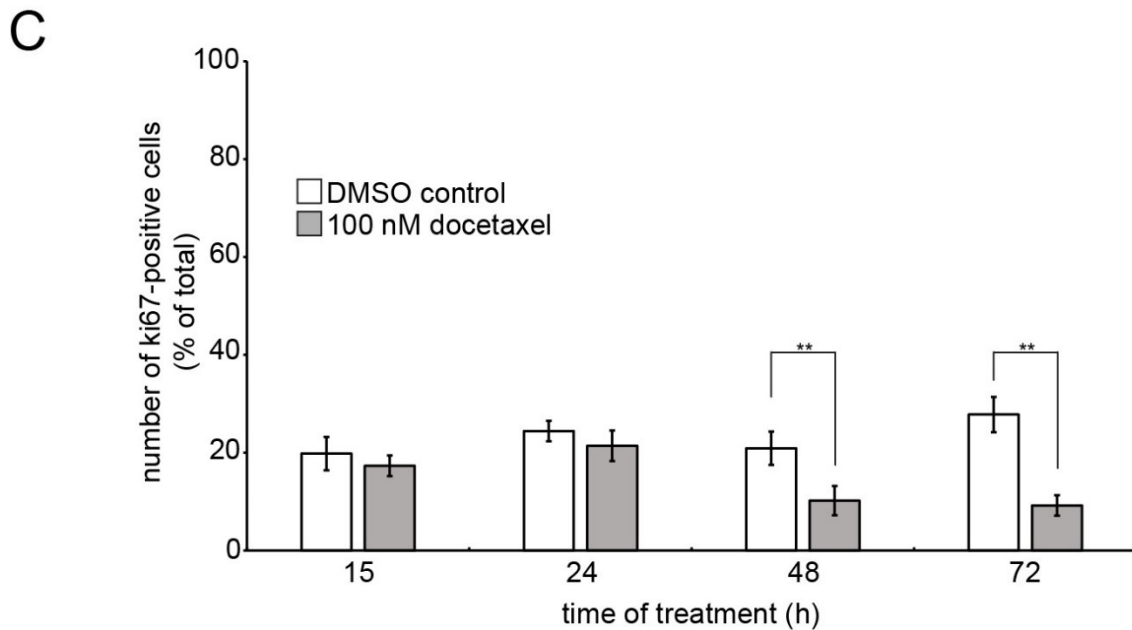control or 100 nM docetaxel for 15, 24, 48, and 72 h. Spheroids were cryosectioned into 10 µm thick slices and stained for ki67. **A and B** Representative confocal images of control (**A**) and docetaxel-treated cultures (**B**). In overlay images, ki67 fluorescent signals, SK-MEL-28, HaCaT, and nuclei are depicted in red, green, yellow, and blue, respectively. Scale bars: 100 µm. **C** Quantitative analysis of ki67-positive cells. Graph displays the amounts of ki67-positive cells as mean ± S.E.M. in percent of the whole cell count per slice with n ≥ 3 independent experiments. ANOVA was applied to calculate statistical significance with **p<0.01. For each experiment and time point, ≥ 3 spheroids were analyzed. *Adapted and modified from Klicks et al 2019 (revised revision).*

DMSO controls showed a continuous increase in the number of external melanoma cells over time (figure 23 A, table 4) and between 82.4 % ± 2.4 % (mean ± S.E.M., at 15 h) and 79.1 % ± 3.2 % (mean ± S.E.M., at 72 h) of those cells were proliferating. On the contrary, treatment with docetaxel led to an increasing loss of external SK-MEL-28 cells (figure 23 B, table 4). Interestingly, survival of internal SK-MEL-28 cells in the fibroblast core was apparently not affected by docetaxel. Since external melanoma cells represented the major source of proliferating cells in untreated tri-cultures, their selective ablation upon docetaxel treatment reduced the fraction of ki67-positive cells in the whole tri-culture from 20.9 % ± 3.4 % (mean ± S.E.M., n = 5 independent experiments, figure 23 C) to 10.2 % ± 3.0 % (mean ± S.E.M., n = 5 independent experiments, figure 23 C) after 48 h of treatment. 72 h after starting the

treatment, the difference was even higher with 27.8 % ± 3.6 % (mean ± S.E.M., n = 3 independent experiments, figure 23 C) compared to 9.2 % ± 2.1 % (mean ± S.E.M., n = 4 independent experiments, figure 23 C) in the absence and presence of docetaxel, respectively. In summary, these data prove that docetaxel affects proliferating cells, which constitute in this model primarily external melanoma cells.

Table 4: Docetaxel gradually decreased the number of external SK-MEL-28 cells.

	DMSO control	100 nM docetaxel
15 h	80.4 ± 6.6	81.1 ± 4.0
24 h	77.6 ± 6.9	58.4 ± 6.2 **
48 h	142.9 ± 20.5	33.1 ± 3.1 **
72 h	135.2 ± 1.9	19.7 ± 3.2 **

3.10 Docetaxel treatment did apparently not affect apoptosis in tri-culture spheroids

Next, the effect of docetaxel on the apoptosis of tri-culture spheroids over time was investigated. Therefore, tri-cultures were incubated with DMSO control or docetaxel as before and collected after 15, 24, 48, and 72 h of treatment. Cryosections were made and stained for cleaved caspase 3. Figure 24 A and B shows representative confocal microscopy images of spheroids treated with DMSO as control (figure 24 A) or docetaxel (figure 24 B). The overall morphology of tri-cultures with increasing numbers of external melanoma cells in the control and decreasing numbers in the docetaxel-treated samples did not change. Quantitative analysis revealed that the fraction of cleaved caspase 3-positive cells in the entire tri-culture was not altered by the treatment with docetaxel. Only at 24 h of treatment, a significant difference was observable with 68.1 % ± 6.7 % (mean ± S.E.M., n = 3 independent experiments, figure 24 C) of cleaved caspase 3-positive cells in the absence of docetaxel compared to 46.9 % ± 10.5 % (mean ± S.E.M., n = 4 independent experiments, figure 24 C) in the presence of docetaxel. This result suggests that apoptosis was either not involved in the drug response or that technical limitations of the model led to an unclear information.

C
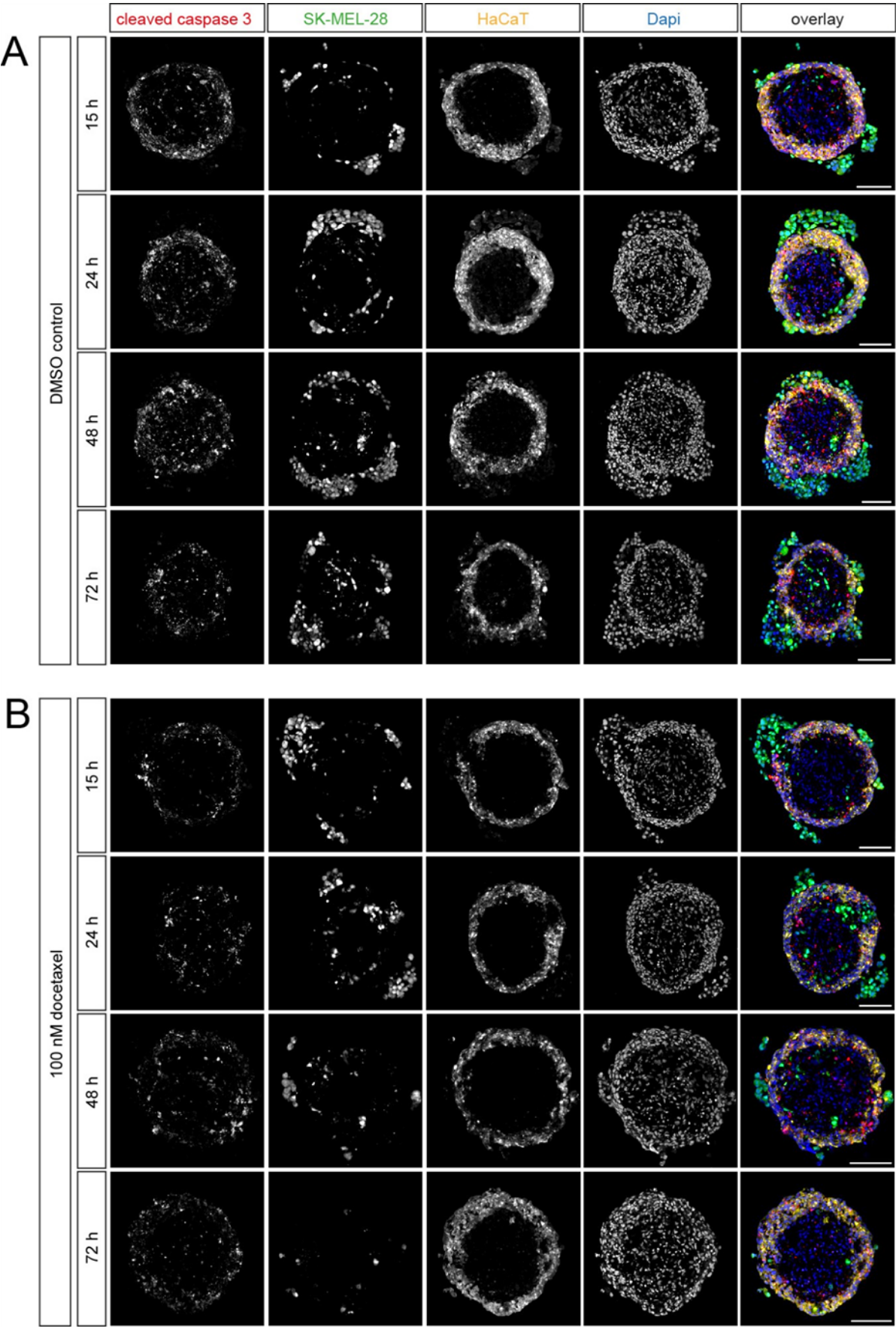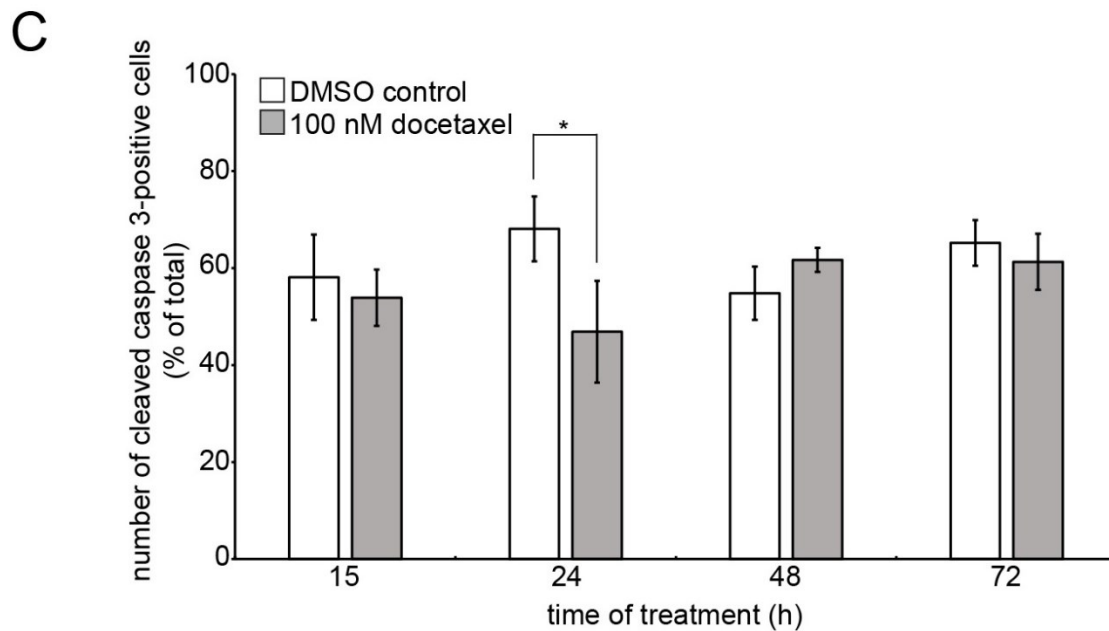
Figure 24: Docetaxel treatment did not alter apoptosis in 3D tri-culture spheroids. Tri-culture spheroids were generated by 3D cultivation of fibroblasts for three days, followed by simultaneous addition of keratinocytes and melanoma cells. HaCaT and SK-MEL-28 cells were labeled with CellTrackerRed CMPTX and CellTrackerGreen CMFDA dyes, respectively. After another two days, tri-culture spheroids were treated with 0.01 ‰ DMSO as control or 100 nM docetaxel for 15, 24, 48, and 72 h. Spheroids were cryosectioned into 10 µm thick slices and stained for cleaved caspase 3. **A and B** Representative confocal images of control (**A**) and docetaxel-treated cultures (**B**). In overlay images, cleaved caspase 3 immunostaining signals are depicted in red, SK-MEL-28 in green, HaCaT in yellow, and nuclei in blue. Scale bars: 100 µm. **C** Quantification of cleaved caspase 3-positive cells. Graph shows the amounts of cleaved caspase 3-positive cells as mean ± S.E.M. in percent of the whole cell count per slice with n ≥ 3 independent experiments and *p<0.05 according to ANOVA. For each experiment and time point, ≥ 3 spheroids were analyzed. *Adapted and modified from Klicks et al 2019 (revised revision)*.

3.11 Docetaxel-induced loss of external SK-MEL-28 cells was avoided by a modified preparation

As shown previously, docetaxel treatment of tri-culture spheroids led to an ablation of external melanoma cells. To understand why they got lost and what possibly happened to those cells, experiments using a 3D mold technique were performed. Since docetaxel might weaken cell-cell interactions, many of the affected cells might have been lost in the previous assays where tri-cultures were transferred by pipetting from the culture plates to a staining/washing place after docetaxel treatment. The use of these agarose molds should avoid this post-treatment stress to the samples. Therefore, tri-culture spheroids were first cultured as before in cell-repellent plates, but were then transferred on day five into an agarose 3D mold. Treatment with docetaxel

and all following processing steps were then carried out in these molds. Actually, the complete molds with the treated spheroids inside were embedded in OCT, cryosectioned, and slices were stained for nuclei and ki67 or cleaved caspase 3. Figure 25 A shows a comparison of representative confocal images of the tri-culture spheroids processed with the agarose mold ('with mold', left panels) and the standard transfer washing/staining station technique ('without mold', right panel). As obvious in figure 25 A, the majority of external SK-MEL-28 cells were lost or still present upon docetaxel treatment when processed without or within the molds, respectively. This was confirmed by quantitative analysis of external melanoma cells, which showed significant differences in the numbers of external melanoma cells between the two methods (figure 25 B). Upon processing without the molds, docetaxel treatment resulted in a significant decrease of the number of external SK-MEL-28 cells from 135 ± 2 to 20 ± 3 (mean ± S.E.M., n ≥ 3 independent experiments, figure 25 B). On the contrary, when processed within the molds, the number of external melanoma cells remained unchanged after docetaxel treatment (figure 25 B). Regarding the number of proliferating cells, the processing technique had only little impact. Actually, in both, with and without the mold, docetaxel treatment led to a significant reduction of the ki67-positive numbers of external melanoma cells (figure 25 C). Nevertheless, the processing was significant when addressing the fraction of apoptotic cells. Using the technique without mold, the number of cleaved caspase 3-positive external melanoma cells decreased from 59 ± 12 cells (mean ± S.E.M., n = 3 independent experiments) to 6 ± 3 cells (mean ± S.E.M., n = 4 independent experiments) in the absence versus presence of docetaxel (figure 25 D). Conversely, when processed within the molds, the number of cleaved caspase 3-positive external SK-MEL-28 cells significantly increased from 25 ± 6 (mean ± S.E.M., n = 4 independent experiments) with DMSO to 56 ± 5 (mean ± S.E.M., n = 4 independent experiments) with docetaxel (figure 25 D). In summary, these data suggest that accurate post-treatment processing is critical for the interpretation of the behavior of external melanoma cells and that both, a reduced proliferation and increased apoptosis, is induced by docetaxel treatment. Moreover, docetaxel-induced apoptosis can, at least to some extent, explain the loss of external melanoma cells in the tri-culture model.
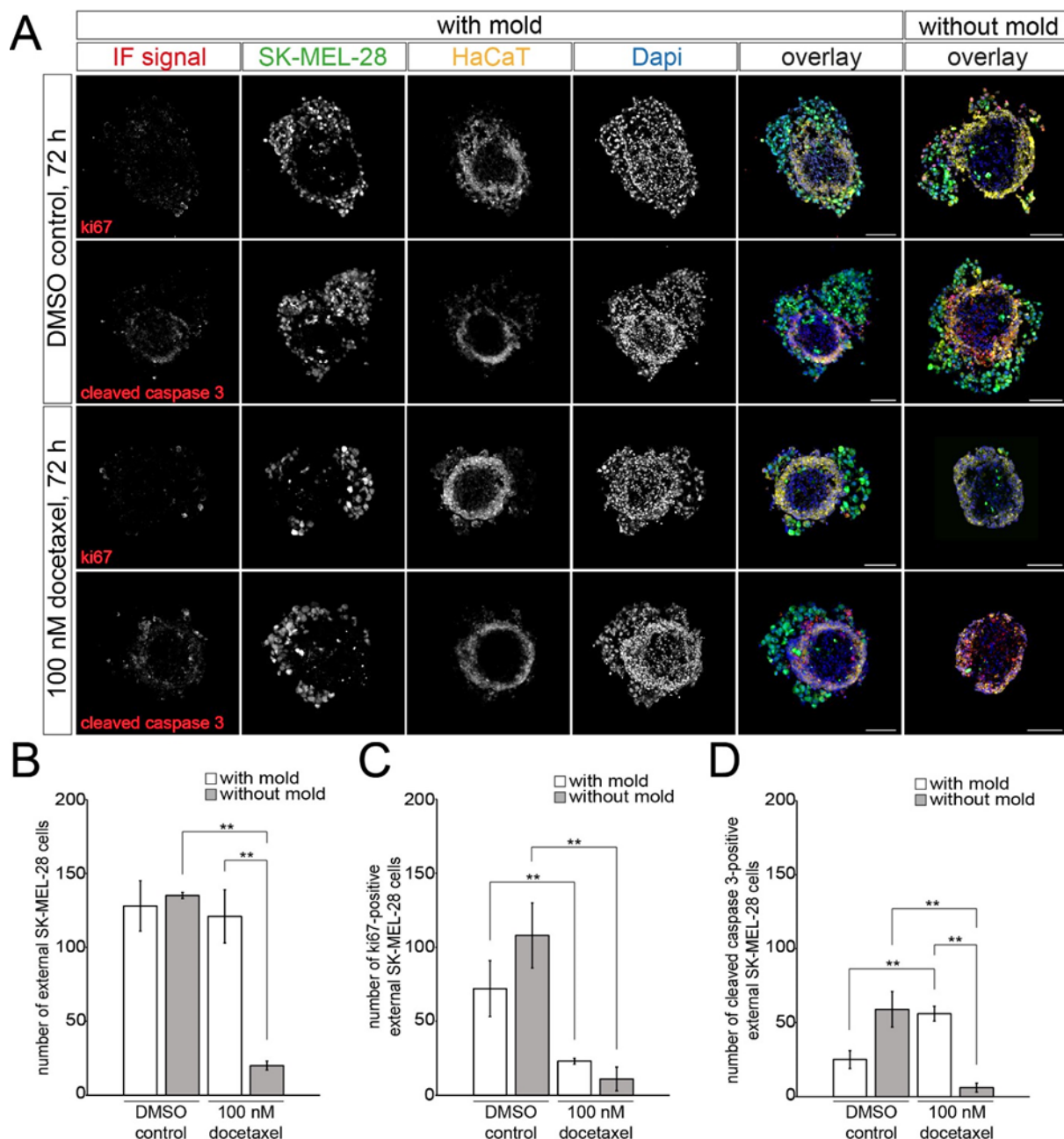
Figure 25: Processing of tri-cultures in special agarose molds led to a docetaxel-induced increase of apoptosis and reduction of proliferation of external melanoma cells. Tri-culture spheroids were made by 3D cultivation of fibroblasts for three days, followed by the simultaneous addition of keratinocytes and melanoma cells. HaCaT cells were labeled with CellTrackerRed CMPTX dye and SK-MEL-28 cells with CellTrackerGreen CMFDA dye. For the mold technique, spheroids were transferred on day five into 3D agarose molds and treated with 0.01 ‰ DMSO as control or 100 nM docetaxel in DMSO for 72 h. Spheroids in the mold were then cryosectioned into 20 µm and spheroids without the mold into 10 µm thick slices, and stained for either ki67 or cleaved caspase 3 as indicated (**A**). Scale bars: 100 µm. **B-D** Quantitative analysis of total numbers of external SK-MEL-28 cells (**B**), as well as amounts of ki67- (**C**) and cleaved caspase 3-positive external SK-MEL-28 cells (**D**) of tri-culture spheroids processed with or without mold. Graph shows mean ± S.E.M. with n ≥ 3 independent experiments. Statistical significance was probed using ANOVA (**p<0.01). For each experiment, ≥ 3 spheroids were analyzed. *Adapted and modified from Klicks et al 2019 (revised revision).*

3.12 Docetaxel treatment of tri-culture spheroids restored differentiation of keratinocytes

In order to address previous findings, in which neoplastic cells in human malignant melanoma biopsies where found to hamper keratinocyte differentiation [228], in our 3D-melanoma model, we stained cryosections of tri-culture spheroids with an antibody against ck10 in the absence and presence of docetaxel. Figure 26 A and B shows representative confocal images of these samples. In the DMSO-treated spheroids, an increase in the number of external SK-MEL-28 cells as well as a constant low level of the keratinocyte differentiation marker ck10 were observed during the experiment time course (figure 26 A). Remarkably, treatment with docetaxel resulted in a restoration of ck10 expression that occurred in parallel to the ablation/apoptosis of external melanoma cells (figure 26 B). Quantitative analysis revealed that the number of peripheral ck10-positive cells was significantly higher in the docetaxel treated spheroids as compared to the controls, starting after 24 h of treatment until the end of the observation period (figure 26 C). Treated tri-culture spheroids reached a number of ck10-positive cells of 36 % ± 5 % (mean ± S.E.M., n = 4 independent experiments, figure 26 C). Overall, these results suggest that the tri-culture model is able to reflect effects of melanoma cells on keratinocyte differentiation as observed in human disease and that such loss of differentiation can be restored by treatment with docetaxel.
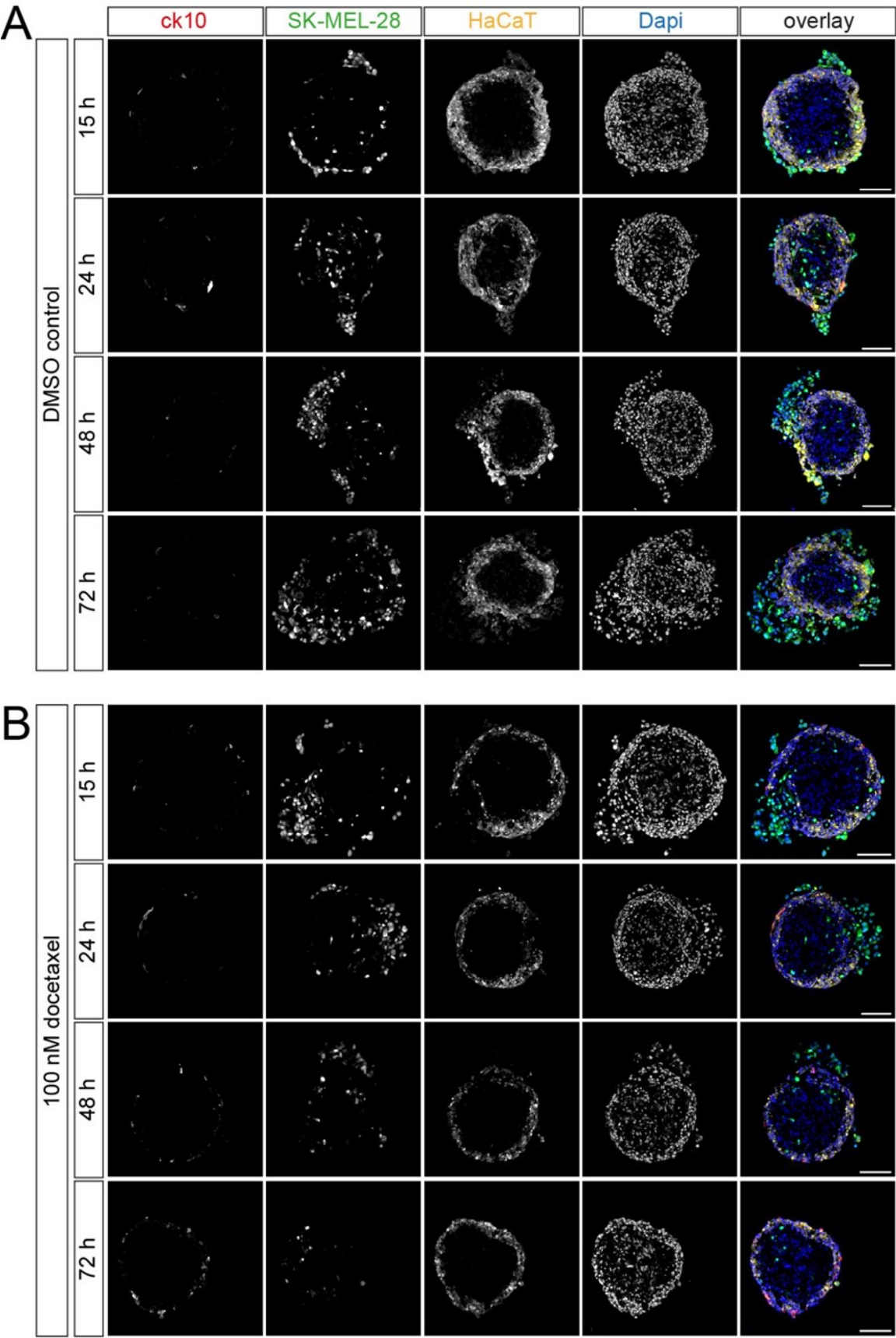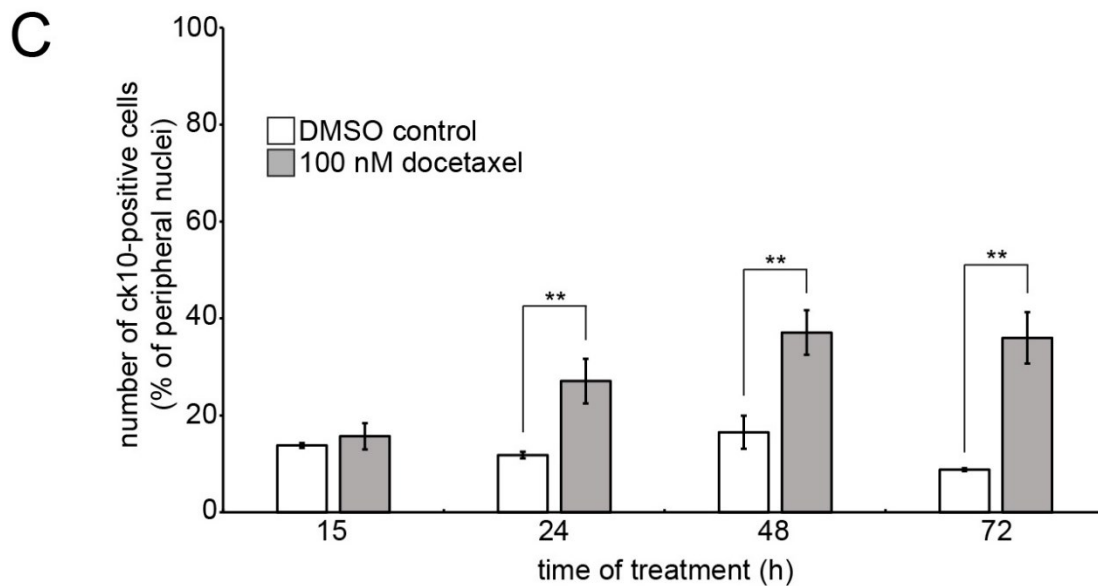
Figure 26: Melanoma cells weakened the expression of the keratinocyte differentiation marker ck10. Tri-culture spheroids were produced by 3D cultivation of fibroblasts for three days, followed by the simultaneous addition of HaCaT and SK-MEL-28 cells. HaCaT and SK-MEL-28 cells were labeled with CellTrackerRed CMPTX dye and CellTrackerGreen CMFDA, respectively. Another two days later, tri-culture spheroids were treated with 0.01 ‰ DMSO as control or 100 nM docetaxel for 15, 24, 48, and 72 h. Spheroids were cryosectioned into 10 µm thick slices and stained for ck10. **A and B** Representative confocal sections of control (**A**) and docetaxel-treated spheroids (**B**). In overlay images, ck10 immunostaining signals, SK-MEL-28, HaCaT, and nuclei are depicted in red, green, yellow, and blue, respectively. Scale bars: 100 µm. **C** Quantification of ck10-positive cells. Graph displays the amounts of ck10-positive cells as mean ± S.E.M. in percent of the peripheral nuclei per slice with n ≥ 3 independent experiments. Significance was tested using ANOVA (**$p < 0.01$). For each experiment and time point, ≥ 3 spheroids were analyzed. *Adapted and modified from Klicks et al 2019 (revised revision).*

3.13 Docetaxel treatment led to enhanced ABCB5-signals in external melanoma cells

Bearing in mind that ABCB5 is capable of inducing multidrug resistance for doxorubicin and temozolomide in melanoma cells [130,133], a correlation between ABCB5 expression and melanoma cell survival to drug treatment was also tested in the tri-culture model. Thus, tri-cultures were incubated with 100 nM docetaxel or DMSO for 48 h, fixed, sliced, and then immunostained for ABCB5 with m3C2-1D12 [133] primary antibody. As described in figure 27 A-F, melanoma cells as well as keratinocytes were the major source that showed ABCB5 immunoreactivity. Quantitative analysis revealed a rise in the number of external melanoma cells with high ABCB5 immunofluorescence intensity upon drug treatment (figure 27 G), while internal melanoma cells were apparently unaffected in this sense (figure 27 H). Interestingly, also keratinocytes were found to exhibit an increased ABCB5 staining upon docetaxel treatment (figure 27 B and E).

DMSO control, 48 h

100 nM docetaxel, 48 h

A

D

B

Dapi

HaCaT

E

Dapi

HaCaT

SK-MEL-28

ABCB5

SK-MEL-28

ABCB5

C

F
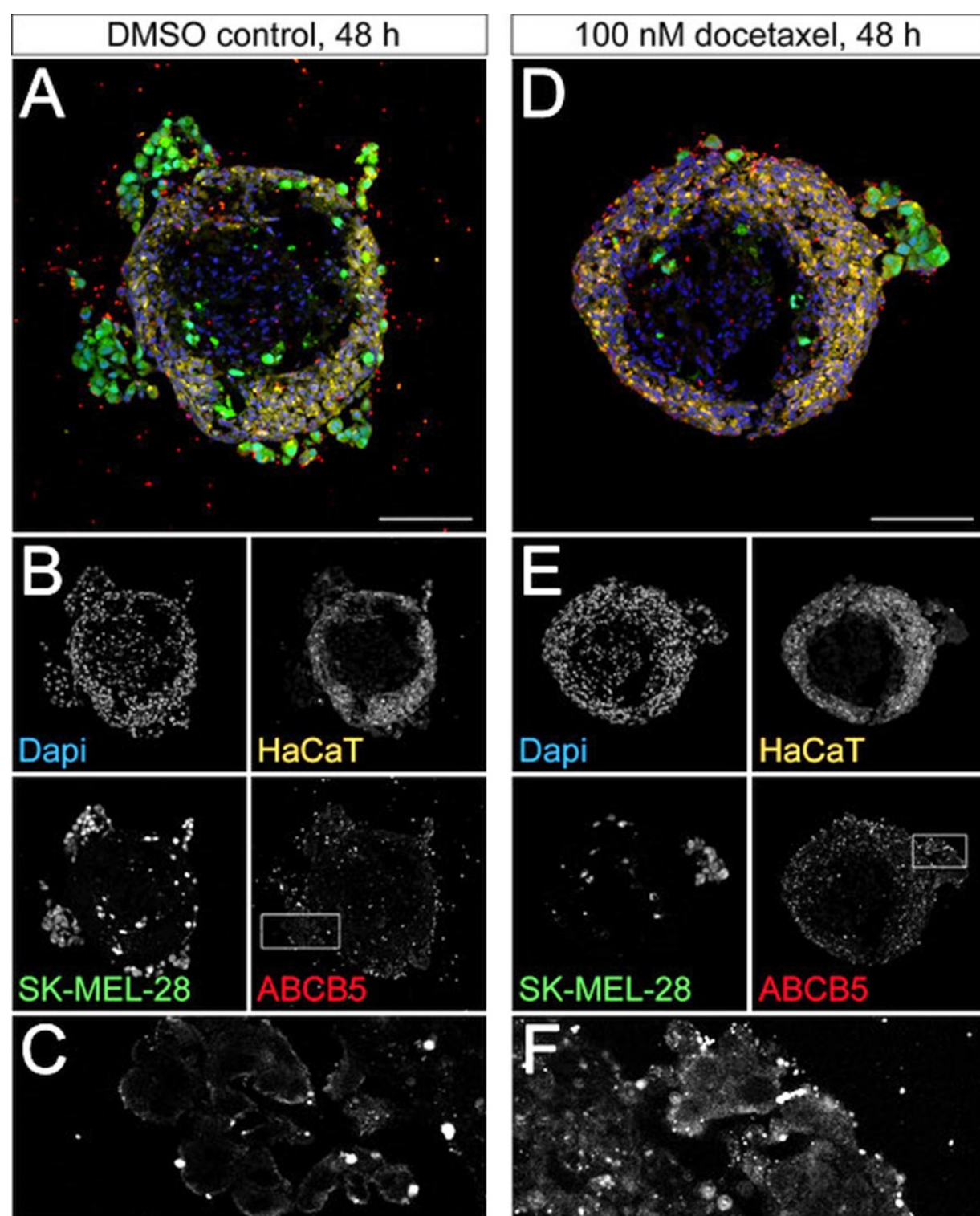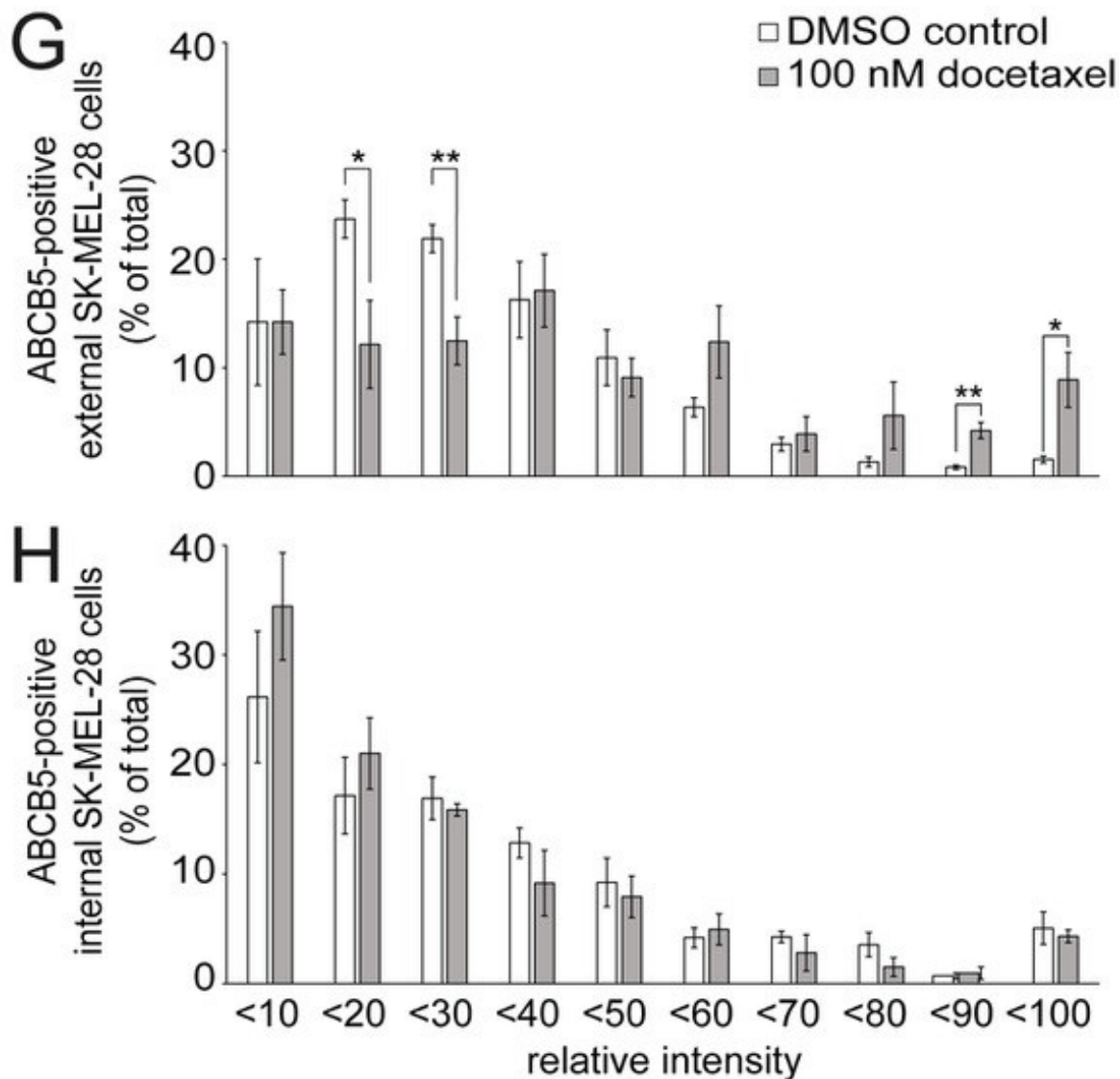
Figure 27: Docetaxel treatment augmented ABCB5-signals in keratinocytes and external melanoma cells. Tri-culture spheroids were generated by 3D cultivation of fibroblasts for three days, followed by the combined addition of keratinocytes and melanoma cells. HaCaT keratinocytes were labeled with CellTrackerRed CMPTX dye and SK-MEL-28 melanoma cells with CellTrackerGreen CMFDA dye. After additional two days, tri-culture spheroids were treated with 0.01 ‰ DMSO as control (**A-C**) or 100 nM docetaxel in DMSO (**D-F**) for 48 h. Spheroids were cryosectioned into 10 µm thick slices and stained with an antibody against ABCB5 from the company TICEBA GmbH. **A and D** Overlay images of the confocal sections shown in B and E. In overlays, ABCB5 signals are depicted in red, SK-MEL-28 cells in green, HaCaT cells in yellow, and nuclei in blue. Scale bars: 100 µm. **C and F** Detail images of ABCB5 stainings from boxed regions in B and E. **G and H** Quantitative analysis of the relative intensity of ABCB5-positive external (**G**) and internal (**H**) SK-MEL-28 cells in percentage of total. Given is mean ± S.E.M. with n = 4 independent experiments, *p<0.05, and **p<0.01 according to ANOVA. For each experiment, ≥ 3 spheroids were analyzed. *Adapted from Klicks et al 2019 (revised revision).*

This observation with a drug-induced enrichment of strongly ABCB5-positive external SK-MEL-28 and HaCaT cells and the lack of effect on internal melanoma cells was

similarly confirmed by another anti-ABCB5 antibody (figure 28). Altogether, these data display either a docetaxel-induced enhancement of ABCB5 expression in weakly expressing cells or a selection of cells with high ABCB5 immunofluorescence.
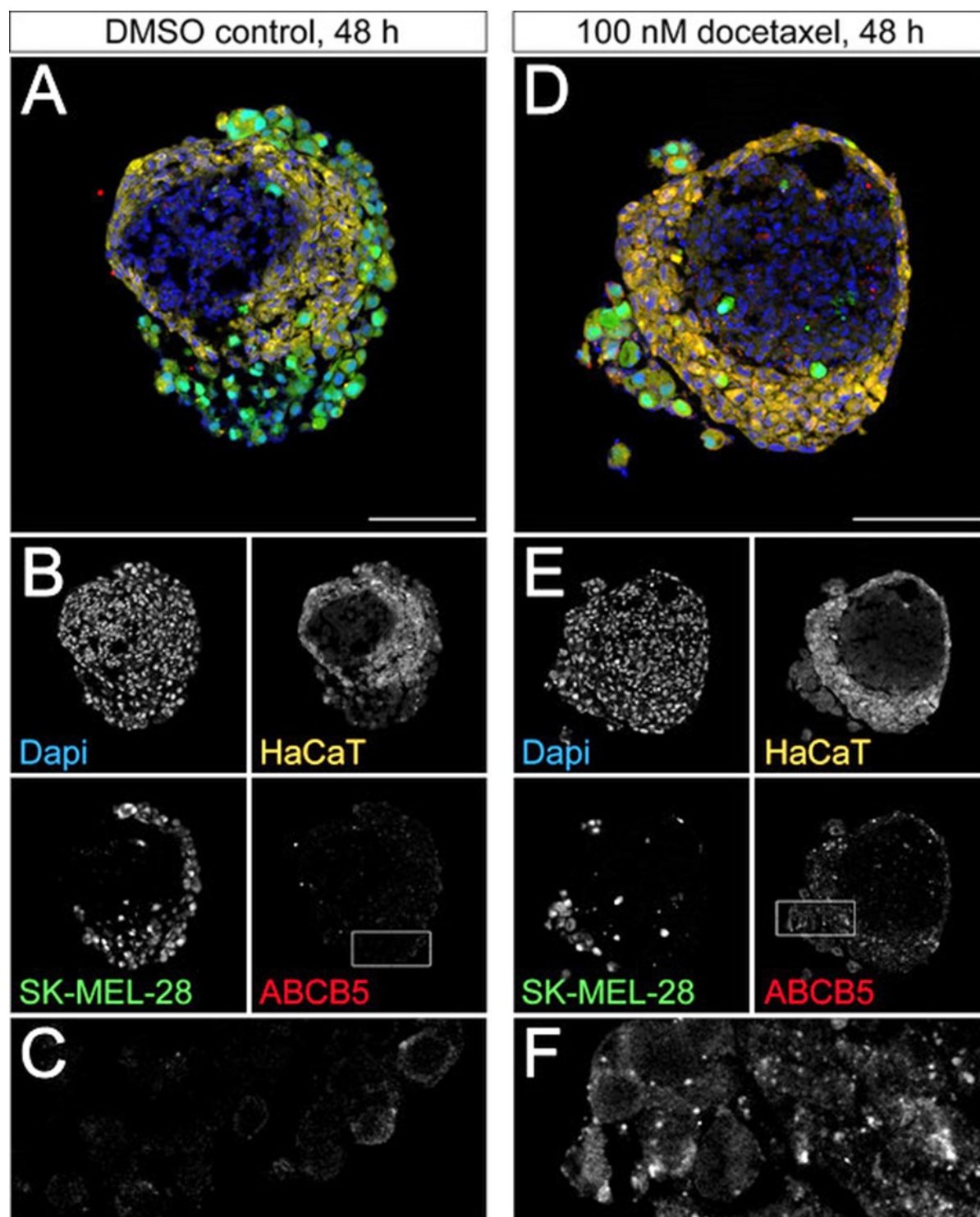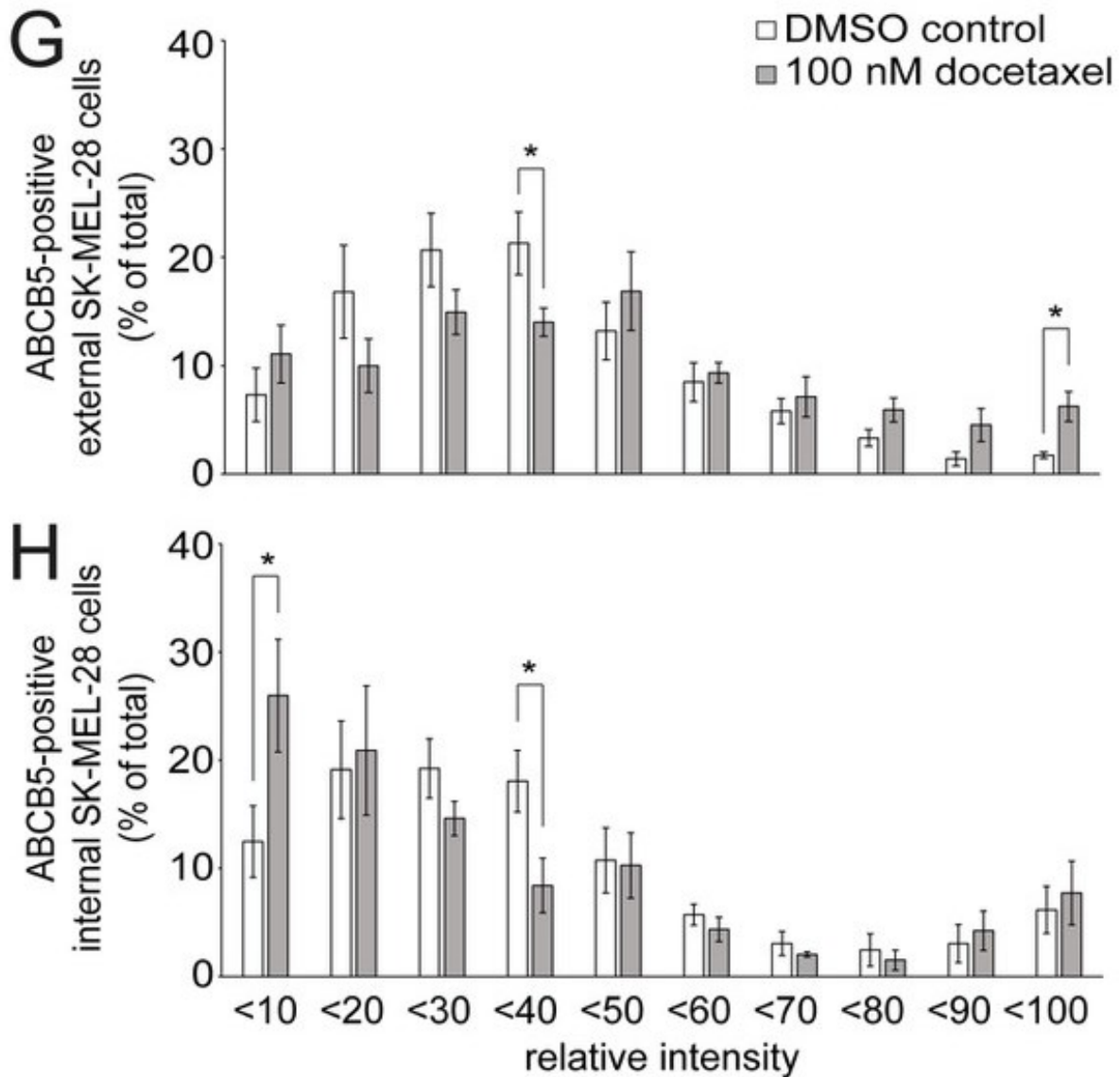
Figure 28: Enrichment of ABCB5-levels in keratinocytes and external melanoma cells upon docetaxel treatment was confirmed by another anti-ABCB5 antibody. Tri-culture spheroids were made by 3D cultivation of CCD-1137Sk cells for three days, followed by the joint addition of HaCaT and SK-MEL-28 cells. HaCaT cells were labeled with CellTrackerRed CMPTX dye and SK-MEL-28 cells with CellTrackerGreen CMFDA dye. Another two days later, tri-culture spheroids were treated with 0.01 ‰ DMSO as control (**A-C**) or 100 nM docetaxel in DMSO (**D-F**) for 48 h. Spheroids were cryosectioned into 10 µm thick slices and stained for ABCB5 (MA5-17026). **A and D** Overlay images of the confocal sections shown in B and E. In overlays, ABCB5 signals, melanoma cells, keratinocytes, and nuclei are represented in red, green, yellow, and blue, respectively. Scale bars: 100 µm. **C and F** Detail images of ABCB5 stainings from boxed regions in B and E. **G and H** Quantitative analysis of the relative intensity of ABCB5-positive external (**G**) and internal (**H**) SK-MEL-28 cells in percentage of total. Given is mean ± S.E.M. with n = 4 independent experiments and *$p < 0.05$ according to ANOVA. For each experiment, ≥ 3 spheroids were analyzed. *Adapted from Klicks et al 2019 (revised revision).*

3.14 Western Blot analysis of melanoma tri-culture largely confirmed immunofluorescence results

Finally, we aimed to confirm/corroborate the immunostaining data on proliferation, apoptosis, and differentiation of tri-cultures by Western Blot analysis. For this, tri-culture spheroids were cultivated as before and treated with DMSO as control or docetaxel. After harvesting, spheroids were homogenized and lysates were subsequently subjected to Western Blot analysis. Using an ABCB5 antibody (figure 29 A and B) expression levels were found to remain constant in both conditions, while cleaved caspase 3 was upregulated upon docetaxel treatment (figure 29 A and B). The analysis of proliferation using a PCNA antibody showed a decrease when treated with docetaxel (figure 29 A and B). Furthermore, expression profiles showed a significant increase in ck10 upon docetaxel treatment (figure 29 B). Thus, apart from ABCB5, all parameters tested here largely reflected the outcomes of the immunofluorescence staining.
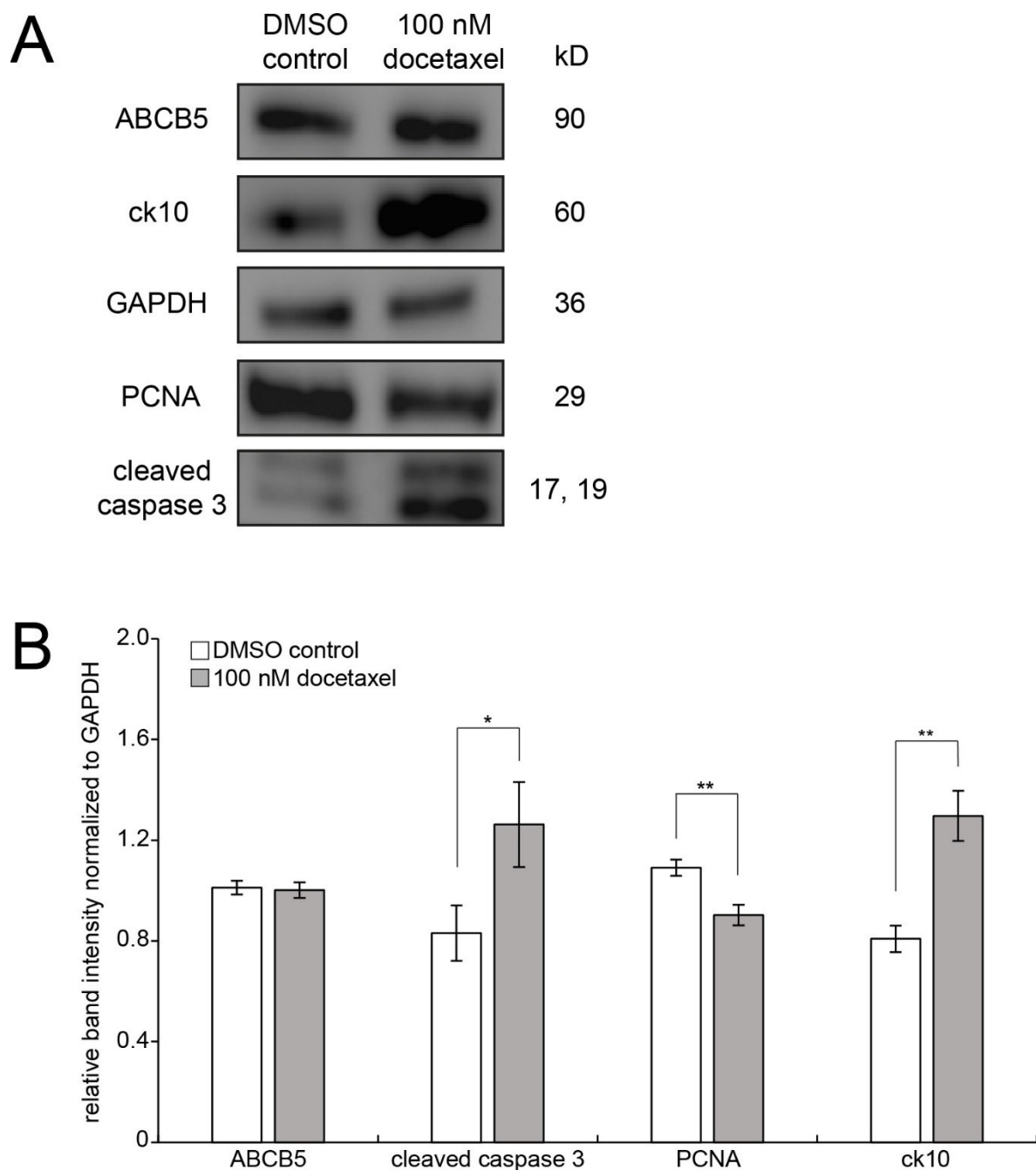
Figure 29: Expression profiles of melanoma tri-cultures largely confirmed immunofluorescence outcomes. Tri-culture spheroids were generated by 3D cultivation of fibroblasts for three days, followed by the simultaneous addition of HaCaT and SK-MEL-28 cells. HaCaT cells were labeled with CellTrackerRed CMPTX dye and SK-MEL-28 cells with CellTrackerGreen CMFDA dye. Another two days later, tri-culture spheroids were treated with 0.01 ‰ DMSO as control or 100 nM docetaxel in DMSO for 48 h. **A** After harvesting the spheroids, lysates were prepared and equal amounts of substrate were loaded on SDS-PAGE for Western Blot analysis with detection of ABCB5, cleaved caspase 3, PCNA, and ck10. **B** Relative intensity of respective bands for ABCB5, cleaved caspase 3, PCNA, and ck10 were measured and normalized to internal GAPDH loading control. Given is mean ± S.E.M. from three independent experimental sets with statistical significance probed using ANOVA (*$p<0.05$; **$p<0.01$).

4 DISCUSSION

3D *in vitro* models are increasingly becoming more and more the preferred choice for researchers and pharma companies to study drug efficacy and mode of action as well as drug combinations. Compared to traditional 2D cell cultures, 3D models are thought to better mimic numerous parameters that are critical for the behavior of cancer cells. Such parameters include cell-cell interactions, oxygen and nutrient gradients, distribution of waste products, substrate stiffness, as well as drug diffusion [122]. Currently, several 3D models exist that are either simple and allow high-throughput, or they are complex and function to mirror the *in vivo* situation or be useful for personalized medicine [49,122,141,148,211,229–233]. The present study aimed to set up a 3D model for early stage melanoma to investigate a series of drug-induced processes in a quantitative and cell-type specific manner. In addition, its performance should be simple, fast, and reproducible. Hence, an easy to handle spheroid-based system was established composed of melanoma cells, human fibroblasts and keratinocytes, the latter two being the major components of a stroma-like environment. In order to avoid batch-to-batch variability and achieve a cost effective system, the established cell lines SK-MEL-28, HaCaT, and CCD-1137Sk fibroblasts were used. To identify generalizable features for 3D culture of neoplastic and normal cells, the prostate cancer cell lines LNCaP and PC-3 were used in addition.

4.1 3D cultivation of stromal, skin, and cancer cells decreased proliferation and simultaneously increased apoptosis compared to 2D cultures

Cells grown under 2D conditions are equally exposed to medium allowing constant oxygen and nutrient supply and removal of waste products [19] (table 5). Presumably, this largely explained that all cell lines used in this study were highly proliferative in 2D cultures with almost no apoptotic cells (figure 12-17). Conversely, cells cultured under 3D conditions are unevenly exposed to nutrients and oxygen (table 5). While cells on the periphery of the 3D structure exhibit most access to nutrients and oxygen and, hence, appear to be proliferative, cells inside the 3D architecture are excluded from this leading to quiescent and necrotic cells (figure 13-17). Gene and protein expression of cells in 2D cultures often display differential levels compared to *in vivo* models. Conversely, 3D models exhibit more similar profiles to the *in vivo* tissue origins concerning this characteristic (table 5).

Table 5: Key differences of 2D and 3D cell cultures (Adapted and modified from Edmondson et al 2014)

Characteristics	2D	3D
Morphology	Flat and stretched cells as monolayer	Natural shape in a 3D architecture
Proliferation	Often faster than *in vivo*	Faster/slower compared to cells cultured in 2D depending on cell type and 3D model
Exposure to medium and drugs	Equally exposed	Medium and drugs may not be able to fully penetrate the 3D structure
Stage of cell cycle	Cells are more likely to be in the same stage	Spheroids are composed of proliferating, quiescent, hypoxic, and necrotic cells
Gene/protein expression	Often different to *in vivo* models	More similar to *in vivo* tissue
Drug sensitivity	Appear to be very sensitive	More resistant compared to 2D cultures, often being more predictive to *in vivo* drug responses

The major difference between normal, non-tumorigenic cells and neoplastic cells is their cell division. Cells divide to form new tissue or to replace old and damaged cells in a highly regulated manner mediated by a complex set of chemical processes. In neoplastic cells, these signals do not exist anymore and cells divide in an uncontrollable way [234]. This feature was also reflected in our study. Spheroids of normal cells, like fibroblasts and keratinocytes, decreased in size over time (figure 10) and exhibited only few proliferating cells (figure 12 and 19 A). Conversely, spheroids of neoplastic cells, like SK-MEL-28, LNCaP and PC-3 cells, increased in size over time (figure 11) and displayed more proliferating cells compared to non-tumorigenic cells (figure 13 and 14). Since fibroblasts are the principal cellular components of connective tissues, maintenance of balance between fibroblast proliferation and differentiation is essential for skin homeostasis [235]. Fibroblasts are activated by skin injury, migrate into damaged tissue and proliferate [236]. Accordingly, proliferation rate is lowered in healthy skin. This finding was reflected in this study by 3D cultivation of CCD-1137Sk fibroblasts. Spheroids were sparsely proliferating at the periphery (figure 19 A). Instead, their volume decreased over time and they got more compact (figure 10 B and B`). Suggesting that oxygen and nutrients did not penetrate the spheroid sufficiently

and waste products could not be removed, apoptotic cells were found to be equally distributed inside the spheroid (figure 19 B). Contrary to the *in vivo* situation, in which basal keratinocytes renew and proliferate to upper layers [44], 3D cultivation of HaCaT cells yielded only few proliferating cells on the periphery of spheroids and between the cavities of Dynarrays where cells were able to grow as monolayer (figure 12). Similar to fibroblast spheroids, the volume of HaCaT spheroids decreased and they got densely packed (figure 10 A and A`) resulting in numerous apoptotic cells throughout the spheroid diameter (figure 15 A and 19 B). Comparing spheroids and Dynarrays, which can be cultivated in a bioreactor allowing continuous flow of medium, the amount of ki67-positive cells did not change (figure 12). However, spheroids displayed higher numbers of apoptotic cells compared to Dynarrays (figure 15). This might be explained by less cell density on Dynarrays. Even co-culturing of HaCaT cells with fibroblasts, which is known to enhance proliferation of keratinocytes [237], did not improve proliferation of HaCaT cells in spheroids. Actually, the number of ki67-positive cells was significantly reduced (figure 19 D). This suggests that 3D cultivation of HaCaT cells as spheroids and on Dynarrays is not appropriate to investigate proliferation and apoptosis of keratinocytes. In contrast, 3D cultivation of cancer cells, like melanoma and prostate cancer, reflects the *in vivo* situation more closely than 2D cultures. Spheroids as well as Dynarrays produced 3D structures with proliferating cells at the periphery and apoptotic cells in the core (figure 13-14 and 16-17) similar to *in vivo* tumors [144,238]. Consequently, spheroids of cancer cells are increasing in size over time [224,239] (figure 11). While the amount of proliferating melanoma cells in spheroids compared to Dynarrays did not differ (figure 13), SK-MEL-28 cells showed more apoptotic cells on Dynarrays compared to spheroids (figure 16) even though Dynarrays were cultivated with superfusion allowing constant nutrient and oxygen supply. This suggests that 3D cultivation in a microfluidic device does not improve survival of cells in that case.

4.2 3D skin and melanoma model reflected stratification of keratinocytes and melanoma-induced loss of keratinocyte differentiation

Concerning keratinocyte differentiation, the 3D skin model presented in this study is very promising. Usually, optimal differentiation of keratinocytes *in vitro* leading to human skin equivalents requires the use of primary cells and multiple external factors like pH and Ca^{2+} gradients as well as air liquid interface [49,230,232]. Since the

implementation of this external control is very time consuming and difficult to perform in high amounts, this was avoided and HaCaT cells were allowed to automatically stratify in monoculture spheroids as well as on top of a fibroblast core (figure 18 and 19 C). Indeed, a partial differentiation with ck14-expressing lower strata and ck10-expressing upper strata was observed. However, our skin model lacked a cornified layer. Compared to HSE models, which involves generation times of several weeks [155], the spheroid-based melanoma tri-culture was already complete for further studies after seven days. It is an open question, whether the observed stratification was achieved by differentiation of HaCaT cells or if pre-differentiated keratinocytes migrated to the outer rim of the spheroid. Nevertheless, a surprising discovery was made regarding keratinocyte differentiation, which is also known from human melanoma. Actually, it was reported that melanoma cells influence the differentiation pattern of human epidermal keratinocytes *in vivo* leading to a loss of ck10 in hyperplastic regions [228]. Accordingly, melanoma cells decreased ck10 expression of HaCaT cells in the 3D tri-culture model (figure 20 and 26). Particularly, such loss of ck10 expression was predominantly found in direct contact with melanoma cells and was restored upon treatment with docetaxel leading to apoptosis of external melanoma cells (figure 26 and 29).

4.3   3D melanoma tri-culture spheroids presented two populations of melanoma cells

One more interesting feature was observed in the presented model, i.e. the division of melanoma cells into external and internal cells. The observation of SK-MEL-28 cells inside the fibroblast core suggests their invasion ability and fits to the fact that this cell line is from the metastatic phase of melanoma [229] and thus known to migrate quickly downwards through the skin [240]. Hence, this melanoma tri-culture model could be used as a simple test system to examine antimigratory effects of various drugs. Besides this future application, it was fascinating to observe different behaviors of the two melanoma cell populations. The first difference was that external melanoma cells were located at the outside of the spheroid in direct contact to keratinocytes. Furthermore, they aggregated to growing clusters. In contrast, internal melanoma cells were found in the fibroblast core and were usually separated from each other not merging (figure 20). One day after the simultaneous addition of HaCaT and SK-MEL-28 cells, melanoma cells were still embedded in the keratinocyte ring. The following day, they were already found rarely in the HaCaT ring, but always in the fibroblast core

(figure 21). The second difference that was visible between internal and external melanoma cells was the effect of docetaxel on those cells. External cells were extremely apoptotic and lost cell-cell interactions, whereas internal cells showed apparently no response to docetaxel. The number of internal melanoma cells remained unchanged even after 72 h of treatment with docetaxel. Their relative amounts of proliferating and apoptotic cells were unchanged. It is not clear whether such uneven behavior was caused by a limited diffusion of the drug into the spheroid or rather by cell-specific variances. It could well be that only drug-resistant cell subpopulations were able to invade the fibroblast core. This characteristic is regularly found in malignant melanoma [241]. Another explanation could be that this drug insensitivity was triggered by some cellular signaling within the core. Anyway, it was fascinating to detect that docetaxel affected proliferation and apoptosis exclusively in melanoma cells and not in keratinocytes or fibroblasts. The last difference between external and internal melanoma cells was according to their expression of the ATP-dependent transporter protein, ABCB5. It was observed that docetaxel led to higher ABCB5 immunofluorescence signals in external but not in internal melanoma cells (figure 27 and 28). This does not mean that internal melanoma cells were unable to increase ABCB5 expression. Differently than expected, they showed lower ABCB5 signals upon docetaxel treatment than before treatment. Again, this loss of drug-induced changes in gene expression could be explained by internal melanoma cells representing a special subpopulation of cells, insufficient penetration of the drug, or disturbance of the local environment. However, the effect of docetaxel on ABCB5 signals observed in external melanoma cells is consistent with an up-regulation of ABCB5 in weakly expressing cells or a selection of strongly expressing cells. Overall, these results match previous studies that described an enhanced ABCB5 expression in malignant melanoma [242], the functional role of ABCB5 in tumor growth [243,244], and the selection of ABCB5-expressing cells upon chemotherapy [130]. However, the enhanced expression of ABCB5 upon docetaxel treatment was not confirmed by Western Blot analysis (figure 29). Here, the expression profile remained unchanged. A reason for this could be the difference in harvesting the samples. Tri-culture spheroids for immunofluorescence analysis were transferred after docetaxel treatment and washed leading to loss of external melanoma cells. In contrast, tri-culture spheroids for Western Blot analysis were collected and completely lysed. In this step, no cells got lost. The hypothesis is that in DMSO treated control spheroids there are many ABCB5-low

external melanoma cells, while in the docetaxel treated spheroids there are only few ABCB5-high external melanoma cells but much more apoptotic cells that lost ABCB5 expression. Thus, these apoptotic cells compensated the few ABCB5-high cells that were seen in immunofluorescence.

4.4 Docetaxel presented a classical agent against melanoma cells

Since the tri-culture spheroids should serve as a model system to study drug candidates, the cytostatic drug, docetaxel, was tested as a test substance. Even if MAPK pathway inhibitors like the approved BRAF inhibitor vemurafenib [117,118] and immunotherapies against CTLA-4 like ipilimumab [121] and PD-1 [122,123] substituted traditional alkylating and cytostatic chemotherapeutics as first-line therapy, the mitotic inhibitor paclitaxel and its derivative docetaxel [245] are still used as adjuvant treatments [124,126,127]. Moreover, they are probed for their use in innovative drugs [226,227,246,247]. Up to now, the here presented model lacks immune cells. Therefore, immunotherapies were not taken into consideration. Although the addition of T-cells and other immune cells is an interesting and possible aspect in the future, this study focused on the response of melanoma cells to a classical agent and its effect on melanoma chemoresistance. Significant effects on external melanoma cell survival were detected after 48 h at 100 nM of docetaxel. Hence, this drug concentration was used in all experiments. In contrast, docetaxel reached a higher effect in 2D cultures of SK-MEL-28 cells (figure 22). This is consistent with previous studies, which reported that docetaxel had a maximal effect on different melanoma cell lines grown in 2D at around 10-20 nM [248] and a changed sensitivity of cells cultured in 2D and 3D in general [249–251].

4.5 3D tri-culture model has beneficial aspects compared to other systems

Other 3D melanoma spheroid models such as the liquid overlay technique [147] are only made of one cell type, the melanoma cells. Therefore, they do not represent the stromal environment of a tumor. This aspect is fulfilled in the 3D tri-culture model of this study by the insert of fibroblasts and keratinocytes. More complex HSE models are often produced by seeding primary fibroblasts in collagen type I followed by the combined addition of primary keratinocytes and melanoma cells [252] or by embedding primary fibroblasts together with melanoma cells in the collagen I matrix [155]. Both methods spontaneously formed melanoma nests leading to variations in number and

sizes of such nests between individual skin reconstructs. Consequently, quantitative validation of these models and prediction of therapeutic impacts are often difficult. In comparison, the presented tri-culture model always generated very similar spheroids with highly reproducible organization of the different cell types. This allowed reliable quantification of drug effects on specific cells. Skin-on-a-chip devices have the advantage of a controlled perfusion of growth factors and nutrients [196]. This cannot be performed in a static system like the melanoma tri-culture spheroid. Abaci and colleagues demonstrated on their skin-on-a-chip platform that the cancer drug doxorubicin may have direct toxic effects on the proliferation and differentiation of keratinocytes [253]. Still, this method is not appropriate for high-throughput screening. Here, a simple spheroid-based model might be more suitable. Since the melanoma tri-culture spheroid model contains stroma as well as tumor cells, it can be used to assess general cell toxicity of a drug by examining the effect on the neighboring non-cancerous cells [254].

4.6 Post-treatment processing was essential for the interpretation of cell behavior

It was obvious that treatment with docetaxel led to a loss of external melanoma cells in tri-culture spheroids (figure 20 B). However, this happened due to the transfer of spheroids after treatment from cell-repellent plates to another place for washing and embedding (figure 25). If this transfer was avoided which means that docetaxel treatment as well as washing and embedding was performed at the same place, apparently all cells, dead and alive, were still present within close proximity to the spheroid (figure 25). It cannot be excluded that the different cell numbers were caused by distinct effect of the drug in the agarose mold versus the plastic plate. However, the most straightforward explanation seems to be that most of the external melanoma cells became loose in response to drug treatment and were lost during the transfer from the plates to the washing place due to mechanical shear stress (figure 30). Given that this treatment-induced loss of cells might also happen in other spheroids and organoids, this finding might be interesting for a broad range of researchers. In case of analyzing either culture size, cell number, or amount of proliferating and apoptotic cells, this influence could lead to incorrect data interpretations.
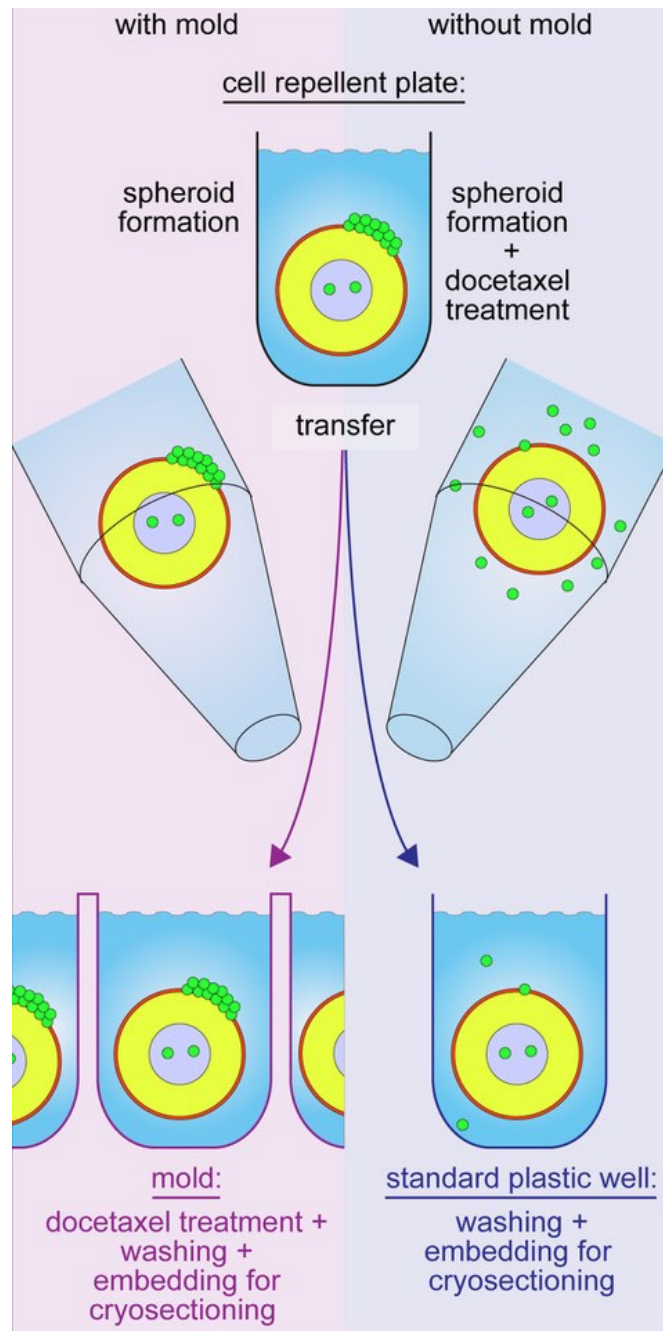
Figure 30: Transfer of tri-culture spheroids after docetaxel treatment led to immense loss of external melanoma cells. Scheme depicts proposed way of losing external SK-MEL-28 cells in response to docetaxel treatment. Spheroid formation was performed in cell-repellent plates. Typically, they were also treated inside the plates and then transferred to another place for washing and embedding. In mold experiments, spheroids were transferred to agarose molds prior treatment with docetaxel. Washing, embedding, and cryosectioning were then carried out in these molds. *Adapted and modified from Klicks et al 2019 (revised revision)*.

4.7 Conclusion

The present work describes a novel, simple spheroid-based melanoma tri-culture model composed of fibroblasts, keratinocytes, and melanoma cells. This model mimicked characteristics found in early stages of melanoma, with loss of keratinocyte differentiation, melanoma cell invasion, and drug-induced selection of ABCB5-expressing cells. A future approach might be the complementation of this system by the addition of further cell types like immune or primary cells to further expand the applicability of such model for screening drug candidates and their mode of action.

5   SUMMARY

Melanoma is the most common form of cancer. Thus, test systems for the development of new drugs and therapies are required that resemble the *in vivo* situation. Currently, most cell-based assays are performed in two-dimensional (2D) cell cultures. While cells cultured in 2D monolayers appear to be flat and stretched allowing for equal exposure to medium and drugs, three-dimensional (3D) structures of cells are more realistic to the *in vivo* situation displaying cells of varying stages of the cell cycle, i.e. proliferating cells on the periphery of the 3D structure, followed by quiescent and necrotic cells in the center. Several 3D cell culture approaches that exhibit varying degrees of complexity have been developed to perform drug testing and mechanistic studies on melanoma. Although 3D cell culture systems of melanoma are superior to traditional 2D approaches, these 3D cultures are either composed of only one cell type, the melanoma cells, or they are so complex that it is challenging to understand the behavior of individual cell types. Additionally, they are often difficult to establish and expensive. Therefore, this work aimed to establish a novel, simple, spheroid-based melanoma model. This study used low-attachment plates to generate spheroids that are composed of up to three different cell types, i.e. stromal, skin, and cancer cells. To study differences in culture conditions and behavior of normal and neoplastic cells, 3D cultures of these cell types were compared. 3D cultivation revealed decreasing volume sizes of normal cells, fibroblasts and keratinocytes, with only few proliferating cells on the periphery of the spheroids. In contrast, neoplastic cells, SK-MEL-28, LNCaP, and PC-3 cells, displayed increasing volume sizes with proliferating cells on the outside of the spheroids. All tested cell types showed a significant reduction of proliferation with a concurrent rise of apoptosis in 3D compared to 2D cultures. The presented tri-culture model allowed the study of cellular behavior in a cell-type specific way and represented different features of early melanoma stages. Fibroblasts formed a collagen IV rich center of the tri-culture spheroid, keratinocytes built up a ring around this center, and melanoma cells arranged highly proliferating clusters on the outside. Some melanoma cells were also found regularly in the fibroblast core. In the absence of melanoma cells, keratinocytes stratified into an inner basal-like ring and more differentiated cells on the periphery. In contrast, addition of melanoma cells clearly reduced keratinocyte differentiation. Upon treatment with the cytostatic drug, docetaxel, this keratinocyte differentiation was restored and apoptosis of external melanoma cells was induced.

Furthermore, docetaxel treatment significantly increased the amount of immunoreactivity to the transporter protein ABCB5 in remaining intact external melanoma cells. Taken together, a novel, simple, spheroid-based melanoma tri-culture model composed of fibroblasts, keratinocytes, and melanoma cells was described. This can now be applied for the development of new drugs and the analysis of their cell-type specific mode of action.

6 ZUSAMMENFASSUNG

Das Melanom, besser bekannt als schwarzer Hautkrebs, ist die häufigste Krebsart. Daher besteht der Bedarf nach einem *in vivo* nahen Testsystem für die Entwicklung neuer Medikamente und Therapien. Derzeit werden die meisten zellbasierten Untersuchungen mit Hilfe der zweidimensionalen (2D) Zellkultur durchgeführt. Zellen, die als 2D Einzelschicht kultiviert werden, sehen phänotypisch flach und gestreckt aus, wohingegen im lebenden Organismus Zellen in einem dreidimensionalen (3D) Verbund wachsen. Dies hat zur Folge, dass in der 2D Zellkultur eine gleichmäßige Exposition zu Medium und Medikamenten vorliegt, welche nicht der *in vivo* Situation entspricht. Zudem zeigen 3D kultivierte Zellen unterschiedliche Stadien des Zellzyklus, das heißt proliferierende Zellen an der Peripherie der 3D Struktur, gefolgt von ruhenden und nekrotischen Zellen im Zentrum. Es wurden bereits einige 3D Zellkulturkonzepte unterschiedlicher Komplexität für Arzneimittelprüfungen und mechanistische Untersuchungen an Melanomen entwickelt. Obwohl 3D Zellkultursysteme von Melanomen den traditionellen 2D Methoden überlegen sind, bestehen bisherige 3D Systeme entweder nur aus einem Zelltyp, den Melanomzellen, oder sind so komplex, dass es schwierig ist, das Verhalten einzelner Zelltypen zu verstehen. Zusätzlich sind diese komplexen 3D Systeme oft schwer zu etablieren und teuer. Daher ist das Ziel dieser Arbeit, ein neuartiges, einfaches, sphäroidbasiertes Melanommodell zu etablieren. Für die Herstellung der Sphäroide wurden beschichtete Platten verwendet, die ein Anheften der Zellen verhindern. In diese wurden bis zu drei verschiedene Zelltypen, Stroma-, Haut- und Krebszellen, ausgesät. Um Unterschiede in den Kultivierungsbedingungen und dem Verhalten von normalen und neoplastischen Zellen zu untersuchen, wurden 3D Kulturen dieser Zelltypen miteinander verglichen. Die 3D Kultivierung ergab einen reduzierten Umfang der Sphäroide von normalen Zellen, Fibroblasten und Keratinozyten, mit nur wenigen proliferierenden Zellen an der Peripherie der Sphäroide. Dagegen präsentierten neoplastische Zellen, SK-MEL-28, LNCaP und PC-3 Zellen, eine zunehmende Größe der Sphäroide mit proliferierenden Zellen an deren Außenseite. In 3D Monokulturen zeigten alle getesteten Zelltypen eine signifikante Abnahme der Proliferation mit gleichzeitigem Anstieg an Apoptose im Vergleich zu 2D. Mit Hilfe des hier vorgestellten Trikulturmodells war es möglich, das zelluläre Verhalten von Stroma-, Haut- und Krebszellen zelltypspezifisch zu untersuchen. Das Trikulturmodell repräsentiert hierbei

ein frühes Melanomstadium. Fibroblasten bildeten ein Kollagen IV-reiches Zentrum im Trikultursphäroid, wohingegen Keratinozyten sich zu einem Ring um dieses Zentrum ansammelten und Melanomzellen sich zu proliferierenden Clustern an der Außenseite anordneten. Einige Melanomzellen wurden auch regelmäßig im Fibroblastenkern beobachtet. In Abwesenheit der Melanomzellen stratifizierten die Keratinozyten zu einem inneren basalähnlichen Ring und stärker differenzierten Zellen an der Peripherie. Dagegen reduzierte die Zugabe von Melanomzellen deutlich die Differenzierung der Keratinozyten. Die Behandlung mit dem Zytostatikum Docetaxel stellte diese Differenzierung der Keratinozyten wieder her und induzierte Apoptose in den externen Melanomzellclustern. Darüber hinaus erhöhte die Docetaxelbehandlung erheblich den Umfang der Immunreaktivität auf das Transporterprotein ABCB5 in den verbliebenen, unbeschädigten, externen Melanomzellen. Zusammenfassend wurde ein neuartiges, einfaches, sphäroidbasiertes Melanomtrikulturmodell beschrieben, welches aus Fibroblasten, Keratinozyten und Melanomzellen besteht. Dieses kann nun zur Entwicklung neuer Wirkstoffe und zur Analyse der zelltypspezifischen Wirkungsweise verwendet werden.

7 REFERENCES

1. Birgersdotter A, Sandberg R, Ernberg I: Gene expression perturbation in vitro - A growing case for three-dimensional (3D) culture systems. Semin. Cancer Biol. 2005

2. Bhadriraju K, Chen CS: Engineering cellular microenvironments to improve cell-based drug testing. Drug Discov. Today. 2002

3. DiMasi JA, Grabowski HG: Economics of new oncology drug development. J. Clin. Oncol. 2007

4. Breslin S, O'Driscoll L: Three-dimensional cell culture: The missing link in drug discovery. *Drug Discov. Today* [Internet] 18: 240–249, 2013 Available from: http://dx.doi.org/10.1016/j.drudis.2012.10.003

5. Hopkins AL: Network pharmacology: The next paradigm in drug discovery. Nat. Chem. Biol. 2008

6. Kola I: The state of innovation in drug development. Clin. Pharmacol. Ther. 2008

7. Lancaster MA, Knoblich JA: Organogenesis in a dish: Modeling development and disease using organoid technologies. *Science (80-.).* [Internet] 345: 1247125–1247125, 2014 Available from: http://www.sciencemag.org/cgi/doi/10.1126/science.1247125

8. Yin X, Mead BE, Safaee H, Langer R, Karp JM, Levy O: Engineering Stem Cell Organoids. Cell Stem Cell. 2016

9. Kaur G, Dufour JM: Cell lines. Valuable tools or useless artifacts. *Spermatogenesis* 2012

10. Breslin S, O'Driscoll L: Three-dimensional cell culture: The missing link in drug discovery. Drug Discov. Today. 2013

11. Gurski LA, Petrelli NJ, Jia X, Farach-Carson MC: 3D Matrices for Anti-Cancer Drug Testing and Development. *Oncol. Issues* 2010

12. Tibbitt MW, Anseth KS: Hydrogels as extracellular matrix mimics for 3D cell culture. Biotechnol. Bioeng. 2009

13. Rimann M, Graf-Hausner U: Synthetic 3D multicellular systems for drug development. Curr. Opin. Biotechnol. 2012

14. Mehta G, Hsiao AY, Ingram M, Luker GD, Takayama S: Opportunities and challenges for use of tumor spheroids as models to test drug delivery and efficacy. *J. Control. Release* 2012

15. Friedrich J, Seidel C, Ebner R, Kunz-Schughart LA: Spheroid-based drug screen: Considerations and practical approach. *Nat. Protoc.* 2009

16. Harrison RG: Observations on the river developing nerve fiber. *Anat Rec* 1907

17. Foty R: A Simple Hanging Drop Cell Culture Protocol for Generation of 3D Spheroids. *J. Vis. Exp.* 2011

18. Kelm JM, Timmins NE, Brown CJ, Fussenegger M, Nielsen LK: Method for generation of homogeneous multicellular tumor spheroids applicable to a wide variety of cell types. *Biotechnol. Bioeng.* 2003

19. Edmondson R, Broglie JJ, Adcock AF, Yang L: Three-Dimensional Cell Culture Systems and Their Applications in Drug Discovery and Cell-Based Biosensors. *Assay Drug Dev. Technol.* 2014

20. van Duinen V, Trietsch SJ, Joore J, Vulto P, Hankemeier T: Microfluidic 3D cell culture: from tools to tissue models. *Curr Opin Biotechnol* [Internet] 35: 118–126, 2015 Available from: http://www.ncbi.nlm.nih.gov/pubmed/26094109

21. Jeong SY, Lee JH, Shin Y, Chung S, Kuh HJ: Co-culture of tumor spheroids and fibroblasts in a collagen matrix-incorporated microfluidic chip mimics reciprocal

activation in solid tumor microenvironment. *PLoS One* 2016

22. Ataç B, Wagner I, Horland R, Lauster R, Marx U, Tonevitsky AG, Azar RP, Lindner G: Skin and hair on-a-chip: in vitro skin models versus ex vivo tissue maintenance with dynamic perfusion. *Lab Chip* [Internet] 13: 3555, 2013 Available from: http://xlink.rsc.org/?DOI=c3lc50227a

23. Wagner I, Materne E-M, Brincker S, Süßbier U, Frädrich C, Busek M, Sonntag F, Sakharov DA, Trushkin E V., Tonevitsky AG, Lauster R, Marx U: A dynamic multi-organ-chip for long-term cultivation and substance testing proven by 3D human liver and skin tissue co-culture. *Lab Chip* [Internet] 13: 3538, 2013 Available from: http://xlink.rsc.org/?DOI=c3lc50234a

24. Schimek K, Busek M, Brincker S, Groth B, Hoffmann S, Lauster R, Lindner G, Lorenz A, Menzel U, Sonntag F, Walles H, Marx U, Horland R: Integrating biological vasculature into a multi-organ-chip microsystem. *Lab Chip* 2013

25. Baker BM, Trappmann B, Stapleton SC, Toro E, Chen CS: Microfluidics embedded within extracellular matrix to define vascular architectures and pattern diffusive gradients. *Lab Chip* 2013

26. Polacheck WJ, German AE, Mammoto A, Ingber DE, Kamm RD: Mechanotransduction of fluid stresses governs 3D cell migration. *Proc. Natl. Acad. Sci.* 2014

27. Altmann B, L??chner A, Swain M, Kohal RJ, Giselbrecht S, Gottwald E, Steinberg T, Tomakidi P: Differences in morphogenesis of 3D cultured primary human osteoblasts under static and microfluidic growth conditions. *Biomaterials* [Internet] 35: 3208–3219, 2014 Available from: http://dx.doi.org/10.1016/j.biomaterials.2013.12.088

28. Wang M, Zhao J, Zhang L, Wei F, Lian Y, Wu Y, Gong Z, Zhang S, Zhou J, Cao K, Li X, Xiong W, Li G, Zeng Z, Guo C: Role of tumor microenvironment in tumorigenesis. J. Cancer. 2017

29. Whiteside TL: The tumor microenvironment and its role in promoting tumor growth. Oncogene. 2008

30. Lovitt C, Shelper T, Avery V: Advanced Cell Culture Techniques for Cancer Drug Discovery. *Biology (Basel).* 2014

31. Dhiman HK, Ray AR, Panda AK: Three-dimensional chitosan scaffold-based MCF-7 cell culture for the determination of the cytotoxicity of tamoxifen. *Biomaterials* 2005

32. Horning JL, Sahoo SK, Vijayaraghavalu S, Dimitrijevic S, Vasir JK, Jain TK, Panda AK, Labhasetwar V: 3-D tumor model for in vitro evaluation of anticancer drugs. *Mol. Pharm.* 2008

33. Barbone D, Yang TM, Morgan JR, Gaudino G, Broaddus VC: Mammalian target of rapamycin contributes to the acquired apoptotic resistance of human mesothelioma multicellular spheroids. *J. Biol. Chem.* 2008

34. Howes AL, Chiang GG, Lang ES, Ho CB, Powis G, Vuori K, Abraham RT: The phosphatidylinositol 3-kinase inhibitor, PX-866, is a potent inhibitor of cancer cell motility and growth in three-dimensional cultures. *Mol. Cancer Ther.* 2007

35. Frankel A, Man S, Elliott P, Adams J, Kerbel RS: Lack of multicellular drug resistance observed in human ovarian and prostate carcinoma treated with the proteasome inhibitor PS-341. *Clin. Cancer Res.* 2000

36. Pickl M, Ries CH: Comparison of 3D and 2D tumor models reveals enhanced HER2 activation in 3D associated with an increased response to trastuzumab. *Oncogene* 2009

37. Breitkreutz D, Mirancea N, Nischt R: Basement membranes in skin: Unique matrix structures with diverse functions? *Histochem. Cell Biol.* 132: 1–10, 2009

38. Klicks J, von Molitor E, Ertongur-Fauth T, Rudolf R, Hafner M: In vitro skin three-dimensional models and their applications. *J. Cell. Biotechnol.* 2017

39. Hayward MG, Keatinge WR: Roles of subcutaneous fat and thermoregulatory reflexes in determining ability to stabilize body temperature in water. *J. Physiol.* 1981

40. Purves D, Augustine GJ, Fitzpatrick D, Katz LC, LaMantia A-S, McNamara JO, Williams SM: Mechanoreceptors Specialized to Receive Tactile Information. *Neuroscience,* 2001

41. Kouklis PD, Hutton E, Fuchs E: Making a connection: Direct binding between keratin intermediate filaments and desmosomal proteins. *J. Cell Biol.* 1994

42. Andrä K, Kornacker I, Jörgl A, Zörer M, Spazierer D, Fuchs P, Fischer I, Wiche G: Plectin-isoform-specific rescue of hemidesmosomal defects in plectin (-/-) keratinocytes. *J. Invest. Dermatol.* 2003

43. Haines RL, Lane EB: Keratins and disease at a glance. *J. Cell Sci.* [Internet] 125: 3923–3928, 2012 Available from: http://jcs.biologists.org/cgi/doi/10.1242/jcs.099655

44. Denecker G, Ovaere P, Vandenabeele P, Declercq W: Caspase-14 reveals its secrets. J. Cell Biol. 2008

45. Candi E, Schmidt R, Melino G: The cornified envelope: A model of cell death in the skin. Nat. Rev. Mol. Cell Biol. 2005

46. Rinnerthaler M, Streubel MK, Bischof J, Richter K: Skin aging, gene expression and calcium. *Exp. Gerontol.* [Internet] 68: 59–65, 2015 Available from: http://dx.doi.org/10.1016/j.exger.2014.09.015

47. Breiden B, Sandhoff K: The role of sphingolipid metabolism in cutaneous permeabilitybarrier formation. *Biochim. Biophys. Acta - Mol. Cell Biol. Lipids* [Internet] 1841: 441–452, 2014 Available from: http://dx.doi.org/10.1016/j.bbalip.2013.08.010

48. Menon GK, Cleary GW, Lane ME: The structure and function of the stratum corneum. Int. J. Pharm. 2012

49. Borowiec AS, Delcourt P, Dewailly E, Bidaux G: Optimal Differentiation of In Vitro Keratinocytes Requires Multifactorial External Control. *PLoS One* 8: 1–15, 2013

50. Nguyen V, Ndoye A, Hall L: Programmed cell death of keratinocytes culminates in apoptotic secretion of a humectant upon secretagogue action of acetylcholine. *J. Cell Sci.* [Internet] 114: 1189–1204, 2001 Available from: http://jcs.biologists.org/content/114/6/1189.short

51. Yousef H, Sharma S: Anatomy, Skin (Integument), Epidermis.

52. Fuchs E, Green H: Changes in keratin gene expression during terminal differentiation of the keratinocyte. *Cell* 19: 1033–1042, 1980

53. Freedberg IM, Tomic-Canic M, Komine M, Blumenberg M: Keratins and the keratinocyte activation cycle. *J. Invest. Dermatol.* [Internet] 116: 633–640, 2001 Available from: http://dx.doi.org/10.1046/j.1523-1747.2001.01327.x

54. Moll R, Divo M, Langbein L: The human keratins: Biology and pathology. *Histochem. Cell Biol.* 129: 705–733, 2008

55. Woodcock-Mitchell J, Eichner R, Nelson WG, Sun TT: Immunolocalization of keratin polypeptides in human epidermis using monoclonal antibodies. *J. Cell Biol.* 1982

56. Kim S, Wong P, Coulombe PA: A keratin cytoskeletal protein regulates protein synthesis and epithelial cell growth. *Nature* 441: 362–365, 2006

57. Rice RH, Green H: Presence in human epidermal cells of a soluble protein precursor of the cross-linked envelope: Activation of the cross-linking by calcium ions. *Cell* 1979

58. Mehrel T, Hohl D, Rothnagel JA, Longley MA, Bundman D, Cheng C, Lichti U, Bisher ME, Steven AC, Steinert PM, Yuspa SH, Roop DR: Identification of a major keratinocyte cell envelope protein, loricrin. *Cell* 1990

59. DALE BA, RESING KA, LONSDALE-ECCLES JD: Filaggrin: A Keratin Filament Associated Protein. *Ann. N. Y. Acad. Sci.* 1985

60. McLean WHI: Filaggrin failure – from ichthyosis vulgaris to atopic eczema and beyond. Br. J. Dermatol. 2016

61. Scholzen T, Gerdes J: The Ki-67 protein: From the known and the unknown. J. Cell. Physiol. 2000

62. Juríková M, Danihel Ľ, Polák Š, Varga I: Ki67, PCNA, and MCM proteins: Markers of proliferation in the diagnosis of breast cancer. Acta Histochem. 2016

63. Purba TS, Brunken L, Hawkshaw NJ, Peake M, Hardman J, Paus R: A primer for studying cell cycle dynamics of the human hair follicle. Exp. Dermatol. 2016

64. Tewari M, Quan Lt, O'Rourke K, Desnoyers S, Zeng Z, Beidler Dr, Poirier Gg, Salvesen Gs, Dixit Vm: Yama/CPP32 beta, a mammalian homolog of CED 3, is a CrmA inhibitable protease that cleaves the death substrate poly(ADP ribose) polymerase. *Cell* 1995

65. Shalini S, Dorstyn L, Dawar S, Kumar S: Old, new and emerging functions of caspases. Cell Death Differ. 2015

66. Krueger JG, Bowcock A: Psoriasis pathophysiology: Current concepts of pathogenesis. *Ann. Rheum. Dis.* 64: 30–36, 2005

67. Yang L, Fan X, Cui T, Dang E, Wang G: Nrf2 Promotes Keratinocyte Proliferation in Psoriasis through Up-Regulation of Keratin 6, Keratin 16, and Keratin 17. *J. Invest. Dermatol.* 2017

68. Thewes M, Stadler R, Korge B, Mischke D: Normal psoriatic epidermis expression of hyperproliferation-associated keratins. *Arch. Dermatol. Res.* 1991

69. Nourshargh S, Larkin S, Das A, Williams T: Interleukin-1-induced leukocyte extravasation across rat mesenteric microvessels is mediated by platelet-activating factor. *Blood* 1995

70. Komine M, Freedberg IM, Blumenberg M: Regulation of epidermal expression of keratin K17 in inflammatory skin diseases. *J. Invest. Dermatol.* 1996

71. Wikner NE, Persichitte KA, Baskin JB, Nielsen LD, Clark RAF: Transforming growth factor-β stimulates the expression of fibronectin by human keratinocytes. *J. Invest. Dermatol.* 1988

72. Vollberg TM, George MD, Jetten AM: Induction of extracellular matrix gene expression in normal human keratinocytes by transforming growth factor β is altered by cellular differentiation. *Exp. Cell Res.* 193: 93–100, 1991

73. Ryynanen J, Sollberg S, Olsen DR, Uitto J: Transforming growth factor-β up-regulates type VII collagen gene expression in normal and transformed epidermal keratinocytes in culture. *Biochem. Biophys. Res. Commun.* 1991

74. Konig A, Bruckner-Tuderman L: Transforming growth factor-β stimulates collagen VII expression by cutaneous cells in vitro. In: *Journal of Cell Biology*, 1992

75. Jiang CK, Tomic-Canic M, Lucas DJ, Simon M, Blumenberg M: TGFβ promotes the basal phenotype of epidermal keratinocytes: Transcriptional induction of k#5 and k#14 keratin genes. *Growth Factors* 1995

76. Yamaguchi Y, Hearing VJ: Melanocytes and their diseases. *Cold Spring Harb. Perspect. Med.* 2014

77. Simon JD, Peles D, Wakamatsu K, Ito S: Current challenges in understanding melanogenesis: Bridging chemistry, biological control, morphology, and function. Pigment Cell Melanoma Res. 2009

78. Kondo T, Hearing VJ: Update on the regulation of mammalian melanocyte function and skin pigmentation. Expert Rev. Dermatol. 2011

79. Hearing VJ: Determination of Melanin Synthetic Pathways. *J. Invest. Dermatol.* [Internet] 131: E8–E11, 2011 Available from: http://linkinghub.elsevier.com/retrieve/pii/S0022202X15610363

80. Cichorek M, Wachulska M, Stasiewicz A, Tymińska A: Skin melanocytes: Biology and development. *Postep. Dermatologii i Alergol.* 2013

81. Tachibana M: Sound needs sound melanocytes to be heard. Pigment Cell Res. 1999

82. Yaar M, Park HY: Melanocytes: A window into the nervous system. J. Invest. Dermatol. 2012

83. Brito FC, Kos L: Timeline and distribution of melanocyte precursors in the mouse heart. *Pigment Cell Melanoma Res.* 2008

84. Hwang H, Liu F, Petrenko NB, Huang J, Schillinger KJ, Patel V V.: Cardiac melanocytes influence atrial reactive oxygen species involved with electrical and structural remodeling in mice. *Physiol. Rep.* 2015

85. Hu DN, Simon JD, Sarna T: Role of ocular melanin in ophthalmic physiology and pathology. Photochem. Photobiol. 2008

86. Zecca L, Tampellini D, Gerlach M, Riederer P, Fariello RG, Sulzer D: Substantia nigra neuromelanin: structure, synthesis, and molecular behaviour. *Mol. Pathol.* 2001

87. Randhawa M, Huff T, Valencia JC, Younossi Z, Chandhoke V, Hearing VJ, Baranova A: Evidence for the ectopic synthesis of melanin in human adipose tissue. *FASEB J.* 2009

88. Jimbow K, Quevedo WC, Fitzpatrick TB, Szabo G: Some aspects of melanin biology: 1950-1975. J. Invest. Dermatol. 1976

89. Hoath SB, Leahy DG: The Organization of Human Epidermis: Functional Epidermal Units and Phi Proportionality. *J. Invest. Dermatol.* 2003

90. Haass NK, Smalley KSM, Li L, Herlyn M: Adhesion, migration and communication in melanocytes and melanoma. Pigment Cell Res. 2005

91. Haass NK, Smalley KSM, Herlyn M: The role of altered cell-cell communication in melanoma progression. J. Mol. Histol. 2004

92. Haass NK, Herlyn M: Normal human melanocyte homeostasis as a paradigm for understanding melanoma. J. Investig. Dermatol. Symp. Proc. 2005

93. Nesbit M, Herlyn M: Adhesion receptors in human melanoma progression. *Invasion Metastasis* 1994

94. Hsu MY, Meier FE, Nesbit M, Hsu JY, Van Belle P, Elder DE, Herlyn M: E-cadherin expression in melanoma cells restores keratinocyte-mediated growth control and down-regulates expression of invasion-related adhesion receptors. *Am. J. Pathol.* 2000

95. Shih IM, Speicher D, Hsu MY, Levine E, Herlyn M: Melanoma cell-cell interactions are mediated through heterophilic Mel- CAM/ligand adhesion. *Cancer Res.* 1997

96. Kraus A, Masat L, Johnson JP: Analysis of the expression of intercellular adhesion molecule-1 and MUC18 on benign and malignant melanocytic lesions using monoclonal antibodies directed against distinct epitopes and recognizing denatured, non-glycosylated antigen. *Melanoma Res.* 1997

97. Lehmann JM, Riethmüller G, Johnson JP: MUC18, a marker of tumor progression in human melanoma, shows sequence similarity to the neural cell adhesion molecules of the immunoglobulin superfamily. *Proc. Natl. Acad. Sci. U. S. A.* 1989

98. Shih IM, Elder DE, Johnson JP: Isolation and Functional Characterization of the A32 Melanoma-associated Antigen. *Cancer Res.* 1994

99. Satyamoorthy K, Muyrers J, Meier F, Patel D, Herlyn M: Mel-CAM-specific genetic suppressor elements inhibit melanoma growth and invasion through loss of gap junctional communication. *Oncogene* 2001

100. Montgomery AMP, Becker JC, Siu CH, Lemmon VP, Cheresh DA, Pancook JD, Zhao X, Reisfeld RA: Human neural cell adhesion molecule L1 and rat homologue NILE are ligands for integrin $\alpha v\beta 3$. *J. Cell Biol.* 1996

101. Voura EB, Ramjeesingh RA, Montgomery AMP, Siu C-H: Involvement of Integrin alpha vbeta 3 and Cell Adhesion Molecule L1 in Transendothelial Migration of Melanoma Cells. *Mol. Biol. Cell* 2001

102. Degen WG, van Kempen LC, Gijzen EG, van Groningen JJ, van Kooyk Y, Bloemers HP, Swart GW: MEMD, a new cell adhesion molecule in metastasizing human melanoma cell lines, is identical to ALCAM (activated leukocyte cell adhesion molecule). *Am. J. Pathol.* 1998

103. Van Kempen LCLT, Van Den Oord JJ, Van Muijen GNP, Weidle UH, Bloemers HPJ, Swart GWM: Activated leukocyte cell adhesion molecule/CD166, a marker of tumor progression in primary malignant melanoma of the skin. *Am. J. Pathol.* 2000

104. Holzmann B, Gosslar U, Bittner M: alpha 4 integrins and tumor metastasis. *Curr Top Microbiol Immunol* 1998

105. Hodis E, Watson IR, Kryukov GV, Arold ST, Imielinski M, Theurillat J-P, Nickerson E, Auclair D, Li L, Place C, DiCara D, Ramos AH, Lawrence MS, Cibulskis K, Sivachenko A, Voet D, Saksena G, Stransky N, Onofrio RC, Winckler W, Ardlie K, Wagle N, Wargo J, Chong K, Morton DL, Stemke-Hale K, Chen G, Noble M, Meyerson M, Ladbury JE, Davies MA, Gershenwald JE, Wagner SN, Hoon DSB, Schadendorf D, Lander ES, Gabriel SB, Getz G, Garraway LA, Chin L: A Landscape of Driver Mutations in Melanoma. *Cell* 150: 251–263, 2012

106. Ascierto PA, Kirkwood JM, Grob JJ, Simeone E, Grimaldi AM, Maio M, Palmieri G, Testori A, Marincola FM, Mozzillo N: The role of BRAF V600 mutation in melanoma. J. Transl. Med. 2012

107. Surgery E, Becquerel CH: New Drug Combination Strategies in Melanoma: Current Status and Future DirectionsNew Drug Combination Strategies in Melanoma: Current Status and Future Directions. *Anticancer Res.* [Internet] 37: 5941–5953, 2017 Available from: http://ar.iiarjournals.org/content/37/11/5941.abstract

108. Wang JX, Fukunaga-Kalabis M, Herlyn M: Crosstalk in skin: melanocytes, keratinocytes, stem cells, and melanoma. J. Cell Commun. Signal. 2016

109. Amaral T, Sinnberg T, Meier F, Krepler C, Levesque M, Niessner H, Garbe C: The mitogen-activated protein kinase pathway in melanoma part I – Activation and primary resistance mechanisms to BRAF inhibition. Eur. J. Cancer. 2017

110. McCain J: The MAPK (ERK) Pathway: Investigational Combinations for the Treatment Of BRAF-Mutated Metastatic Melanoma. *P T* 2013

111. Swaika A, Crozier JA, Joseph RW: Vemurafenib: An evidence-based review of its clinical utility in the treatment of metastatic melanoma. Drug Des. Devel. Ther. 2014

112. Davies MA: The role of the PI3K-AKT pathway in melanoma. Cancer J. 2012

113. Tsao H, Chin L, Garraway LA, Fisher DE: Melanoma: From mutations to medicine. *Genes Dev.* 26: 1131–1155, 2012

114. Heistein JB, Acharya U: Cancer, Melanoma, Malignant.

115. Ward WH, Lambreton F, Goel N, Yu JQ, Farma JM: Clinical Presentation and Staging of Melanoma. In: *Cutaneous Melanoma: Etiology and Therapy*, 2017

116. Guerry D, Synnestvedt M, Elder DE, Schultz D: Lessons from tumor progression: the invasive radial growth phase of melanoma is common, incapable of metastasis, and indolent. *J. Invest. Dermatol.* 100: 342S–345S, 1993

117. Chapman PB, Hauschild A, Robert C, Haanen JB, Ascierto P, Larkin J, Dummer R: Improved survival with vemurafenic in melanoma with BRAF V600E mutation. *N Eng J Med* 364: 2507–2516, 2011

118. Flaherty KT: Narrative Review: BRAF Opens the Door for Therapeutic Advances in Melanoma. *Ann. Intern. Med.* 153: 587, 2010

119. Alluri N, Jimeno A: Trametinib for the treatment of melanoma. *Drugs of Today* 2013

120. Ascierto PA, Schadendorf D, Berking C, Agarwala SS, van Herpen CML, Queirolo P, Blank CU, Hauschild A, Beck JT, St-Pierre A, Niazi F, Wandel S, Peters M, Zubel A, Dummer R: MEK162 for patients with advanced melanoma harbouring NRAS or Val600 BRAF mutations: A non-randomised, open-label phase 2 study. *Lancet Oncol.* 2013

121. Wolchok JD, Hodi FS, Weber JS, Allison JP, Urba WJ, Robert C, O'Day SJ, Hoos A, Humphrey R, Berman DM, Lonberg N, Korman AJ: Development of ipilimumab: A novel immunotherapeutic approach for the treatment of advanced melanoma. *Ann. N. Y. Acad. Sci.* 1291: 1–13, 2013

122. Levesque MP, Cheng PF, Raaijmakers MIG, Saltari A, Dummer R: Metastatic melanoma moves on: translational science in the era of personalized medicine. *Cancer Metastasis Rev.* 36: 7–21, 2017

123. Gutzmer R, Koop A, Meier F, Hassel JC, Terheyden P, Zimmer L, Heinzerling L, Ugurel S, Pföhler C, Gesierich A, Livingstone E, Satzger I, Kähler KC: Programmed cell death protein-1 (PD-1) inhibitor therapy in patients with advanced melanoma and preexisting autoimmunity or ipilimumab-triggered autoimmunity. *Eur. J. Cancer* 2017

124. Megahed AI, Koon HB: What Is the Role of Chemotherapy in the Treatment of Melanoma? *Curr. Treat. Options Oncol.* 15: 321–335, 2014

125. Domingues B, Lopes J, Soares P, Populo H: Melanoma treatment in review. *ImmunoTargets Ther.* Volume 7: 35–49, 2018

126. Mishra H, Mishra PK, Ekielski A, Jaggi M, Iqbal Z, Talegaonkar S: Melanoma treatment: from conventional to nanotechnology. *J. Cancer Res. Clin. Oncol.* 2018

127. Malissen N, Grob J-J: Metastatic Melanoma: Recent Therapeutic Progress and Future Perspectives. *Drugs* 78: 1197–1209, 2018

128. Wagle N, Emery C, Berger MF, Davis MJ, Sawyer A, Pochanard P, Kehoe SM, Johannessen CM, MacConaill LE, Hahn WC, Meyerson M, Garraway LA: Dissecting therapeutic resistance to RAF inhibition in melanoma by tumor genomic profiling. *J. Clin. Oncol.* 2011

129. Gottesman MM: Mechanisms of Cancer Drug Resistance. *Annu. Rev. Med.* 2002

130. Chartrain M, Riond J, Stennevin A, Vandenberghe I, Gomes B, Lamant L, Meyer N, Gairin JE, Guilbaud N, Annereau JP: Melanoma chemotherapy leads to the selection of ABCB5-expressing cells. *PLoS One* 2012

131. Chen KG, Valencia JC, Lai B, Zhang G, Paterson JK, Rouzaud F, Berens W, Wincovitch SM, Garfield SH, Leapman RD, Hearing VJ, Gottesman MM: Melanosomal sequestration of cytotoxic drugs contributes to the intractability of malignant melanomas. *Proc. Natl. Acad. Sci.* 2006

132. Gottesman MM, Fojo T, Bates SE: Multidrug resistance in cancer: role of ATP–

dependent transporters. *Nat. Rev. Cancer* 2002

133. Frank NY, Margaryan A, Huang Y, Schatton T, Waaga-Gasser AM, Gasser M, Sayegh MH, Sadee W, Frank MH: ABCB5-mediated doxorubicin transport and chemoresistance in human malignant melanoma. *Cancer Res.* 2005

134. Cheung ST, Cheung PFY, Cheng CKC, Wong NCL, Fan ST: Granulin-epithelin precursor and ATP-dependent binding cassette (ABC)B5 regulate liver cancer cell chemoresistance. *Gastroenterology* 2011

135. Wilson BJ, Schatton T, Zhan Q, Gasser M, Jie M, Saab KR, Schanche R, Waaga-Gasser AM, Gold JS, Huang Q, Murphy GF, Frank MH, Frank NY: ABCB5 identifies a therapy-refractory tumor cell population in colorectal cancer patients. *Cancer Res.* 2011

136. Frank NY, Pendse SS, Lapchak PH, Margaryan A, Shlain D, Doeing C, Sayegh MH, Frank MH: Regulation of progenitor cell fusion by ABCB5 P-glycoprotein, a novel human ATP-binding cassette transporter. *J. Biol. Chem.* 278: 47156–65, 2003

137. Chen KG, Szakács G, Annereau JP, Rouzaud F, Liang XJ, Valencia JC, Nagineni CN, Hooks JJ, Hearing VJ, Gottesman MM: Principal expression of two mRNA isoforms (ABCB5α and ABCB5β) of the ATP-binding cassette transporter gene ABCB5 in melanoma cells and melanocytes. *Pigment Cell Res.* 2005

138. Huang Y, Anderle P, Bussey KJ, Barbacioru C, Shankavaram U, Dai Z, Reinhold WC, Papp A, Weinstein JN, Sadée W: Membrane Transporters and Channels. *Cancer Res.* 64: 4294–4301, 2004

139. Szakács G, Annereau J-P, Lababidi S, Shankavaram U, Arciello A, Bussey KJ, Reinhold W, Guo Y, Kruh GD, Reimers M, Weinstein JN, Gottesman MM: Predicting drug sensitivity and resistance. *Cancer Cell* 6: 129–137, 2004

140. Schatton T, Murphy GF, Frank NY, Yamaura K, Waaga-Gasser AM, Gasser M, Zhan Q, Jordan S, Duncan LM, Weishaupt C, Fuhlbrigge RC, Kupper TS, Sayegh MH, Frank MH: Identification of cells initiating human melanomas. *Nature* [Internet] 451: 345–9, 2008 Available from: http://dx.doi.org/10.1038/nature06489

141. Beaumont K, Mohana-Kumaran N, Haass N: Modeling Melanoma In Vitro and In Vivo. *Healthcare* [Internet] 2: 27–46, 2013 Available from: http://www.mdpi.com/2227-9032/2/1/27/

142. Halpern B, Pejsachowicz B, Febvre HL, Barski G: Differences in patterns of aggregation of malignant and non-malignant mammalian cells. *Nature* 1966

143. Sutherland RM, Mccredie JA, Inch WR: Growth of Multicell Spheroids in Tissue Culture as a Model of Nodular Carcinomas. *JNCI J. Natl. Cancer Inst.* 1971

144. Phung YT, Barbone D, Broaddus VC, Ho M: Rapid generation of in vitro multicellular spheroids for the study of monoclonal antibody therapy. *J. Cancer* 2011

145. Lin SJ, Jee SH, Hsaio WC, Lee SJ, Young TH: Formation of melanocyte spheroids on the chitosan-coated surface. *Biomaterials* 2005

146. Okochi M, Matsumura T, Yamamoto S, Nakayama E, Jimbow K, Honda H: Cell behavior observation and gene expression analysis of melanoma associated with stromal fibroblasts in a three-dimensional magnetic cell culture array. *Biotechnol. Prog.* 29: 135–142, 2013

147. Smalley KSM: Multiple signaling pathways must be targeted to overcome drug resistance in cell lines derived from melanoma metastases. *Mol. Cancer Ther.* [Internet] 5: 1136–1144, 2006 Available from: http://mct.aacrjournals.org/cgi/doi/10.1158/1535-7163.MCT-06-0084

148. Smalley KS, Lioni M, Noma K, Haass NK, Herlyn M: *In vitro* three-dimensional

tumor microenvironment models for anticancer drug discovery. *Expert Opin. Drug Discov.* [Internet] 3: 1–10, 2008 Available from: http://www.tandfonline.com/doi/full/10.1517/17460441.3.1.1

149. Haass NK, Sproesser K, Nguyen TK, Contractor R, Medina CA, Nathanson KL, Herlyn M, Smalley KSM: The mitogen-activated protein/extracellular signal-regulated kinase kinase inhibitor AZD6244 (ARRY-142886) induces growth arrest in melanoma cells and tumor regression when combined with docetaxel. *Clin. Cancer Res.* 2008

150. Zhuang L, Lee CS, Scolyer RA, McCarthy SW, Palmer AA, Zhang XD, Thompson JF, Bron LP, Hersey P: Activation of the extracellular signal regulated kinase (ERK) pathway in human melanoma. *J. Clin. Pathol.* 2005

151. Marrero B, Messina JL, Heller R: Generation of a tumor spheroid in a microgravity environment as a 3D model of melanoma. *Vitr. Cell. Dev. Biol. - Anim.* 45: 523–534, 2009

152. Peura M, Siltanen A, Saarinen I, Soots A, Bizik J, Vuola J, Harjula A, Kankuri E: Paracrine factors from fibroblast aggregates in a fibrin-matrix carrier enhance keratinocyte viability and migration. *J. Biomed. Mater. Res. - Part A* 95 A: 658–664, 2010

153. Ströbel S, Buschmann N, Neeladkandhan A, Messner S, Kelm JM: Characterization of a novel in vitro 3D skin microtissue model for efficacy and toxicity testing. *Toxicol. Lett.* 2016

154. Ivascu A, Kubbies M: Rapid Generation of Single-Tumor Spheroids for High-Throughput Cell Function and Toxicity Analysis. *J. Biomol. Screen.* [Internet] 11: 922–932, 2006 Available from: http://journals.sagepub.com/doi/10.1177/1087057106292763

155. Vörsmann H, Groeber F, Walles H, Busch S, Beissert S, Walczak H, Kulms D: Development of a human three-dimensional organotypic skin-melanoma spheroid model for in vitro drug testing. *Cell Death Dis.* 4: 2013

156. Rebelo SP, Costa R, Estrada M, Shevchenko V, Brito C, Alves PM: HepaRG microencapsulated spheroids in DMSO-free culture: novel culturing approaches for enhanced xenobiotic and biosynthetic metabolism. *Arch. Toxicol.* [Internet] 89: 1347–1358, 2014 Available from: http://dx.doi.org/10.1007/s00204-014-1320-9

157. Smyrek I, Stelzer EHK: Quantitative three-dimensional evaluation of immunofluorescence staining for large whole mount spheroids with light sheet microscopy. *Biomed. Opt. Express* [Internet] 8: 484, 2017 Available from: https://www.osapublishing.org/abstract.cfm?URI=boe-8-2-484

158. Raleigh JA, Miller GG, Franko AJ, Koch CJ, Fuciarelli AF, Kelly DA: Fluorescence immunohistochemical detection of hypoxic cells in spheroids and tumours. *Br J Cancer* [Internet] 56: 395–400, 1987 Available from: http://www.ncbi.nlm.nih.gov/pmc/articles/PMC2001823/pdf/brjcancer00509-0014.pdf

159. Carlson MW, Alt-Holland A, Egles C, Garlick JA: Three-dimensional tissue models of normal and diseased skin. Curr. Protoc. Cell Biol. 2008

160. Zanoni TB, Tiago M, Fai??o-Flores F, de Moraes Barros SB, Bast A, Hageman G, de Oliveira DP, Maria-Engler SS: Basic Red 51, a permitted semi-permanent hair dye, is cytotoxic to human skin cells: Studies in monolayer and 3D skin model using human keratinocytes (HaCaT). *Toxicol. Lett.* [Internet] 227: 139–149, 2014 Available from: http://dx.doi.org/10.1016/j.toxlet.2014.03.007

161. Bell E, Ehrlich HP, Buttle DJ, Nakatsuji T: Living tissue formed in vitro and accepted as skin-equivalent tissue of full thickness. *Science (80-.).* 211: 1052–

1054, 1981

162. Alameda JP, Navarro M, Ramirez A, Page A, Suarez-Cabrera C, Moreno-Maldonado R, Paramio JM, Farina MD, Del RM, Fernandez-Acenero MJ, Bravo A, Casanova ML: IKKalpha regulates the stratification and differentiation of the epidermis: implications for skin cancer development. *Oncotarget.* 7: 76779–76792, 2016

163. Schoop VM, Mirancea N, Fusenig NE: Epidermal organization and differentiation of HaCat keratinocytes in organotypic coculture with human dermal fibroblasts. *J. Invest. Dermatol.* [Internet] 112: 343–353, 1999 Available from: http://dx.doi.org/10.1046/j.1523-1747.1999.00524.x

164. Denda M, Denda S: Air-exposed keratinocytes exhibited intracellular calcium oscillation. *Ski. Res. Technol.* 13: 195–201, 2007

165. Smola H, Thiekotter G, Fusenig NE: Mutual induction of growth factor gene expression by epidermal- dermal cell interaction. *J.Cell Biol.* 122: 417–429, 1993

166. Soboleva AG, Mezentsev A, Zolotorenko A, Bruskin S, Pirusian E: Three-dimensional skin models of psoriasis. Cells Tissues Organs. 2014

167. Kober J, Gugerell A, Schmid M, Kamolz LP, Keck M: Generation of a Fibrin Based Three-Layered Skin Substitute. *Biomed Res. Int.* 2015: 2015

168. Brohem CA, Massaro RR, Tiago M, Marinho E, Jasiulionis MG, Almeida RL De, Rivelli DP, Albuquerque RC, Oliveira TF De, Loureiro APDM, Okada S: Pigment Cell & melanoma. 2011

169. Berking C, Herlyn M: Human skin reconstruct models: A new application for studies of melanocyte and melanoma biology. Histol. Histopathol. 2001

170. Meier F, Nesbit M, Hsu MY, Martin B, Van Belle P, Elder DE, Schaumburg-Lever G, Garbe C, Walz TM, Donatien P, Crombleholme TM, Herlyn M: Human melanoma progression in skin reconstructs: Biological significance of bFGF. *Am. J. Pathol.* 156: 193–200, 2000

171. Meier F, Busch S, Lasithiotakis K, Kulms D, Garbe C, Maczey E, Herlyn M, Schittek B: Combined targeting of MAPK and AKT signalling pathways is a promising strategy for melanoma treatment. *Br. J. Dermatol.* 2007

172. Van Den Bogaard EH, Tjabringa GS, Joosten I, Vonk-Bergers M, Van Rijssen E, Tijssen HJ, Erkens M, Schalkwijk J, Koenen HJPM: Crosstalk between keratinocytes and T cells in a 3D microenvironment: A model to study inflammatory skin diseases. *J. Invest. Dermatol.* 2014

173. Hern DL, Hubbell JA: Incorporation of adhesion peptides into nonadhesive hydrogels useful for tissue resurfacing. *J. Biomed. Mater. Res.* 39: 266–276, 1998

174. Hosseinkhani H, Hiraoka Y, Li CH, Chen YR, Yu DS, Hong P Da, Ou KL: Engineering three-dimensional collagen-IKVAV matrix to mimic neural microenvironment. *ACS Chem. Neurosci.* 4: 1229–1235, 2013

175. Okugawa Y, Hirai Y: Extracellular epimorphin modulates epidermal differentiation signals mediated by epidermal growth factor receptor. *J. Dermatol. Sci.* [Internet] 69: 236–242, 2013 Available from: http://dx.doi.org/10.1016/j.jdermsci.2012.11.006

176. Zhao X, Lang Q, Yildirimer L, Lin ZY, Cui W, Annabi N, Ng KW, Dokmeci MR, Ghaemmaghami AM, Khademhosseini A: Photocrosslinkable Gelatin Hydrogel for Epidermal Tissue Engineering. *Adv. Healthc. Mater.* 2016

177. Müller I, Kulms D: A 3D Organotypic Melanoma Spheroid Skin Model. *J. Vis. Exp.* 2018

178. Rossi A, Appelt-Menzel A, Kurdyn S, Walles H, Groeber F: Generation of a Three-dimensional Full Thickness Skin Equivalent and Automated Wounding

Video Link. *J. Vis. Exp* 2015

179. Lee V, Singh G, Trasatti JP, Bjornsson C, Xu X, Tran TN, Yoo S-S, Dai G, Karande P: Design and Fabrication of Human Skin by Three-Dimensional Bioprinting. *Tissue Eng. Part C Methods* [Internet] 20: 473–484, 2014 Available from: http://online.liebertpub.com/doi/abs/10.1089/ten.tec.2013.0335

180. Yoo S-S: 3D-printed biological organs: medical potential and patenting opportunity. *Expert Opin. Ther. Pat.* [Internet] 25: 507–511, 2015 Available from: http://www.tandfonline.com/doi/full/10.1517/13543776.2015.1019466

181. Hull CW, Arcadia C: Apparatus for production of three-dimensional objects by stereolithography. Appar. Prod. Three-Dimensional Objects by Stereolithography. 1986

182. Barron JA, Wu P, Ladouceur HD, Ringeisen BR: Biological laser printing: A novel technique for creating heterogeneous 3-dimensional cell patterns. *Biomed. Microdevices* 2004

183. Xu T, Kincaid H, Atala A, Yoo JJ: High-Throughput Production of Single-Cell Microparticles Using an Inkjet Printing Technology. *J. Manuf. Sci. Eng.* 2008

184. Lee W, Son J, Yoo S-S, Park J-K: Facile and Biocompatible Fabrication of Chemically Sol−Gel Transitional Hydrogel Free-Standing Microarchitectures. *Biomacromolecules* [Internet] 12: 14–18, 2010 Available from: http://dx.doi.org/10.1021/bm101246u

185. Son J, Bae CY, Park JK: Freestanding stacked mesh-like hydrogel sheets enable the creation of complex macroscale cellular scaffolds. *Biotechnol. J.* 11: 585–591, 2016

186. Lee W, Lee V, Polio S, Keegan P, Lee JH, Fischer K, Park JK, Yoo SS: On-demand three-dimensional freeform fabrication of multi-layered hydrogel scaffold with fluidic channels. *Biotechnol. Bioeng.* 105: 1178–1186, 2010

187. Jia W, Gungor-Ozkerim PS, Zhang YS, Yue K, Zhu K, Liu W, Pi Q, Byambaa B, Dokmeci MR, Shin SR, Khademhosseini A: Direct 3D bioprinting of perfusable vascular constructs using a blend bioink. *Biomaterials* 2016

188. Lee YB, Polio S, Lee W, Dai G, Menon L, Carroll RS, Yoo SS: Bio-printing of collagen and VEGF-releasing fibrin gel scaffolds for neural stem cell culture. *Exp. Neurol.* 2010

189. Knowlton S, Anand S, Shah T, Tasoglu S: Bioprinting for Neural Tissue Engineering. Trends Neurosci. 2018

190. Lee VK, Dai G, Zou H, Yoo SS: Generation of 3-D glioblastoma-vascular niche using 3-D bioprinting. *2015 41st Annu. Northeast Biomed. Eng. Conf. NEBEC 2015* 3–4, 2015

191. Lee W, Debasitis JC, Lee VK, Lee JH, Fischer K, Edminster K, Park JK, Yoo SS: Multi-layered culture of human skin fibroblasts and keratinocytes through three-dimensional freeform fabrication. *Biomaterials* 2009

192. Koch L, Deiwick A, Schlie S, Michael S, Gruene M, Coger V, Zychlinski D, Schambach A, Reimers K, Vogt PM, Chichkov B: Skin tissue generation by laser cell printing. *Biotechnol. Bioeng.* 109: 1855–1863, 2012

193. Min D, Lee W, Bae IH, Lee TR, Croce P, Yoo SS: Bioprinting of biomimetic skin containing melanocytes. *Exp. Dermatol.* 2018

194. Wang X-F, Song Y, Liu Y-S, Sun Y, Wang Y, Wang Y, Lyu P-J: Osteogenic Differentiation of Three-Dimensional Bioprinted Constructs Consisting of Human Adipose-Derived Stem Cells In Vitro and In Vivo. *PLoS One* [Internet] 11: e0157214, 2016 Available from: http://dx.plos.org/10.1371/journal.pone.0157214

195. Sung JH, Esch MB, Prot J-M, Long CJ, Smith A, Hickman JJ, Shuler ML:

Microfabricated mammalian organ systems and their integration into models of whole animals and humans. *Lab Chip* [Internet] 13: 1201, 2013 Available from: http://xlink.rsc.org/?DOI=c3lc41017j

196. Bhatia SN, Ingber DE: Microfluidic organs-on-chips. Nat. Biotechnol. 2014

197. Duffy DC, McDonald JC, Schueller OJA, Whitesides GM: Rapid prototyping of microfluidic systems in poly (dimethylsiloxane). *Anal. Chem.* 70: 4974–4984, 1998

198. Groeber F, Engelhardt L, Lange J, Kurdyn S, Schmid FF, R??cker C, Mielke S, Walles H, Hansmann J: A first vascularized skin equivalent as an alternative to animal experimentation. *ALTEX* 33: 415–422, 2016

199. Abaci HE, Guo Z, Coffman A, Gillette B, Lee WH, Sia SK, Christiano AM: Human Skin Constructs with Spatially Controlled Vasculature Using Primary and iPSC-Derived Endothelial Cells. *Adv. Healthc. Mater.* 5: 1800–1807, 2016

200. Lee S, Jin S-P, Kim YK, Sung GY, Chung JH, Sung JH: Construction of 3D multicellular microfluidic chip for an in vitro skin model. *Biomed. Microdevices* [Internet] 19: 22, 2017 Available from: http://link.springer.com/10.1007/s10544-017-0156-5

201. O'Neill AT, Monteiro-Riviere NA, Walker GM: Characterization of microfluidic human epidermal keratinocyte culture. *Cytotechnology* 56: 197–207, 2008

202. Kogut I, Roop DR, Bilousova G: Differentiation of Human Induced Pluripotent Stem Cells into a Keratinocyte Lineage. 2014

203. Hewitt KJ, Shamis Y, Hayman RB, Margvelashvili M, Dong S, Carlson MW, Garlick JA: Epigenetic and phenotypic profile of fibroblasts derived from induced pluripotent stem cells. *PLoS One* 6: 2011

204. Ohta S, Imaizumi Y, Okada Y, Akamatsu W, Kuwahara R, Ohyama M, Amagai M, Matsuzaki Y, Yamanaka S, Okano H, Kawakami Y: Generation of human melanocytes from induced pluripotent stem cells. *PLoS One* 6: 1–10, 2011

205. Ramadan Q, Ting FCW: In vitro micro-physiological immune-competent model of the human skin. *Lab Chip* [Internet] 16: 1899–1908, 2016 Available from: http://xlink.rsc.org/?DOI=C6LC00229C

206. Hou L, Hagen J, Wang X, Papautsky I, Naik R, Kelley-Loughnane N, Heikenfeld J: Artificial microfluidic skin for in vitro perspiration simulation and testing. *Lab Chip* [Internet] 13: 1868, 2013 Available from: http://xlink.rsc.org/?DOI=c3lc41231h

207. Wagner I, Materne EM, Brincker S, Süßbier U, Frädrich C, Busek M, Sonntag F, Sakharov DA, Trushkin E V., Tonevitsky AG, Lauster R, Marx U: A dynamic multi-organ-chip for long-term cultivation and substance testing proven by 3D human liver and skin tissue co-culture. *Lab Chip* 2013

208. Maschmeyer I, Hasenberg T, Jaenicke A, Lindner M, Lorenz AK, Zech J, Garbe LA, Sonntag F, Hayden P, Ayehunie S, Lauster R, Marx U, Materne EM: Chip-based human liver-intestine and liver-skin co-cultures - A first step toward systemic repeated dose substance testing in vitro. *Eur. J. Pharm. Biopharm.* [Internet] 95: 77–87, 2015 Available from: http://dx.doi.org/10.1016/j.ejpb.2015.03.002

209. Maschmeyer I, Lorenz AK, Schimek K, Hasenberg T, Ramme AP, Hübner J, Lindner M, Drewell C, Bauer S, Thomas A, Sambo NS, Sonntag F, Lauster R, Marx U: A four-organ-chip for interconnected long-term co-culture of human intestine, liver, skin and kidney equivalents. *Lab Chip* [Internet] 15: 2688–2699, 2015 Available from: http://xlink.rsc.org/?DOI=C5LC00392J

210. Wufuer M, Lee G, Hur W, Jeon B, Kim BJ, Choi TH, Lee S: Skin-on-a-chip model simulating inflammation, edema and drug-based treatment. *Sci. Rep.* [Internet]

6: 37471, 2016 Available from: http://www.nature.com/articles/srep37471

211. Marconi A, Quadri M, Saltari A, Pincelli C: Progress in melanoma modelling in vitro. *Exp. Dermatol.* 27: 578–586, 2018

212. Mori N, Morimoto Y, Takeuchi S: Skin integrated with perfusable vascular channels on a chip. *Biomaterials* [Internet] 116: 48–56, 2017 Available from: http://dx.doi.org/10.1016/j.biomaterials.2016.11.031

213. Pandya HJ, Dhingra K, Prabhakar D, Natarajan SK, Vasan AS, Kulkarni A: HHS Public Access. 632–642, 2018

214. Lucarini V, Sanchez M, Mattei F, Belardelli F, Schiavoni G, Sestili P, Gabriele L, De Ninno A, Spada M, Fragale A, Gerardino A, Businaro L, Sistigu A: A multidisciplinary study using in vivo tumor models and microfluidic cell-on-chip approach to explore the cross-talk between cancer and immune cells . *J. Immunotoxicol.* 11: 337–346, 2014

215. Ataç B, Wagner I, Horland R, Lauster R, Marx U, Tonevitsky AG, Azar RP, Lindner G: Skin and hair on-a-chip: In vitro skin models versus ex vivo tissue maintenance with dynamic perfusion. *Lab Chip* 2013

216. van Meer BJ, de Vries H, Firth KSA, van Weerd J, Tertoolen LGJ, Karperien HBJ, Jonkheijm P, Denning C, IJzerman AP, Mummery CL: Small molecule absorption by PDMS in the context of drug response bioassays. *Biochem. Biophys. Res. Commun.* [Internet] 482: 323–328, 2017 Available from: http://dx.doi.org/10.1016/j.bbrc.2016.11.062

217. Sung JH, Shuler ML: Prevention of air bubble formation in a microfluidic perfusion cell culture system using a microscale bubble trap. *Biomed. Microdevices* 11: 731–738, 2009

218. Lochovsky C, Yasotharan S, Günther A: Bubbles no more: in-plane trapping and removal of bubbles in microfluidic devices. *Lab Chip* [Internet] 12: 595–601, 2012 Available from: http://xlink.rsc.org/?DOI=C1LC20817A

219. Giselbrecht S, Gietzelt T, Gottwald E, Trautmann C, Truckenmüller R, Weibezahn KF, Welle A: 3D tissue culture substrates produced by microthermoforming of pre-processed polymer films. *Biomed. Microdevices* 2006

220. Truckenmüller R, Giselbrecht S, Rivron N, Gottwald E, Saile V, Van Den Berg A, Wessling M, Van Blitterswijk C: Thermoforming of film-based biomedical microdevices. *Adv. Mater.* 23: 1311–1329, 2011

221. Giselbrecht S, Gottwald E, Truckenmueller R, Trautmann C, Welle A, Guber A, Saile V, Gietzelt T, Weibezahn K-F: Microfabrication of chip-sized scaffolds for three-dimensional cell cultivation. *J. Vis. Exp.* 1–6, 2008

222. Wuchter P, Saffrich R, Giselbrecht S, Nies C, Lorig H, Kolb S, Ho AD, Gottwald E: Microcavity arrays as an in vitro model system of the bone marrow niche for hematopoietic stem cells. *Cell Tissue Res.* 2016

223. Laemmli UK: Cleavage of structural proteins during the assembly of the head of bacteriophage T4. *Nature* 1970

224. Ballangrud ÅM, Yang WH, Dnistrian A, Lampen NM, Sgouros G: Growth and characterization of LNCaP prostate cancer cell spheroids. In: *Clinical Cancer Research*, 1999

225. Eroglu Z, Kong KM, Jakowatz JG, Samlowski W, Fruehauf JP: Phase II clinical trial evaluating docetaxel, vinorelbine and GM-CSF in stage IV melanoma. *Cancer Chemother. Pharmacol.* 68: 1081–1087, 2011

226. Doddapaneni BS, Kyryachenko S, Chagani SE, Alany RG, Rao DA, Indra AK, Alani AWG: A three-drug nanoscale drug delivery system designed for preferential lymphatic uptake for the treatment of metastatic melanoma. *J.*

Control. Release 220: 503–514, 2015

227. Mi Y, Mu C, Wolfram J, Deng Z, Hu TY, Liu X, Blanco E, Shen H, Ferrari M: A Micro/Nano Composite for Combination Treatment of Melanoma Lung Metastasis. *Adv. Healthc. Mater.* 5: 936–946, 2016

228. Kodet O, Lacina L, Krejčí E, Dvořánková B, Grim M, Štork J, Kodetová D, Vlček Č, Šáchová J, Kolář M, Strnad H, Smetana K: Melanoma cells influence the differentiation pattern of human epidermal keratinocytes. *Mol. Cancer* 14: 1, 2015

229. Carey TE, Takahashi T, Resnick LA, Oettgen HF, Old LJ: Cell surface antigens of human malignant melanoma: mixed hemadsorption assays for humoral immunity to cultured autologous melanoma cells. *Proc. Natl. Acad. Sci.* [Internet] 73: 3278–3282, 1976 Available from: http://www.pnas.org/cgi/doi/10.1073/pnas.73.9.3278

230. Deyrieux AF, Wilson VG: In vitro culture conditions to study keratinocyte differentiation using the HaCaT cell line. *Cytotechnology* 54: 77–83, 2007

231. Santiago-Walker A, Li L, Haass NK, Herlyn M: Melanocytes: From morphology to application. *Skin Pharmacol. Physiol.* 22: 114–121, 2009

232. Wilson VG: Growth and Differentiation of HaCaT Keratinocytes. Methods Mol. Biol. 2014

233. van den Broek LJ, Bergers LIJC, Reijnders CMA, Gibbs S: Progress and Future Prospectives in Skin-on-Chip Development with Emphasis on the use of Different Cell Types and Technical Challenges. *Stem Cell Rev. Reports* [Internet] 2017 Available from: http://link.springer.com/10.1007/s12015-017-9737-1

234. DeBerardinis RJ, Lum JJ, Hatzivassiliou G, Thompson CB: The Biology of Cancer: Metabolic Reprogramming Fuels Cell Growth and Proliferation. Cell Metab. 2008

235. Schmidt M, Gutknecht D, Simon JC, Schulz JN, Eckes B, Anderegg U, Saalbach A: Controlling the balance of fibroblast proliferation and differentiation: Impact of thy-1. *J. Invest. Dermatol.* 2015

236. Singer AJ, Clark RAF: Mechanisms of disease - Cutaneous wound healing. *N. Engl. J. Med.* 1999

237. Wang Z, Wang Y, Farhangfar F, Zimmer M, Zhang Y: Enhanced keratinocyte proliferation and migration in co-culture with fibroblasts. *PLoS One* 2012

238. Holle AW, Young JL, Spatz JP: In vitro cancer cell-ECM interactions inform in vivo cancer treatment. Adv. Drug Deliv. Rev. 2016

239. Ziskin MC: Growth of Mammalian Multicellular Tumor Spheroids. *Cancer Res.* 1983

240. Haridas P, McGovern JA, McElwain SDL, Simpson MJ: Quantitative comparison of the spreading and invasion of radial growth phase and metastatic melanoma cells in a three-dimensional human skin equivalent model. *PeerJ* 2017

241. Helmbach H, Rossmann E, Kern MA, Schadendorf D: Drug-resistance in human melanoma. Int. J. Cancer. 2001

242. Gambichler T, Petig AL, Stockfleth E, Stï¿½cker M: Expression of SOX10, ABCB5 and CD271 in melanocytic lesions and correlation with survival data of patients with melanoma. *Clin. Exp. Dermatol.* 41: 709–716, 2016

243. Wilson BJ, Saab KR, Ma J, Schatton T, Pütz P: NIH Public Access. 74: 4196–4207, 2015

244. Wilson BJ, Saab KR, Ma J, Schatton T, Pütz P, Zhan Q, Murphy GF, Gasser M, Waaga-Gasser AM, Frank NY, Frank MH: ABCB5 maintains melanoma-initiating cells through a proinflammatory cytokine signaling circuit. *Cancer Res.* 2014

245. Ringel I, Horwitz SB: Studies with RP 56976 (taxotere): A semisynthetic

analogue of taxol. *J. Natl. Cancer Inst.* 1991

246. Zhong P, Qiu M, Zhang J, Sun H, Cheng R, Deng C, Meng F, Zhong Z: cRGD-installed docetaxel-loaded mertansine prodrug micelles: redox-triggered ratiometric dual drug release and targeted synergistic treatment of B16F10 melanoma. *Nanotechnology* 28: 295103, 2017

247. Gu Z, Wang Q, Shi Y, Huang Y, Zhang J, Zhang X, Lin G: Nanotechnology-mediated immunochemotherapy combined with docetaxel and PD-L1 antibody increase therapeutic effects and decrease systemic toxicity. *J. Control. Release* 286: 369–380, 2018

248. Kiejda KA, Hersey P, Mhaidat NM, Zhang XD, Wang Y: Docetaxel-induced apoptosis in melanoma cells is dependent on activation of caspase-2. *Mol. Cancer Ther.* 2007

249. Chemo-sensitivity of Two-dimensional Monolayer and Three-dimensional Spheroid of Breast Cancer MCF-7 Cells to Daunorubicin, Docetaxel, and Arsenic Disulfide. *Anticancer Res.* 2018

250. Lovitt CJ, Shelper TB, Avery VM: Evaluation of chemotherapeutics in a three-dimensional breast cancer model. *J. Cancer Res. Clin. Oncol.* 2015

251. Melissaridou S, Wiechec E, Magan M, Jain MV, Chung MK, Farnebo L, Roberg K: The effect of 2D and 3D cell cultures on treatment response, EMT profile and stem cell features in head and neck cancer. *Cancer Cell Int.* 2019

252. Meier F, Nesbit M, Hsu MY, Martin B, Van Belle P, Elder DE, Schaumburg-Lever G, Garbe C, Walz TM, Donatien P, Crombleholme TM, Herlyn M: Human melanoma progression in skin reconstructs: Biological significance of bFGF. *Am. J. Pathol.* 2000

253. Abaci HE, Gledhill K, Guo Z, Christiano AM, Shuler ML: Pumpless microfluidic platform for drug testing on human skin equivalents. *Lab Chip* 15: 882–888, 2015

254. Lee JT, Li L, Brafford PA, Van Den Eijnden M, Halloran MB, Sproesser K, Haass NK, Smalley KSM, Tsai J, Bollag G, Herlyn M: PLX4032, a potent inhibitor of the B-Raf V600E oncogene, selectively inhibits V600E-positive melanomas. *Pigment Cell Melanoma Res.* 2010

8 PUBLICATIONS

Klicks, J., von Molitor, E., Ertongur-Fauth, T., Rudolf, R. & Hafner, M. In vitro skin three-dimensional models and their applications. *J. Cell. Biotechnol.* (2017). doi:10.3233/JCB-179004

Rustamov, V., Keller, F., **Klicks, J.**, Hafner, M. & Rudolf, R. Bone Sialoprotein Shows Enhanced Expression in Early, High-Proliferation Stages of Three-Dimensional Spheroid Cell Cultures of Breast Cancer Cell Line MDA-MB-231. *Front. Oncol.* (2019). doi:10.3389/fonc.2019.00036

Klicks, J., Maßlo, C., Kluth, A., Rudolf, R. & Hafner, M. A novel spheroid-based co-culture model mimics loss of keratinocyte differentiation, melanoma cell invasion, and drug-induced selection of ABCB5-expressing cells. (revised revision)

9 CURRICULUM VITAE

PERSONALIEN

Name und Vorname:	Julia Klicks
Geburtsdatum:	22.08.1990
Geburtsort:	Mannheim, Deutschland
Familienstand:	verheiratet
Vater:	Thomas Dörner
Mutter:	Gabriele Dörner

SCHULISCHER WERDEGANG

2000 – 2009	Ludwig-Frank Gymnasium, Mannheim

UNIVERSITÄRER WERDEGANG

09/2009 – 08/2013	Biologische Chemie an der Hochschule Mannheim Abschluss: Bachelor of Science Note: 2,0
03/2013 – 06/2013	Bachelorthesis Deutsches Krebsforschungszentrum Heidelberg in der Helmholtz-Gemeinschaft, Abteilung für Angewandte Tumorvirologie Thema: Untersuchungen zur antineoplastischen Wirksamkeit des onkolytischen Parvovirus H-1 an *in vitro* und *in vivo* Modellen MYCN amplifizierter Neuroblastome
09/2013 – 08/2015	Biotechnology – Biomedical Science and Technology an der Hochschule Mannheim Abschluss: Master of Science Note: 1,5
09/2014 – 03/2015	Masterthesis Washington University, School of Medicine, Department of Pediatrics, St. Louis Children's Hospital, St. Louis, Missouri, USA Thema: Role of sonic hedgehog signaling in adrenocortical development and tumorigenesis

10 ACKNOWLEDGMENT